CHAPTER 5

CHOLESTEROL AND NAPHTHALENE-BASED UNSYMMETRICAL LIQUID CRYSTALLINE DIMERS: SYNTHESIS, CHARACTERIZATION, AND INSIGHTS INTO ITS MESOMORPHIC BEHAVIOUR

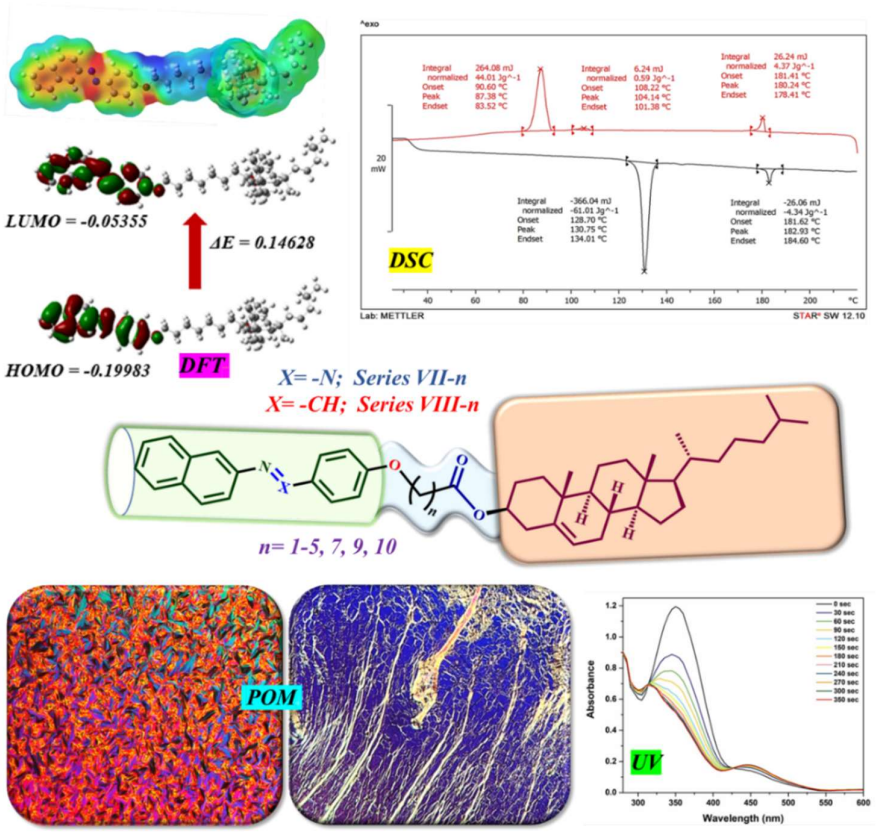

5.1 Introduction

Chiral liquid crystals (LCs) are notable for their unique physical properties. In biological membranes, cholesterol plays a crucial role in regulating fluidity and acts as a membrane reinforcer by affecting the membranes' mechanical and transport properties. Cholesterol is a significant biologically active organic compound and is a key source of chiral mesophases due to their distinctive structural features. The first report on the phase behaviour of cholesterol-based dimers appeared in 1994.[1] The incorporation of cholesterol allows for the induction of chirality in liquid crystals, influencing the formation of various phases[2–8]. Chirality plays a pivotal role in the exploration of liquid crystalline dimers, particularly those incorporating cholesteryl groups, which are not only significant for fundamental research but also hold technological promise.[9–11] Various chiral non-symmetric liquid crystalline dimers have been synthesized, often featuring a cholesteryl group covalently linked to a mesogenic core via a flexible spacer, leading to the manifestation of multiple mesophases such as chiral smectic phase (Sm*), twist grain boundary phases (TGB*), chiral nematic phase (N*), and blue phases (BPs)[12–17]. Moreover, cholesteric liquid crystals exhibit distinctive properties such as circular dichroism, strong optical rotation, and selective reflection, making them a hot research topic in the field of liquid crystal materials[18,19] with tailored properties for applications in displays, photonic devices, and optical modulation. Cholesterol-calamitic dimers have gained significant recognition among reported dimer formations.[20] Various liquid crystalline phases have been identified in substances containing a cholesteryl moiety connected via a spacer to one or more variety of aromatic/ aliphatic/ heterocyclic ring systems with suitable linkages including ethers, azo-, azomethine, aromatic ester, biphenyl, or terphenyl units[21].

Azo bond linking unit exhibits a remarkable property wherein it undergoes isomerization between cis and trans structures under different light induction, a feature particularly prominent in azobenzene liquid crystals[22–24]. This conformational alteration induced by light radiation confers special photo-responsive characteristics to the materials, rendering them suitable for applications in photochromic phase change and optical storage[25,26]. **Fig. 5.1** depicts a few examples of unsymmetrical dimers with cholesterol and azo moiety.

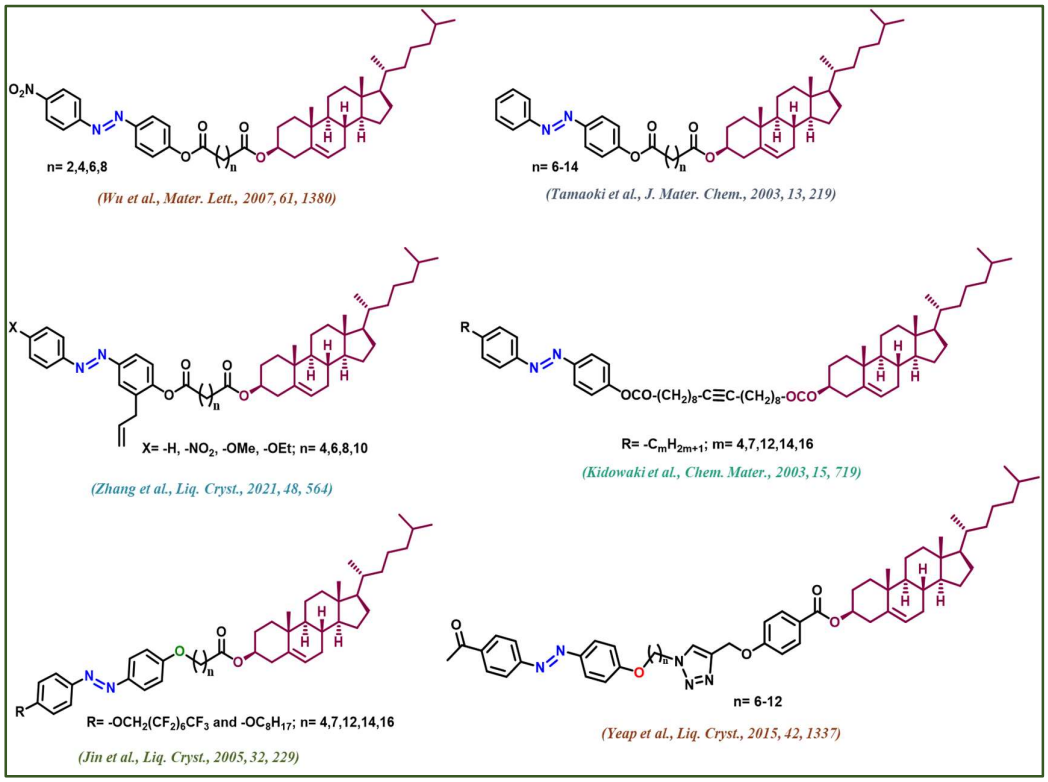

Fig. 5.1 Examples of Unsymmetrical dimers with Cholesterol and azo moiety

Changcheng Wu introduced a series of dimers featuring cholesteryl ester and 4′-nitroazobenzene groups, with different methylene spacer lengths.[27] Meanwhile, Mallia and Tamaoki et al. described a series of photoresponsive chiral dimesogenic compounds.[28] Kidowaki et al. reported LC dimers with a unique spacer of docosanedioic acid and have studied the effect of varying terminal chain length.[29] Zhang et al. described a range of LC dimers comprising both a cholesteryl group and substituted azobenzene, along with a branched allyl chain.[30] Jin et al. presented findings on two sets of asymmetric dimers composed of cholesterol and azobenzene-based components linked by ω-oxyalkanoyl spacers with different lengths.[31] Yeap et al. reported novel non-symmetrical dimers comprising side units of azobenzene and 1,2,3-triazole-cholesterol.[32] Numerous studies have investigated unsymmetrical dimers comprising cholesterol and Schiff base, featuring varying lengths of terminal alkoxy chains and flexible spacer lengths.[33–37]

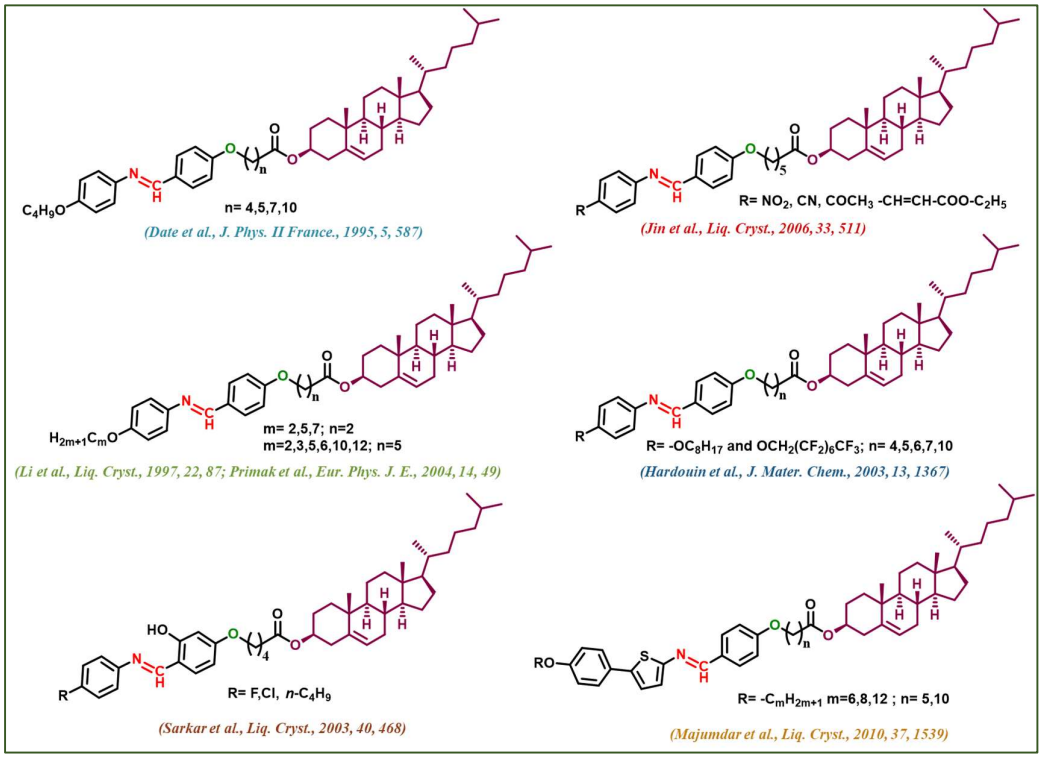

Fig. 5.2 Examples of Unsymmetrical dimers with Cholesterol and azomethine moiety

The Schiff base linking unit, characterized by the -CH=N- bond, possesses notable polarity and rigidity, facilitating strong intermolecular interactions. Incorporating this unit into liquid crystal molecular structures can enhance mesophase formation due to these interactions[38–40]. **Fig. 5.2** depicts a few examples of unsymmetrical dimers with cholesterol and azomethine/Schiff base moiety. Reports have also documented unsymmetrical dimers incorporating cholesterol and Schiff base, characterized by diverse terminal groups possessing electron-attracting properties.[41] Studies have been conducted by Jin et al. to compare the liquid crystalline characteristics of dimers composed of cholesterol and Schiff base components containing alkoxy and perfluoroalkoxy tails.[42,43]

5.2 Objectives:

Cholesterol-based liquid crystals are important due to their unique optical properties. Their ability to form chiral nematic phases makes them valuable in creating reflective displays and temperature-sensitive devices. To enhance our comprehension of the structure-property relationships in cholesterol-based dimers incorporating azo/Schiff

base linakages, and to assess the impact of various flexible spacers on their phase behaviour, we synthesized two new series of Cholesteric-Calamitic dimers. These dimers feature cholesteryl ester along with either naphthyl azo or naphthyl azomethine moieties. The mesogenic units in these compounds are connected via ester and ether bonds, with different flexible spacers ranging in length from 1-5, 7, 9, and 10 methylene groups. The abbreviated name NpAzOH, the word "Np' denotes naphthalene moiety and Az" indicates the azo linkage. In NpAmOH, "Am" denotes azomethine linkage. ***Series VII-n*** dimers are dimers in which one end bears cholesterol group and the other end bears azonaphthyl moiety and ***Series VIII-n*** have azomethine naphthyl moiety at the other end.

5.3 Results and Discussion

5.3.1 Synthesis

The synthesis of liquid crystalline dimers from series-***VII-n*** and series-***VIII-n*** was carried out following a standardized method outlined in Scheme 1 and Scheme 2, respectively. The preparation of key intermediates including (E)-4-(naphthalen-2-yldiazenyl)phenol (***NpAzOH***) and (E)-4-((naphthalen-2-ylimino)methyl)phenol ***(NpAmOH)*** was detailed in Section 2A.5.3. Cholesteryl ω-bromoalkanoates (***ChBr-n***) (n=1-5,7,9,10) were synthesized through the esterification of ω-bromoalkanoic acid with cholesterol using Steglich esterification with a coupling reagent, typically DCC (dicyclohexylcarbodiimide) and DMAP (4-dimethylaminopyridine), under mild conditions.[44] The Williamson etherification reaction involving ***ChBr-n*** and ***NpAzOH/NpAmOH*** results in the formation of our unsymmetrical Cholesterol-Naphthalene dimers.

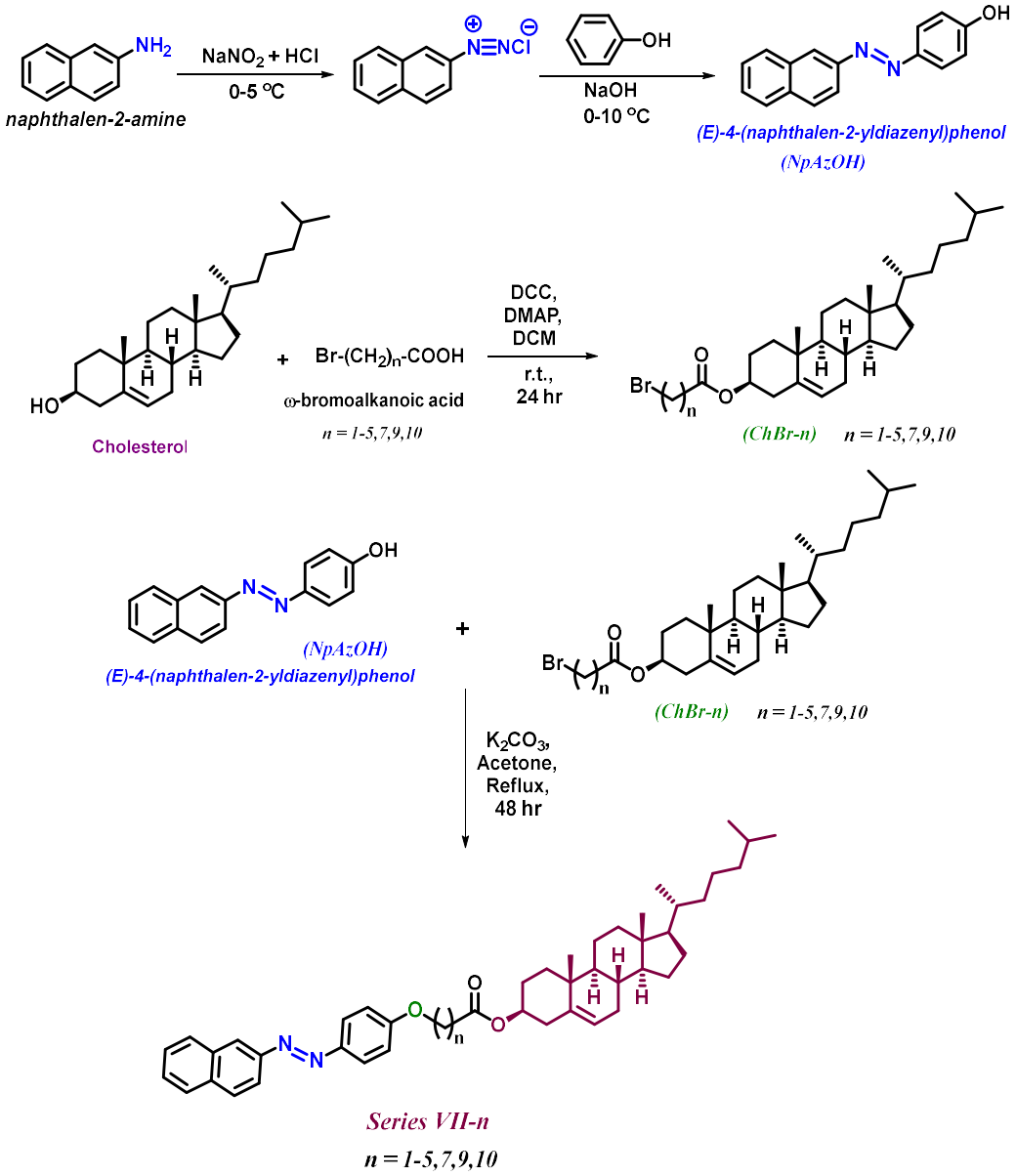

Scheme 5.1: Synthesis scheme for the dimers of series *VII-n*

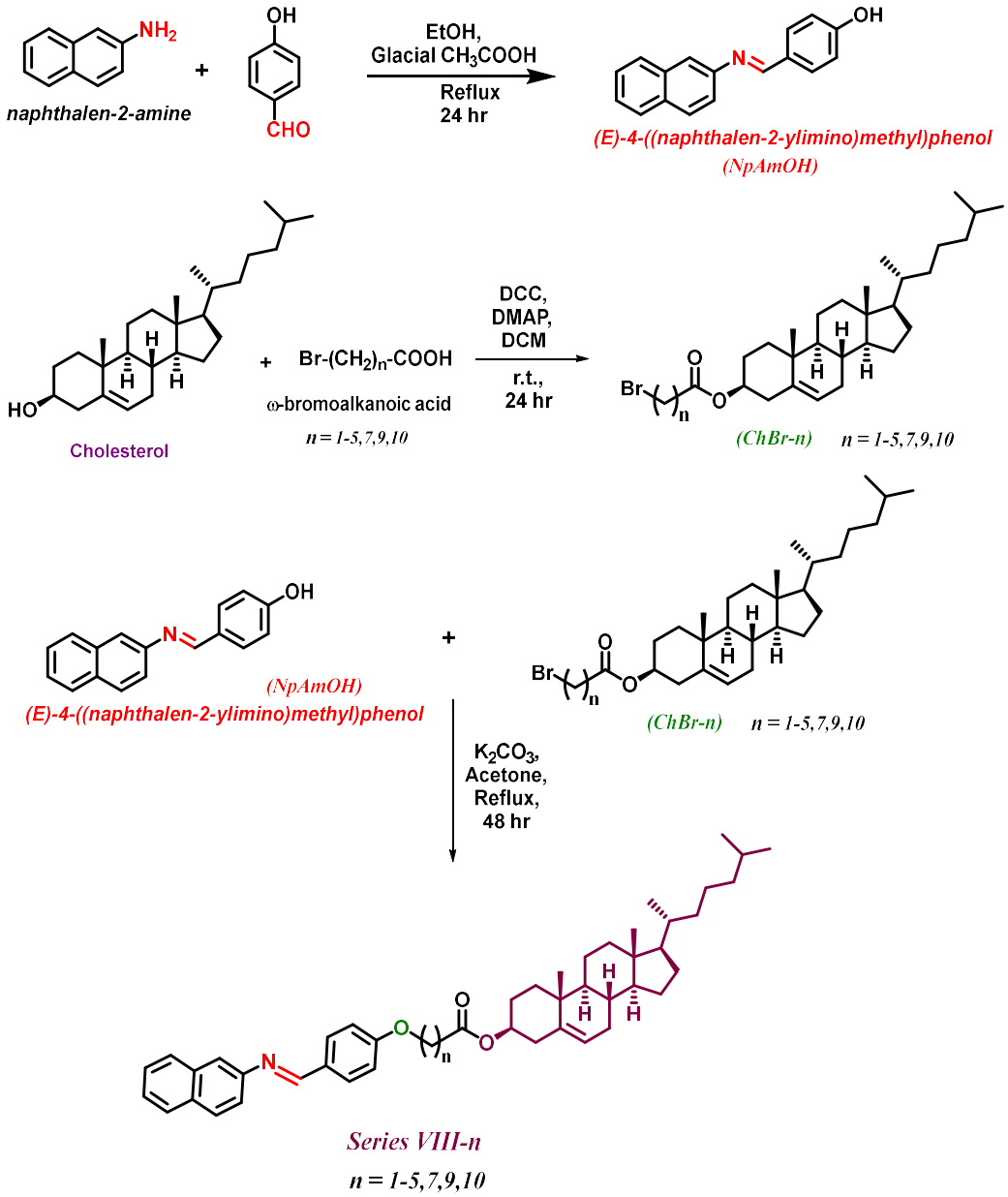

Scheme 5.2: Synthesis scheme for the dimers of series *VIII-n*

5.3.2 Chemistry

Through the use of various analytical methods, including FT-IR, ^{1}H NMR, ^{13}C NMR, mass spectrometry and elemental analysis, the correct structures of the prepared dimers were verified. The structures of ***VII-7*** and ***VIII-7*** are described in detail as representative of the series.

In the FT-IR spectra of dimer ***VII-7***, C-H stretching bands for aliphatic and aromatic C-H, appeared between 2800-3100 cm^{-1}. The C-H stretching bands of the cholesteryl groups also appeared around 2865-2944 cm^{-1}, and, azo (-N=N-) group stretching bands

at 1600–1610 cm^{-1}, and aromatic (-C=C-) stretching bands at 1553-1507 cm^{-1}, the C=O stretching bands indicating ester bonds were observed at 1725-1750 cm^{-1}, C-O stretching for ether linkages were seen around 1240-1260 cm^{-1}. Series ***VIII-n,*** featuring an imine linkage instead of azo, exhibited similar structures. In the FT-IR spectra of ***VIII-7***, imine (-CH=N-) group stretching bands were found at 1605-1595 cm^{-1}.

The ^{1}H-NMR spectra of ***VII-7*** display peaks as described here: The aromatic protons were observed between δ 8.43-6.93 ppm. The olefinic proton of cholesterol gives a triplet at δ 5.39-5.29 ppm. The cholesteric proton of the carbon attached to oxygen (COO-C<u>H</u>-) appears as a multiplet at δ 4.55-4.53 ppm. In the flexible spacer chain, the methylene protons on carbons attached to oxygen (-OCH_2) show triplets at δ 3.99-3.95 ppm, while the chain protons attached to the ester group (-CH_2-COO) exhibit a triplet at δ 2.24-2.22 ppm. Peaks for the alkyl protons (cholesterol and flexible spacer chain methylene protons) appeared around δ 0.58-2.19 ppm. For ***VIII-7***, all other signals were nearly identical. The imine proton of the Schiff base linkage was observed as a singlet at δ 8.56 ppm.

In the ^{13}C NMR spectra of ***VII-7***, signals for methylene carbons of the flexible spacer and aliphatic carbons of cholesterol were observed around δ 10-60 ppm, The ester carbonyl carbon appeared at δ 172 ppm, alkene carbons at δ 160-114 ppm, the (-O<u>C</u>H_2) group at δ 69 ppm, and the (-<u>C</u>H_2-COO) group at δ 30-40 ppm. The cholesteric carbon attached to oxygen (COO-<u>C</u>H-) appeared at δ 73 ppm. The imine carbon was observed at δ 160 ppm in ^{13}C NMR for ***VIII-7***. The mass spectrum was recorded using a Time-of-Flight Mass Spectrometer (TOF-MS) in positive ion mode. The spectrum showcases various peaks, each corresponding to different ionized fragments. The presence of a peak at m/z 758.38 for ***VII-7*** and m/z 757.28 for ***VIII-7*** as a molecular ion peak $[M+H]^+$ confirms the molecular weight of the compounds.

5.3.3 Mesomorphic Behaviour

The phase transition temperatures and mesomorphic behaviour of all the compounds were investigated using Differential Scanning Calorimetry (DSC) while the textures of mesophase were observed using Polarizing Optical Microscope (POM).

5.3.3.1 Differential scanning calorimetry study (DSC)

The thermograms were recorded utilising DSC (DSC-822, Mettler Toledo having Stare software). During both heating and cooling cycles, all phase transitions of the

compounds were monitored at a rate of 10 ºC min^{-1}. Transition temperatures (in ºC) and associated enthalpy of transition (ΔH) in (kJ mol^{-1}) of dimers ***VII-n*** are as presented in **Table 5.1** and dimers ***VIII-n*** are as presented in **Table 5.2**.

Table 5.1: Transition temperatures (in ºC) and associated enthalpy of transition (ΔH) in (kJ mol^{-1}) of *VII*-n

Dimer *VII*-n	n	Transition temperatures (°C) and ΔH (kJ mol^{-1})	
		Heating	Cooling
***VII*-1**	1	Cr 241.04 (63.11) Iso	Iso 198.02 (-57.76) Cr
***VII*-2**	2	Cr 188.54 (58.04) Iso	Iso 163.16 (-49.93) Cr
***VII*-3**	3	Cr 179.95 (57.16) N* 219.92 (3.92) Iso	Iso 214.72 (-3.67) N* 138.34 (-35.93) Cr
***VII*-4**	4	Cr 159.00 (70.84) N* 173.94 (1.44) Iso	Iso 171.93 (-1.23) N* 100.38 (-53.97) Cr
***VII*-5**	5	Cr 156.13 (36.66) N* 210.47 (3.02) Iso	Iso 207.11 (-2.77) N* 148.05[#] SmC* 98.03 (-32.08) Cr
***VII*-7**	7	Cr 130.93 (44.69) N* 181.35 (3.59) Iso	Iso 177.38 (-3.70) N* 119.36 (-0.46) SmC* 90.71 (-37.28) Cr
***VII*-9**	9	Cr 111.02 (25.74) SmC* 137.51 (0.40) N* 172.58 (2.76) Iso	Iso 168.86 (-3.01) N* 133.06 (-0.45) SmC* 94.20 (-24.86) Cr
***VII*-10**	10	Cr 126.11 (21.18) N* 147.16 (2.21) Iso	Iso 141.46 (-0.88) N* 97.52 (-21.38) Cr

SmC, Chiral smectic C; N*, Chiral Nematic; Iso, Isotropic liquid; Cr, Crystalline solid; [#] Phase change observed by POM.*

Table 5.2: Transition temperatures (in °C) and associated enthalpy of transition (ΔH) in (kJ mol^{-1}) of *VIII*-n

Dimer *VIII*-n	n	Transition temperatures (°C) and ΔH (kJ mol^{-1})	
		Heating	Cooling
***VIII*-1**	1	Cr 238.08 (56.93) Iso	Iso 203.87 (-45.14) Cr
***VIII*-2**	2	Cr 183.08 (43.78) Iso	Iso 160.87 (-39.65) Cr
***VIII*-3**	3	Cr 167.63 (38.80) N* 216.04 (3.46) Iso	Iso 212.56 (-3.18) N* 150.01 (-33.54) Cr
***VIII*-4**	4	Cr 149.14 (55.12) N* 169.52 (1.33) Iso	Iso 166.90 (-0.98) N* 83.26 (-39.93) Cr
***VIII*-5**	5	Cr 146.38 (38.27) N* 199.49 (4.29) Iso	Iso 192.33 (-2.72) N* 125.55 (-37.22) Cr
***VIII*-7**	7	Cr 130.75 (46.25) N* 182.93 (3.29) Iso	Iso 180.24 (-3.31) N* 104.14 (-0.44) SmC* 87.38 (-33.36) Cr
***VIII*-9**	9	Cr 132.51 (40.33) N* 158.68 (2.77) Iso	Iso 151.94 (-2.19) N* 101.00 (-0.52) SmC* 79.70 (-21.89) Cr
***VIII*-10**	10	Cr 116.13 (18.72) N* 142.02 (2.20) Iso	Iso 140.96 (-1.60) N* 79.25 (-18.14) Cr

SmC, Chiral smectic C; N*, Chiral Nematic; Iso, Isotropic liquid; Cr, Crystalline solid*

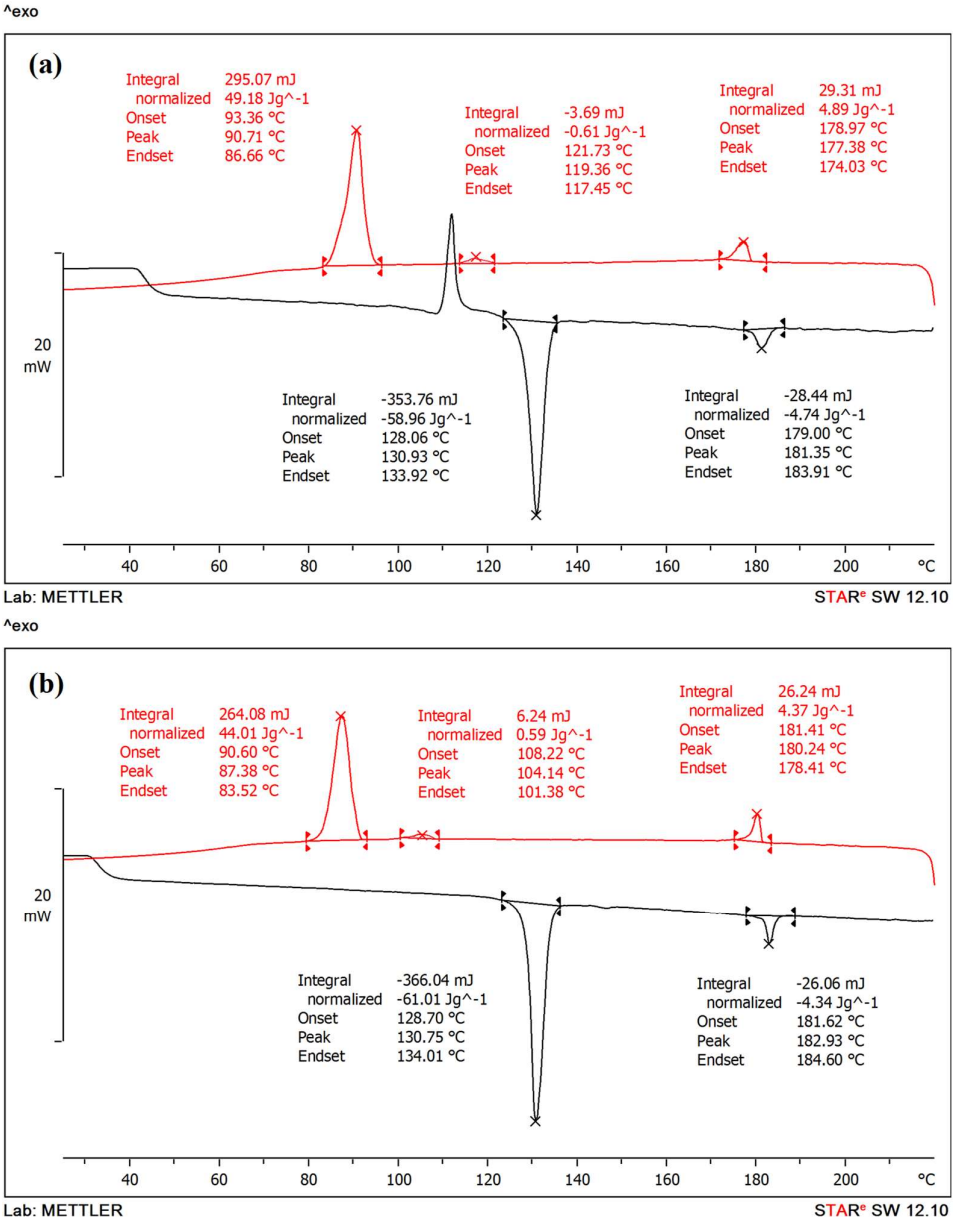

Fig. 5.3: DSC thermogram of Dimers (a) *VII-7* and (b) *VIII-7*

The Differential Scanning Calorimetry (DSC) thermogram for dimers ***VII-7*** is illustrated in **Fig. 5.3(a)**. During the heating process, the transition from crystalline (Cr) to cholesteric phase (N*) occurs at 130.93 °C, with an enthalpy change (ΔH) of 44.69 kJ mol^{-1}. Following this, the transition to the isotropic liquid state happens at 181.35 °C accompanied by an enthalpy change of 3.59 kJ mol^{-1}. Notably, the cooling scan reveals a reversible transition phenomenon, indicating the presence of an additional SmC* phase. Dimer ***VII-7*** have shown three exothermic transitions (Iso-to-N*, N*-to-SmC*

and SmC*-to-Cr) in cooling cycle at 177.38 °C (ΔH= 3.70 kJ mol^{-1}), 119.36 °C (ΔH= 0.46 kJ mol^{-1}) and 90.71 °C (ΔH= 37.28 kJ mol^{-1}) respectively.

Dimers ***VIII-7*** exhibit both enantiotropic chiral nematic (N*) and monotropic SmC* mesophases. Upon heating, it undergoes endothermic transitions, Cr-to-N* and N*-to-Iso at 130.75 °C (ΔH= 46.25 kJ mol^{-1}) and 182.93 °C (ΔH= 3.29 kJ mol^{-1}). During the cooling cycle, three exothermic peaks are observed: at 180.24 °C (ΔH= 3.31 kJ mol^{-1}), at 104.14 (ΔH= 0.44 kJ mol^{-1}) and at 87.38 °C (ΔH= 33.36 kJ mol^{-1}) for Iso-to-N*, N*-to-SmC* and SmC*-to-Cr transitions respectively (**Fig. 5.3b**).

5.3.3.2 Polarising Optical Microscopy (POM)

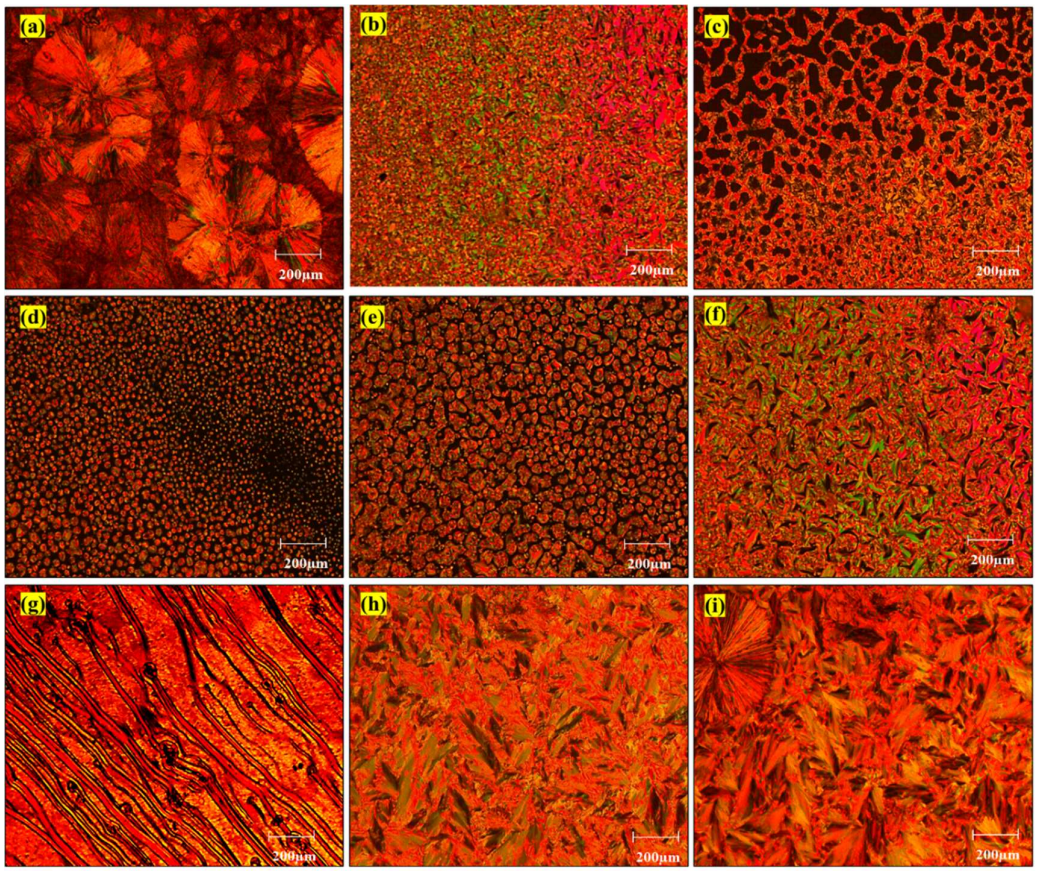

Fig. 5.4: Optical microphotographs of dimer *VII-7* (a) Crystalline state at 141 °C, (b) N* phase (at 143 °C) during heating, (c) N*-Iso transition at 186 °C, (d) chiral nematic droplets at 184 °C upon cooling, (e) coalescence of droplets, (f) Pseudofocal conic texture for N* at 183 °C (g) oily streak of sheared N* phase at 181 °C (h) SmC* at 117 °C (i) SmC*-Cr transition at 89 °C.

The optical microphotographs of dimer ***VII-7*** reveal a series of distinct textures associated with various phase transitions during heating and cooling. At 141 °C, the material exhibits a crystalline state (**Fig. 5.4a**). As the temperature increases to 143 °C, a pseudo focal-conic texture characteristic of the cholesteric (N*) phase appears (**Fig. 5.4b**). Further heating to 186 °C induces the N*-Iso transition (**Fig. 5.4c**). Upon cooling from the isotropic phase, elliptical-shaped chiral nematic droplets emerge at 184 °C (**Fig. 5.4d**), which subsequently coalesce to form a fan-like texture at 183 °C (**Fig. 5.4e, f**), typical of the cholesteric phase. At 181 °C, the sheared N* phase exhibits an oily streak pattern (**Fig. 5.4g**). As cooling continues, a broken focal-conic texture with chiral lines indicative of the SmC* phase is observed at 117 °C (**Fig. 5.4h**), followed by the SmC*-Cr transition at 89 °C (**Fig. 5.4i**). These observations align well with the reported textures for cholesteric and smectic phases.

Other dimers in both series exhibited a high-temperature cholesteric (N*) phase. This phase was identified by the appearance of an oily streak texture upon heating and a focal conic fan texture upon cooling, which closely resembles the SmA mesophase. However, upon mechanical shearing, it transforms into the distinct Grandjean planar texture characteristic of the N* phase under crossed polarizers. The pitch of the cholesteric phase is highly temperature-dependent, leading to the selective reflection phenomenon. As a result, different colours in the visible spectrum are reflected in the cholesteric mesophase as the temperature decreases.

The optical microphotographs of dimer ***VIII-7*** reveal a series of phase transitions, each exhibiting distinct textures, showing a behaviour very similar to that of dimer ***VII-7***. At 130 °C, the dimer is in its crystalline state (**Fig. 5.5a**). When heated to 133 °C, a pseudo focal-conic texture appears, confirms the presence of the cholesteric phase (**Fig. 5.5b**). This phase transitions to the isotropic liquid at 187 °C (**Fig. 5.5c**). As the temperature decreases, elliptical-shaped chiral nematic droplets form at 186 °C (**Fig. 5.5d**), which then develop into a pseudo focal-conic texture at 185 °C (**Fig. 5.5e**) for N*. Further cooling results in an oily streak pattern in the sheared N* phase at 181 °C (**Fig. 5.5f**). The N* at 104 °C (**Fig. 5.5g**), followed by a broken focal-conic texture of the SmC* phase with chiral lines at 102 °C, characteristic of the SmC* phase (**Fig. 5.5h**). Finally, the SmC* phase transitions to the crystalline state at 91 °C (**Fig. 5.5i**).

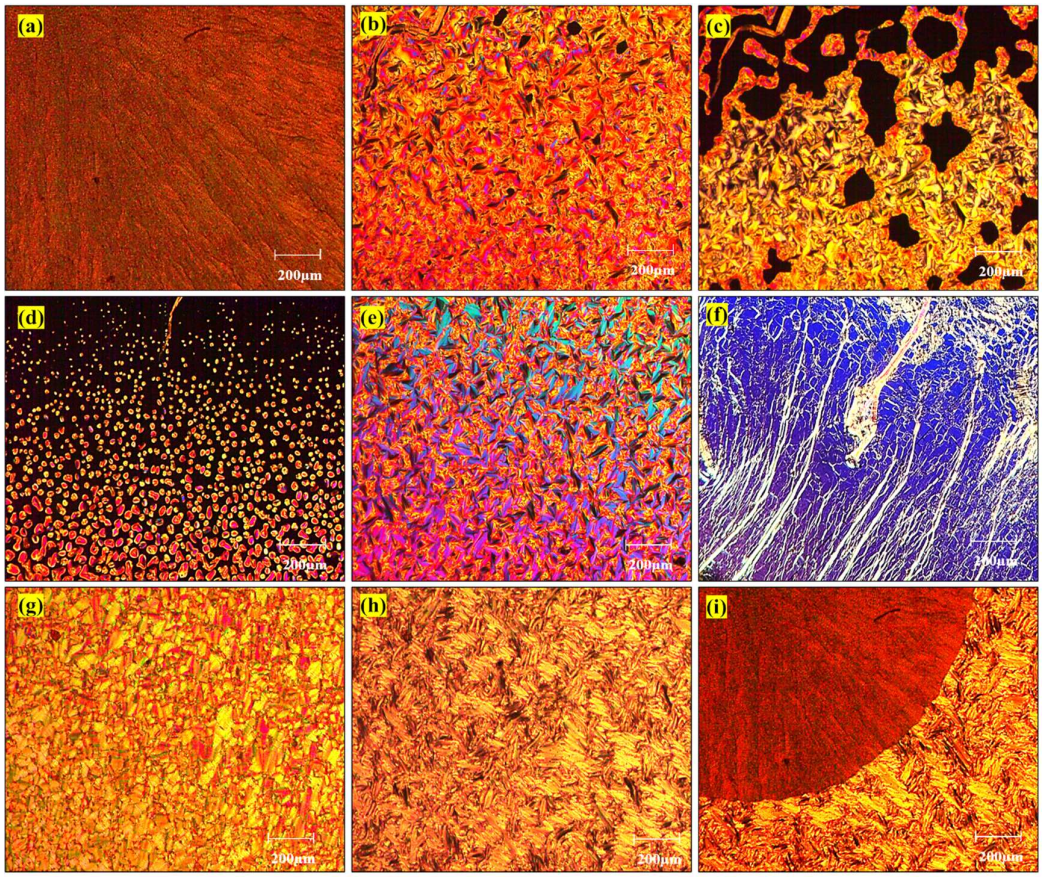

Fig. 5.5: Optical microphotographs of dimer *VIII-7* (a) Crystalline state at 130 °C, (b) N* phase (at 133 °C) during heating, (c) N*-Iso transition at 187 °C, (d) chiral nematic droplets upon cooling at 186 °C, (e) N* phase at 185 °C, (f) N* phase on shear at 181 °C (g) N* phase at 104 °C (h) SmC* at 102 °C (i) SmC*-Cr transition at 91 °C.

The optical microphotographs in **Fig. 5.6** display various textures of different dimers observed under POM. The images capture several characteristic textures of the N* and SmC* phases. For dimer ***VIII-4***, a pseudo focal-conic texture of the N* phase appeared at 133 °C (**Fig. 5.6a**). Dimer ***VIII-5*** exhibits a similar pseudo focal-conic texture at 240 °C (**Fig. 5.6b**) and an oily streak pattern indicative of a sheared N* phase (**Fig. 5.6c**). The same pseudo focal-conic texture is observed for dimer ***VIII-9*** at 240 °C (**Fig. 5.6d**), accompanied by an oily streak pattern of the sheared N* phase (**Fig. 5.6e**). For dimer ***VII-4***, the N* phase is also seen at 240 °C (**Fig. 5.6f**). Dimer ***VII-9*** shows a pseudo focal-conic texture at 133 °C (**Fig. 5.6g**) and an oily streak pattern of the sheared N* phase (**Fig. 5.6h**). Additionally, dimer ***VII-9*** demonstrates a broken focal-conic texture

characteristic of the SmC* phase at 102 °C (**Fig. 5.6i**). These observations highlight the diverse textural manifestations of the N* and SmC* phases across different dimers.

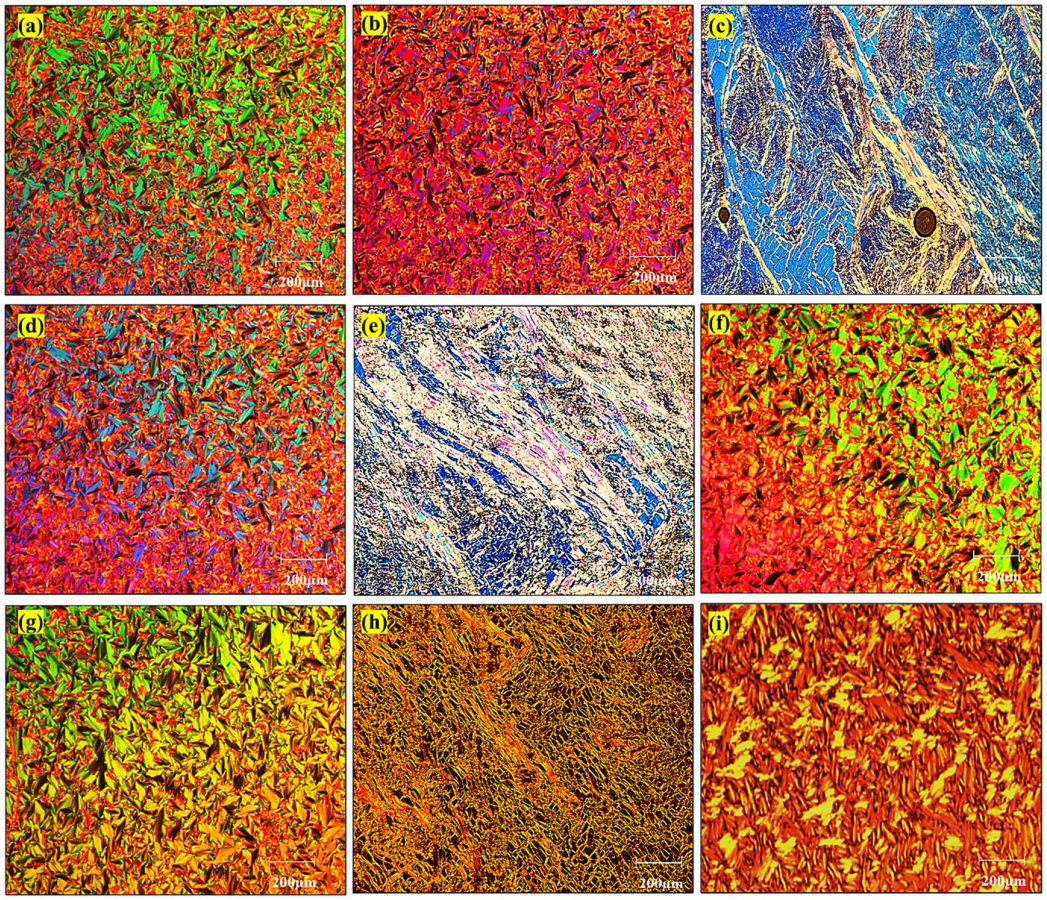

Fig. 5.6: Optical microphotographs of the textures for the LC phases of dimers: (a) Pseudo focal-conic texture of the N* phase (at 133 °C) for *VIII-4* (b) pseudo focal-conic texture of the N* phase of *VIII-5* (T = 240°C) (c) planar texture with oily streaks- N* phase for *VIII-5* (d) N* phase of *VIII-9* (T = 240°C) (e) sheared N* phase for *VIII-9* (f) N* for *VII-4* (T = 240°C) (g) N* phase (at 133 °C) for *VII-9 (h)* sheared N* phase for *VII-9* (i) SmC* at 102 °C for *VII-9*

5.3.3.3 Variable temperature X-ray diffraction (VT-XRD):

Variable temperature X-ray diffraction (VT-XRD) studies were carried out on the ***VII-9*** dimer to explore the cholesteric (N*) to smectic phase transition. (**Fig. 5.7**) The sample was filled in Lindemann capillaries (0.7 mm diameter) by melting and then the sample was heated to 150 °C and given 45min exposure. The sample was then heated

further to the isotropic phase at 180 °C. During the cooling process, diffraction scans were recorded at 155 °C, 115 °C, and 110 °C.

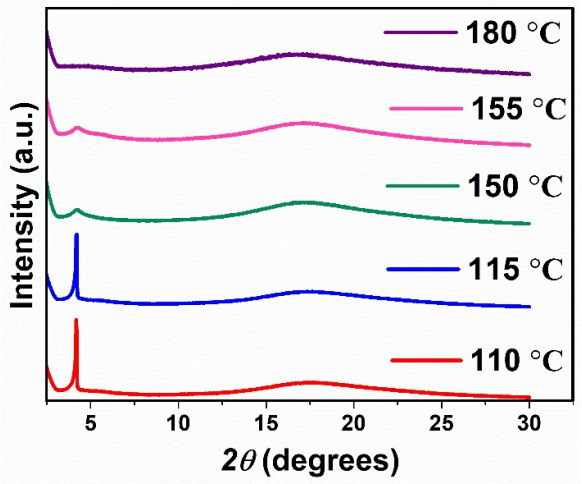

Fig. 5.7: X-ray diffraction spectra of *VII-9* at different temperatures showing the transition from N* to SmC* phase.

At 155°C, a broad, diffused peak appeared in the small-angle region, alongside a very broad halo in the wide-angle region, which is characteristic of the cholesteric (N*) phase found in sterol derivatives.[45] As the temperature was lowered to 115 °C and 110 °C, the small-angle diffraction peak became sharper, indicating a gradual transition to a smectic-like molecular arrangement. This sharpening of the peak reflects the enhanced molecular ordering characteristic of the smectic phase. The diffraction patterns confirmed the coexistence of cholesteric and smectic phases in the ***VII-9*** dimer, which was further corroborated by optical analysis under crossed polarizers.

5.3.3.4 Structure-property relationship

Cholesterol has a tetracyclic ring system with a hydroxyl group on the one ring and a side chain on the other ring. This structure imparts rigidity through the tetracyclic ring and flexibility through the functionalization of the hydroxyl group with flexible tails, facilitating their organization into liquid crystalline forms. In addition to that, azo/azomethine naphthalenes contribute rigidity to the dimeric structure, while various flexible spacers provide flexibility to these dimers.

Graphical illustration can show how factors such as spacer chain length and odd-even effects influence clearing temperatures and phase behaviour. The x-axis of the graph represents the number of carbons in the flexible spacer chain (n), while the y-axis shows the transition temperatures (°C). Each point on the graph represents a specific dimer,

with its transition temperature plotted against its spacer chain length. (**Fig. 5.8**) Generally, as the number of carbons in the flexible spacer chain increases, clearing temperatures tend to decrease. This trend is due to the increased flexibility and reduced intermolecular forces associated with longer spacer chains.

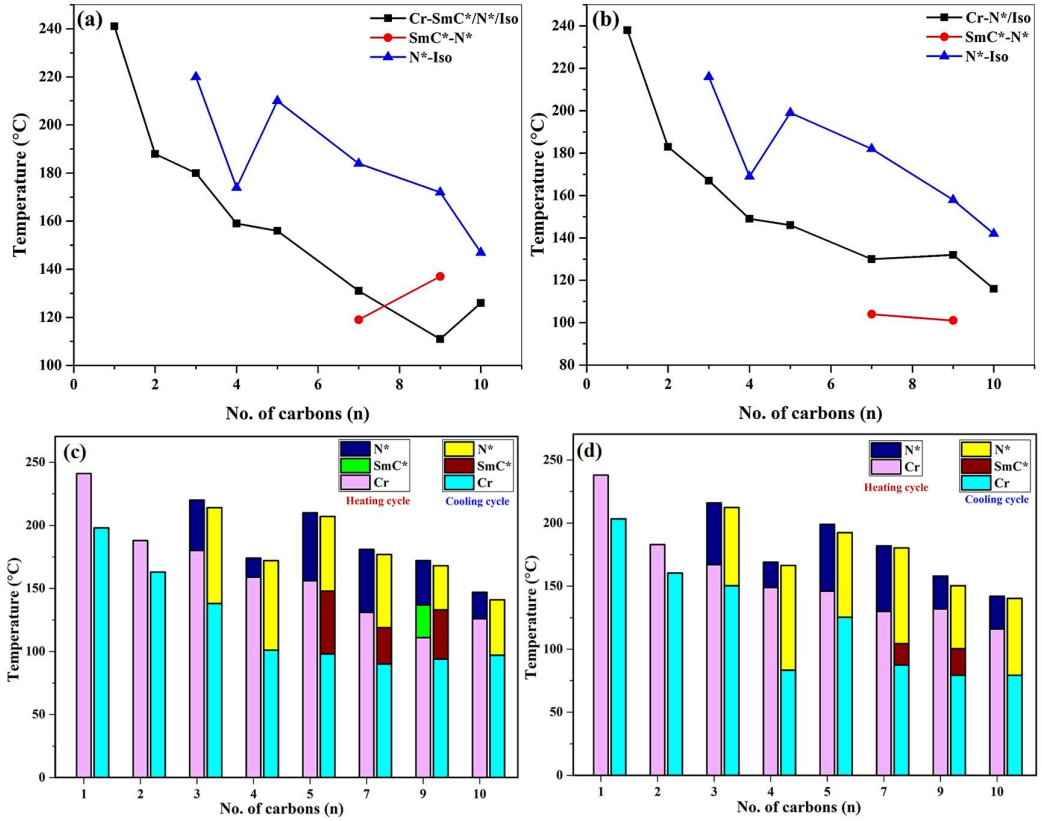

Fig. 5.8: Line graph of the transition temperature vs. no. of carbons in flexible spacer for dimers of *Series* (a) *VII-n and* (b) *VIII-n*. Bar graph showing mesophase stability for dimers of *Series* (c) *VII-n* and (d) *VI-n*

The structure-property relationship in this series reveals that the molecular arrangement and phase behaviour are influenced by the length and type of spacers. The first two members (n=1,2) of each series do not exhibit mesogenic properties due to their short, flexible spacers. Members with n=3−5,7,9,10 demonstrate enantiotropic chiral nematic phases, indicative of their ability to form aligned liquid crystalline phases with thermal reversibility. Notably, higher members with odd spacers (n=5,7,9) show SmC* phases, suggesting that the increased length and odd number of methylene spacers enhance the molecular interactions necessary for chiral smectic C phases. The line graph analysis shows a distinct difference in phase behaviour between dimer ***VII-9*** and ***VIII-9***, where ***VII-9*** only exhibits an enantiotropic smectic phase, while ***VIII-9*** shows a monotropic

smectic phase. This variance could be due to the slightly nonplanar arrangement of the azomethine naphthalene, affecting the packing and stability of the smectic phases. Furthermore, the presence of smectic phases in the higher members is attributed to the longer chain lengths, which facilitate the formation of layered structures, enhancing the stability and manifestation of smectic phases. This structural attribute underscores the crucial role of chain length in determining the liquid crystalline properties of the series. Although ***VII-10*** and ***VIII-10*** do not exhibit the SmC* phase, this can be attributed to the fact that they are odd-membered dimers. The odd-membered structure disrupts the linearity required for a more ordered arrangement, such as in the smectic phase. **Fig. 5.8 (c** and **d)** clearly demonstrates that the mesophase stability of the dimers is more pronounced during the cooling cycle compared to the heating cycle, indicating that the ordered phases are more persistent upon cooling. Dimers in series ***VII-n*** exhibit slightly higher thermal stability, indicated by higher clearing temperatures ($T_{Cr/N-Iso}$), compared to those in series ***VIII-n.***

5.3.4 Thermogravimetric analysis (TGA)

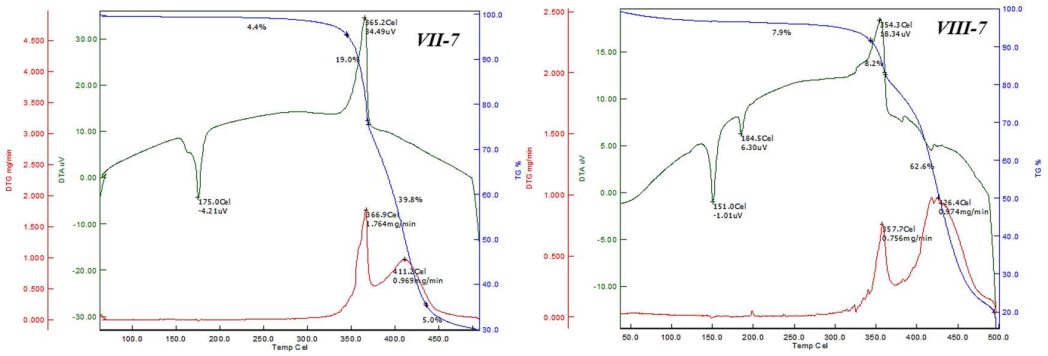

Fig. 5.9: TGA graph for *VII-7* and *VIII-7*

The TGA analysis reveals a substantial mass loss at 365 °C for ***VII-7*** and at 354 °C for ***VIII-7***, indicating the main thermal decomposition of the compound. (**Fig. 5.9**) This is further corroborated by the DTG curve, which shows a peak corresponding to this decomposition.

5.3.5 Photochromic behaviour

Photoisomerization, driven by the π-π* transition, allows cis-trans isomer conversion, making azobenzene a dynamic compound. Experiments using a dual beam spectrophotometer with a 1 cm quartz cuvette and a 365 nm filter showed the UV-Visible spectra of the ***VII-7***. The strong peak at 350 nm was identified as the π-π*

transition for the trans isomer and the n-π* transition indicated by the peak at 440 nm. **Fig. 5.10(a)** depicts the UV-vis spectra for ***VII-7*** under various UV exposure times, showing a decrease in the absorption maxima at 350 nm, followed by a slight increase at 440 nm. It was observed that approximately 3 minutes were required to reach a photostationary state.

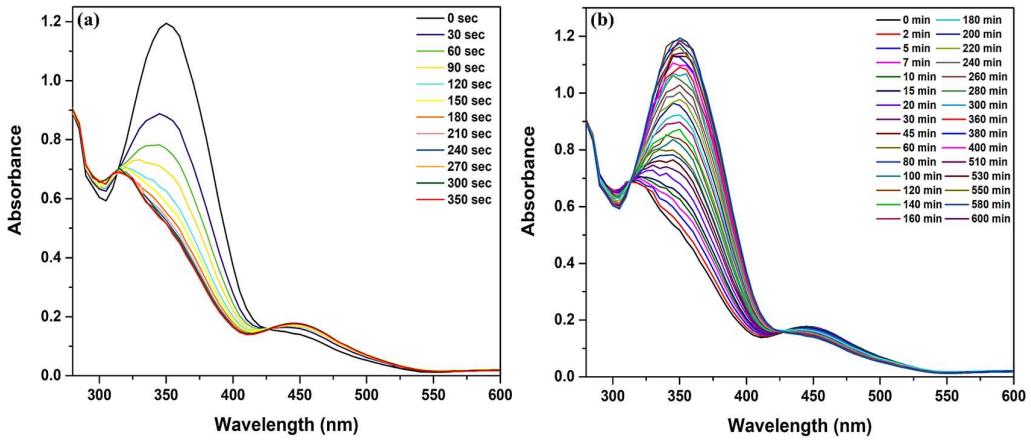

Fig. 5.10: Absorption spectra of VII-7 (a) at different UV exposure times (b) Thermal back relaxation

The photo conversion efficiency (CE) of the trans-cis isomerization was calculated using the formula $[\boldsymbol{CE = (A_{t_0} - A_{t_\infty}) \,/\, A_{t_0} \times 100\%}]$**.** With the absorbance values before UV exposure ($\boldsymbol{A_{t_0}}$) being 1.19459 and after UV exposure ($\boldsymbol{A_{t_\infty}}$) being 0.51654, the CE for ***VII-7*** was determined to be 56.7%. **Fig. 5.10(b)** illustrates the thermal back relaxation process. After reaching a photostationary state, the compound was kept in the dark, and absorbance was measured until complete conversion to the trans form was achieved. Two isosbestic points confirmed the absence of side reactions. The reverse isomerization took approximately 10 hours to revert to the stable trans configuration. The plot (**Fig. 5.11**) illustrates absorbance of ***VII-7*** during UV illumination, and the subsequent back relaxation as a function of time.

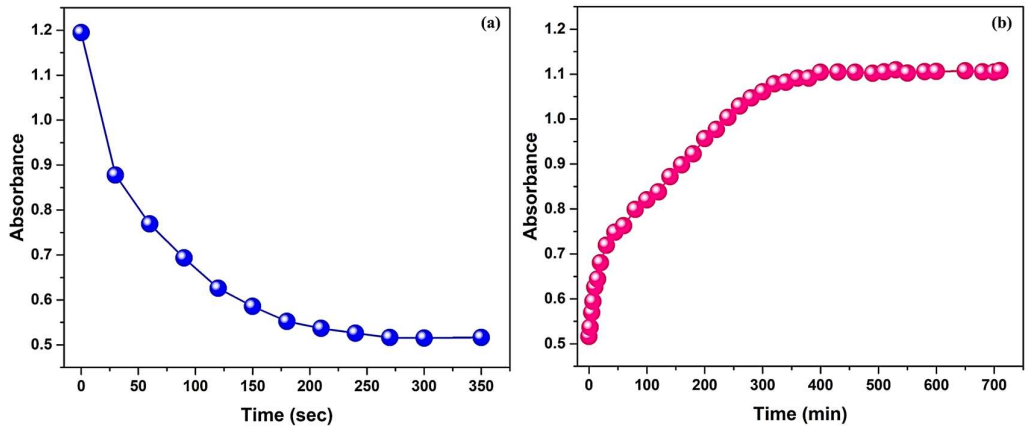

Fig. 5.11: Plot of VII-7 as a function of time: (a) during UV illumination showing the trans-cis isomerization process, and (b) back relaxation

We conducted studies on all dimers of series VII-n, recording the absorption spectra under three conditions: without UV radiation, after exposure to short UV (254 nm), and after exposure to long UV (365 nm). **Fig. 5.12** displays the absorption spectra for the VII-n series under these conditions.

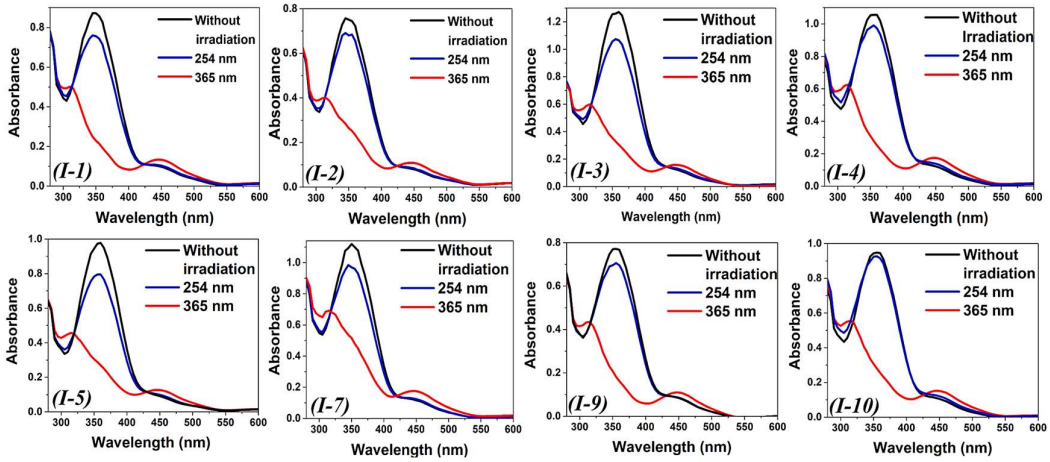

Fig. 5.12: **Absorption spectra for series VII-n under different conditions: without UV radiation, after exposure to short UV (254 nm), and after exposure to long UV (365 nm).**

5.3.6. Computational studies

In our study, we used Density Functional Theory (DFT) with Becke's three-parameter hybrid functional (B3LYP) and the 6-31G basis set. The theoretical calculations were performed using Gaussian 09 software to analyse molecular properties, including optimized structures and vibrational frequencies. We started by optimizing the energy

of different conformations to find the minimum-energy geometrical structure. This optimized structure was then used to calculate frequencies and thermodynamic properties. We use a consistent colour scheme to depict molecular structures: carbon atoms are shown in grey, nitrogen in blue, oxygen in red, and hydrogen in white. These atoms are connected by sigma and pi bonds, creating the complex three-dimensional arrangements of the molecules we are studying. For visualization, **Fig. 5.13** presents the optimized molecular structures for dimers from both series, offering valuable insights into their structural characteristics as determined through our DFT-based computational approach.

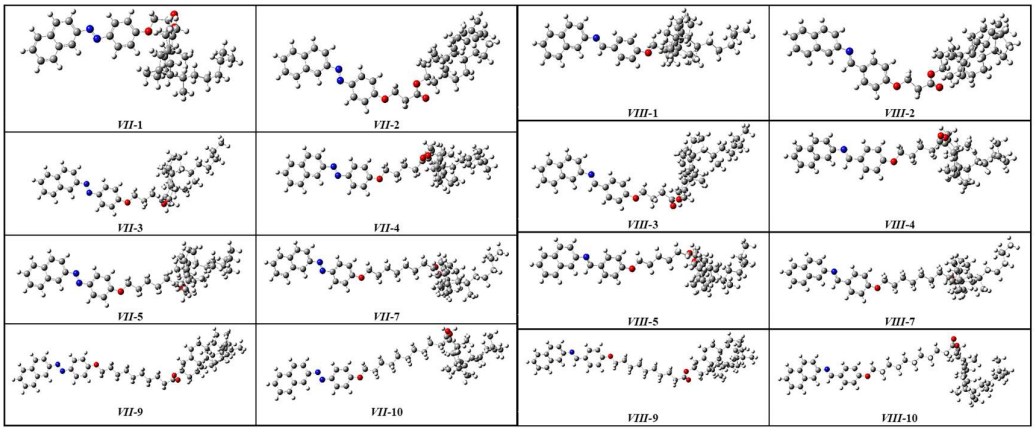

Fig. 5.13: Optimized molecular structures of dimers of *Series VII-n* and *VIII-n*

Quantum mechanical descriptors are crucial in Density Functional Theory (DFT) studies for predicting and understanding chemical behaviour. Global hardness (η) measures a molecule's resistance to deformation or charge transfer, while global softness (δ) is its inverse, indicating the ease of electron redistribution. Chemical reactivity (χ) reflects a molecule's tendency to gain or lose electrons, and the electrophilicity index (ω) quantifies a molecule's ability to accept electrons. Together, these descriptors provide insights into molecular stability, reactivity, and interaction tendencies, aiding in the design and analysis of chemical systems. However, in the both present series, there is no significant change in these parameters.

5.3.6.1 Frontier molecular orbitals (FMOs) and Molecular electrostatic potential (MEP)

An accurate description of the highest occupied molecular orbital (HOMO) and the lowest unoccupied molecular orbital (LUMO), including their atomic orbital composition, absolute energies, and relative energy gaps, provides crucial insights into

the photophysical properties of molecules. The HOMO and LUMO energies, which are presented in **Table 5.3**, are complemented by 3D iso-surface plots shown in **Fig. 5.14**.

Table 5.3: Quantum mechanical descriptors

Dimer	*HOMO*	*LUMO*	*I* (eV)	*A* (eV)	*ΔE* (eV)	*η*	*δ*	*χ*	*ω*
***VII*-1**	-0.201	-0.084	5.587	2.164	3.422	1.711	0.584	3.876	4.389
***VII*-2**	-0.204	-0.078	5.558	2.137	3.421	1.710	0.585	3.848	4.328
***VII*-3**	-0.205	-0.080	5.587	2.164	3.422	1.711	0.584	3.876	4.389
***VII*-4**	-0.204	-0.079	5.558	2.137	3.421	1.710	0.585	3.848	4.328
***VII*-5**	-0.204	-0.078	5.549	2.131	3.418	1.709	0.585	3.840	4.315
***VII*-7**	-0.207	-0.082	5.621	2.221	3.400	1.700	0.588	3.921	4.522
***VII*-9**	-0.202	-0.076	5.507	2.077	3.431	1.715	0.583	3.792	4.191
***VII*-10**	-0.203	-0.077	5.517	2.101	3.416	1.708	0.586	3.809	4.248
***VIII*-1**	-0.205	-0.06	5.481	1.508	3.973	1.986	0.503	3.494	3.073
***VIII*-2**	-0.200	-0.054	5.457	1.480	3.977	1.988	0.503	3.469	3.026
***VIII*-3**	-0.201	-0.055	5.481	1.508	3.973	1.986	0.503	3.494	3.073
***VIII*-4**	-0.201	-0.054	5.457	1.480	3.977	1.988	0.503	3.469	3.026
***VIII*-5**	-0.200	-0.054	5.453	1.473	3.979	1.990	0.503	3.463	3.014
***VIII*-7**	-0.200	-0.054	5.438	1.457	3.981	1.990	0.502	3.447	2.986
***VIII*-9**	-0.199	-0.052	5.418	1.422	3.997	1.998	0.500	3.420	2.926
***VIII*-10**	-0.199	-0.053	5.423	1.441	3.983	1.991	0.502	3.432	2.957

I, Ionization Potential; *A*, Electron Affinity; *ΔE*, Energy gap; *η*, Global hardness; *δ*, Global softness; *χ*, Chemical reactivity; *ω*, Electrophilicity index;

The energy gap between HOMO and LUMO serves as an indicator of a molecule's kinetic stability and its reactivity pattern. A larger HOMO-LUMO gap suggests higher kinetic stability and lower chemical reactivity because it becomes energetically unfavourable to add electrons to a high-lying LUMO or to remove electrons from a low-lying HOMO. In this study, the HOMO-LUMO energy gaps for the molecules in series *VII-n* range from 3.40 to 3.43 eV, while those in series *VIII-n* range from 3.97 to 3.99 eV, indicating that these dimers are relatively stable. Additionally, the electron density in the HOMO and LUMO is predominantly localized in the aromatic regions of the molecules.

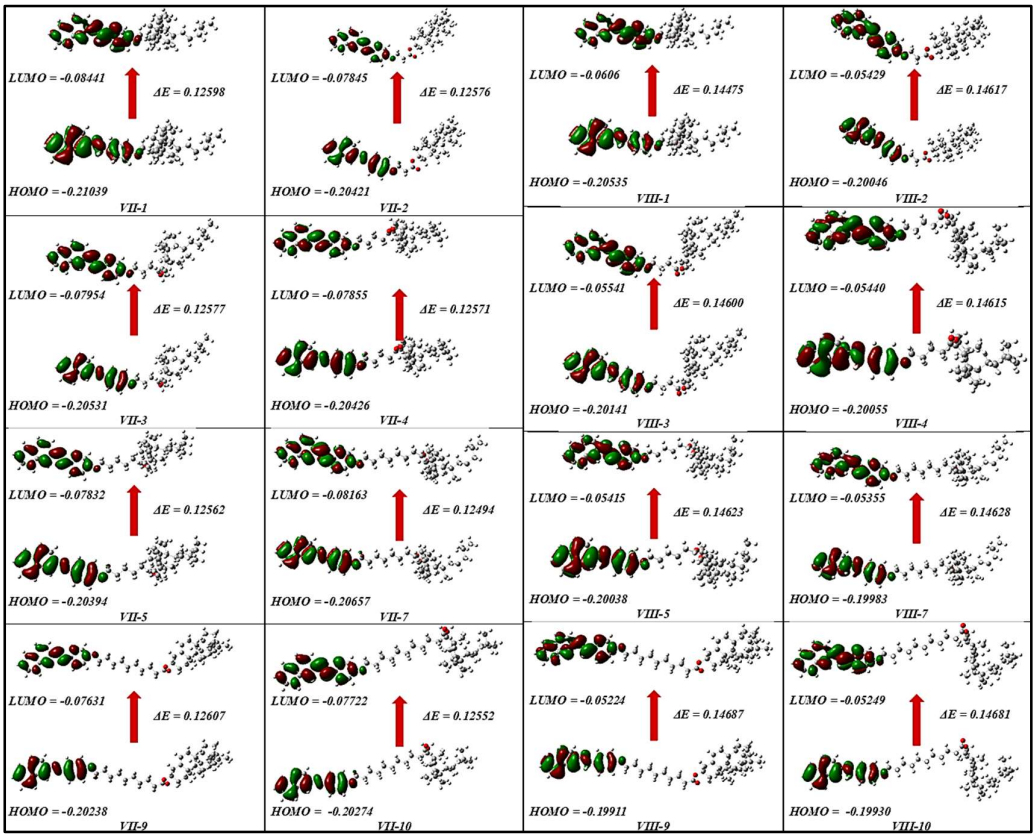

Fig. 5.14: FMOs for the dimers of *Series VII-n* and *V-III-n* (Values of HOMO, LUMO and ΔE are in a.u.)

Fig. 5.15 shows the molecular electrostatic potential (MEP) contours of the dimers from Series ***VII-n*** and ***VIII-n***. The negative electrostatic potential (ESP) is observed on the oxygen atoms, particularly on the ester carbonyl and phenolic oxygen atoms, as indicated by the red contour in the electrostatic potential map. Additionally, a slight negative ESP is present on the nitrogen atoms of the azo and azomethine linkages. The positive ESP on the cholesteryl moiety, phenyl rings, and alkyl chains indicates regions of electron deficiency (mostly in blue colour regions), which can interact with the negatively charged areas, promoting the formation of ordered structures. This balance of positive and negative ESP regions is crucial for the self-assembly and mesophase formation in liquid crystal materials, potentially improving their electro-optical properties and making them suitable for advanced applications in display technologies.

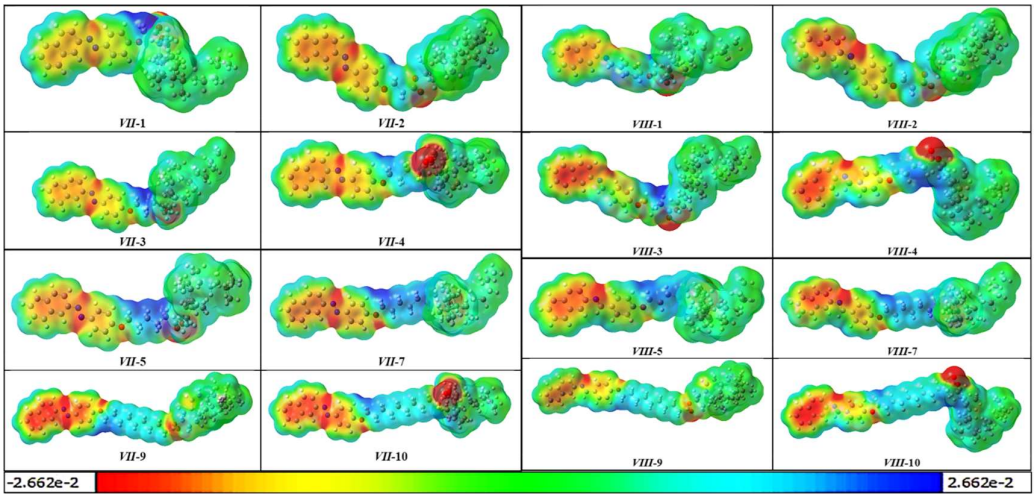

Fig. 5.15: MEP contours of the dimers of *Series VII-n* and *VIII-n*

5.3.6.2 Vibrational studies

The vibrational frequencies calculated for the compounds were compared with the experimental values from FT-IR spectra, revealing a strong correlation that validates the DFT calculations' accuracy. The geometries were further validated through vibrational frequency analysis, which indicated the absence of any imaginary frequencies. **Fig. 5.16** illustrates the comparison between experimental vibrational frequencies and those calculated at the B3LYP/6-31G level for the dimers ***VII-7*** and ***VIII-7.***

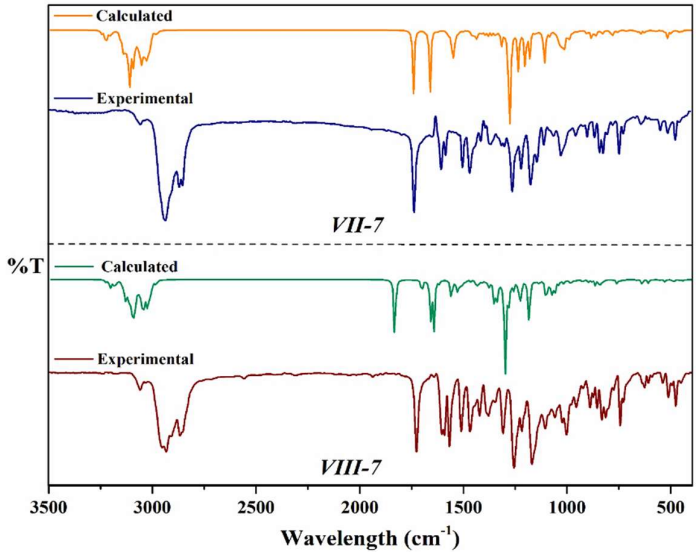

Fig. 5.16: Comparison of the vibrational frequency obtained from the experiment and calculated at B3LYP-6-31G level theory (gas phase) for dimers *VII-7* and *VIII-7*

The comparison of theoretical and experimental IR spectra for the vibrational modes of phenyl and naphthalene rings, along with other functional groups, indicates a high degree of correlation, confirming the reliability of the theoretical calculations. In the experimental FT-IR spectra of dimer ***VII-7***, the observed C-H stretching bands for alkyl and benzylic groups (2800-3100 cm^{-1}) and C-H stretching bands of cholesteryl groups (2865-2944 cm^{-1}) showed good agreement with the theoretical C-H stretching vibrations (3000-2800 cm^{-1}). Additionally, both out-of-plane and in-plane C-H bending vibrations (850-700 cm^{-1}) were consistent between theoretical predictions and experimental observations. The experimental spectra exhibited N=N group stretching bands (1600-1610 cm^{-1}) and aromatic C=C stretching bands (1553-1507 cm^{-1}), which matched well with the theoretical C=C stretching vibrations (1570-1500 cm^{-1}) and N=N double bond vibrations at 1600 cm^{-1}. Furthermore, C=O stretching bands for ester bonds (1725-1750 cm^{-1}) and C-O stretching bands for ether linkages (1240-1260 cm^{-1}) aligned with theoretical predictions. Similarly, the FT-IR spectra of dimer ***VIII-7***, which features an imine linkage instead of an azo group, revealed imine (-CH=N-) group stretching bands at 1605-1595 cm^{-1}, which appeared around 1600 cm^{-1} in theoretical calculations.

5.4 Conclusion

This chapter involves the synthesis and characterization of two novel series of cholesterol-based unsymmetrical liquid crystalline dimers, incorporating either naphthyl azo or naphthyl azomethine moieties. Differential Scanning Calorimetry and Polarizing Optical Microscopy were used to investigate phase transition temperatures and mesomorphic behaviour. The study revealed that spacer chain length significantly impacts these properties. Dimers with shorter spacers (n=1, 2) did not exhibit mesogenic properties, while those with longer spacers (n=3–5, 7, 9, 10) displayed enantiotropic chiral nematic phases and, in some cases, smectic phases. UV-visible spectroscopy studies indicated efficient trans-cis isomerization, with a photo conversion efficiency (CE) of 56.7% for the ***VII-7*** dimer. Density Functional Theory (DFT) calculations provided insights into the optimized molecular structures and vibrational frequencies. Overall, the findings underscore the crucial role of spacer chain length and molecular rigidity in determining the liquid crystalline properties of these cholesterol-based dimers.

5.5 Experimental Section

5.5.1 Materials

All the starting materials and reagents were purchased from (S.R.L. Chemicals, Mumbai) and used without further purification. Solvents like acetone, ethyl acetate and petroleum ether (60-80) were de-moisturized and purified before use.

5.5.2. Measurements

The instruments used are the same as in section **2A.5.2.** X-ray diffraction (XRD) measurements on powder samples were carried out using PANalytical, Empyrean diffractometer using Cu-Kα (λ = 1.54 Å) beam. The sample was filled in Lindemann capillaries (0.7 mm diameter).

5.5.3. Synthesis and Characterization

5.5.3.1 Cholesteryl-ω-(4-((E)-naphthalen-2-yldiazenyl)phenoxy)alkanoate

5.5.3.1.1 (E)-4-(naphthalen-2-yldiazenyl)phenol (NpAzOH)

The synthesis of (E)-4-(naphthalen-2-yldiazenyl)phenol (NpAzOH) is described in Chapter 2, Section 2A.5.3.1.

5.5.3.1.2 Cholesteryl ω-bromoalkanoates (ChBr-n)

A mixture of ω-bromo alkanoic acid (1) (2.58 mmol, 1 equivalent), cholesterol (2.58 mmol, 1 equivalent), and DMAP (0.12 mmol, 0.05 equivalent) in DCM was stirred vigorously. A solution of DCC in dry DCM was added at ice-cold conditions, and the mixture was stirred at room temperature for 24 hours. The resulting white precipitate of N, N'-Dicyclohexylurea was filtered off through a celite and neutral alumina mixture. The filtrate was diluted with DCM and washed with 0.5N HCl, 10% Na_2CO_3 solution, brine, and water. It was then dried over anhydrous Na_2SO_4. The crude product was purified through column chromatography and recrystallized from hexane to obtain a white solid. All the ChBr-n were synthesized and confirmed with the reported literature.[44]

5.5.3.1.3 Synthesis of Cholesteryl-ω-(4-((E)-naphthalen-2-yldiazenyl)phenoxy) alkanoate (VII-n)

In a round bottom flask with a reflux system and stirring for 15 minutes, (E)-4-(naphthalen-2-yldiazenyl) phenol (**NpAzOH**) (0.52 mmol) and **ChBr-n** (0.5 mmol) were dissolved in acetone. Additions of anhydrous K_2CO_3 (2.17 g, 15.7 mmol) and a

catalytic amount of KI were added to the reaction mixture, and the system was refluxed for about 48 h (monitored by TLC). The hot solution was filtered and washed with acetone after the reaction was finished. The filtrate was then collected and evaporated in a rotary evaporator. Cold petroleum ether was added to the concentrated extracts, and the resulting precipitate was filtered and washed two times with this same solvent. Column chromatography is used to purify the resulting compound. (96:4 pet ether: ethyl acetate)

5.5.3.1.4 Characterization of dimers VII-n

Cholesteryl 2-(4-((E)-naphthalen-2-yldiazenyl)phenoxy)acetate (VII-1):

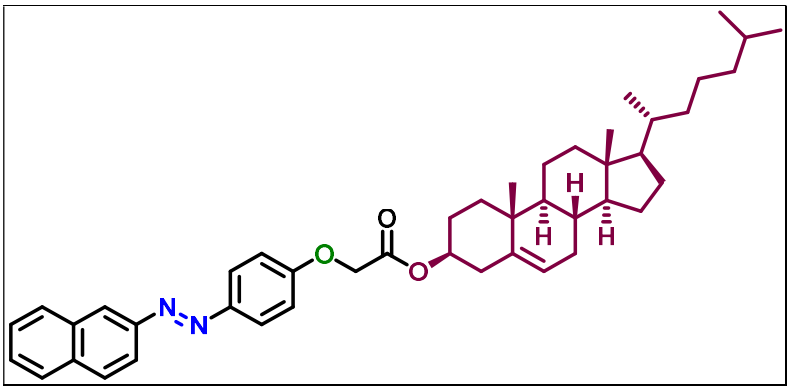

Orange solid, Yield: 69 %; **IR** ν_{max}/cm^{-1}: 3053.62, 2928.52 (C_{sp3}-H), 2851.86, 1729.20 (ester C=O), 1602.38 (-N=N-), 1253.90 (C-O), 1138.28, 836.97; **^{1}H NMR (400 MHz, $CDCl_3$): δ (In ppm)**: 8.34 (s, 1H, Ar-H), 7.98 (d, *J* = 2 Hz, 1H, Ar-H), 7.93 (d, *J* = 3.2 Hz, 1H, Ar-H), 7.91 (d, *J* = 8.8 Hz, 2H, Ar-H), 7.83 (d, *J* = 9.2 Hz, 2H, Ar-H), 7.47 (d, *J* = 9.2 Hz, 2H, Ar-H), 6.97 (d, *J* = 8.8 Hz, 2H, Ar-H), 5.32 (brd, J = 3.6 Hz, 1H, olefinic), 4.62 (m, 1H, CHOCO), 4.58 (t, J = 6.0 Hz, 2H, OCH_2), 2.30-2.28 (m, 4H, 2 X allylic CH_2), 1.91–0.90 (m, 30H, 6 X CH, 9 X CH_2, 2 X CH_3), 0.80 (d, *J* = 2.3 Hz, 6H, 2 X CH_3), 0.59 (s, 3H, CH_3) ; **^{13}C NMR (400MHz, $CDCl_3$): δ (In ppm):** 173.25 (C=O), 159.02 (Ar C-O-), 150.27, 139.67, 134.59, 129.24, 129.09, 129.03, 127.93, 127.40, 126.92, 126.62, 124.71, 122.67, 117.37, 114.75, 73.87 (CHOCO), 68.00 (Ar-O-C-), 56.68, 56.13, 50.02, 42.31, 39.73, 39.53, 38.18, 36.99, 36.19, 35.80, 34.59, 31.92, 31.86, 28.24, 28.03, 27.84, 24.29, 23.84, 22.58, 21.04, 19.33, 11.86; **Elemental Analysis**: $C_{45}H_{58}N_2O_3$:(cal): C, 80.08; H, 8.66; N, 4.15; found C, 79.99; H, 8.62; N, 4.13; %;

Cholesteryl 3-(4-((E)-naphthalen-2-yldiazenyl)phenoxy)propanoate (VII-2):

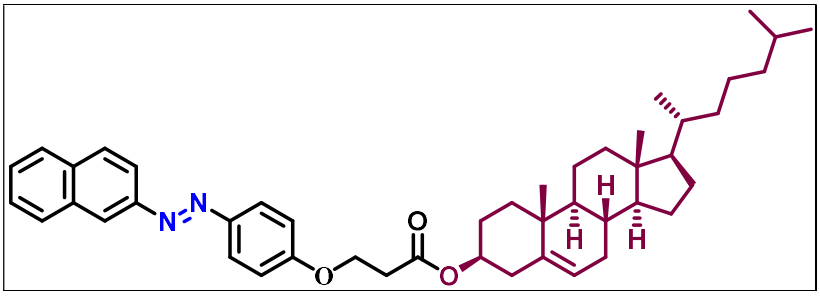

Orange solid, Yield: 71 %; **IR** ν_{max}/cm^{-1}: 3053.93, 2933.83 (C_{sp3}-H), 2868,51, 1732.01 (ester C=O), 1600.70 (-N=N-), 1248.22 (C-O), 1143.06, 836.54; **^{1}H NMR (400 MHz, $CDCl_3$): δ (In ppm)**: 8.42 (s, 1H, Ar-H), 7.98 (d, *J* = 2 Hz, 1H, Ar-H), 7.92 (d, *J* = 2 Hz, 1H, Ar-H), 7.89 (d, *J* = 8.8 Hz, 2H, Ar-H), 7.83 (d, *J* = 9.2 Hz, 2H, Ar-H), 7.46 (d, *J* = 9.2 Hz, 2H, Ar-H), 6.94 (d, *J* = 8.8 Hz, 2H, Ar-H), 5.38 (brd, *J* = 3.6 Hz, 1H, olefinic), 4.64 (m, 1H, CHOCO), 3.98 (t, *J* = 6.0 Hz, 2H, OCH_2), 2.26-2.22 (m, 4H, 2 X allylic CH_2), 2.09–0.89 (m, 32H, 6 X CH, 9 X CH_2, 2 X CH_3, 1 X CH_2-COO), 0.80 (d, *J* = 2.3 Hz, 6H, 2 X CH_3), 0.58 (s, 3H, CH_3) ; **^{13}C NMR (400MHz, $CDCl_3$): δ (In ppm):** 169.97 (C=O), 160.14 (Ar C-O-), 150.25, 139.18, 134.62, 129.30, 129.09, 129.03, 127.94, 127.37, 126.92, 126.69, 124.75, 123.16, 117.19, 114.97, 75.48 (CHOCO), 65.65 (Ar-O-C-), 56.65, 56.10, 49.96, 42.30, 39.69, 39.52, 37.97, 36.88, 36.18, 35.81, 34.59, 31.90, 31.82, 28.25, 28.04, 27.69, 24.29, 23.84, 22.86, 22.60, 21.03, 19.33, 11.87; **Elemental Analysis**: $C_{46}H_{60}N_2O_3$:(cal): C, 80.19; H, 8.78; N, 4.07; found C, 80.13; H, 8.72; N, 4.02; %;

Cholesteryl 4-(4-((E)-naphthalen-2-yldiazenyl)phenoxy)butanoate (VII-3):

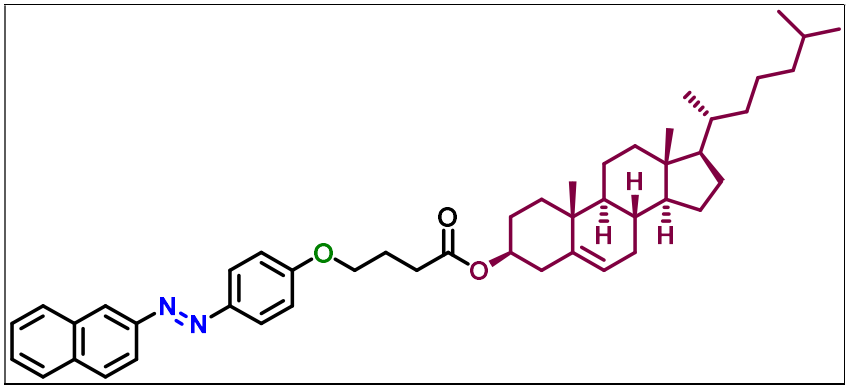

Orange solid, Yield: 70 %; **IR** ν_{max}/cm^{-1}: 3053.38, 2934.90 (C_{sp3}-H), 2848.51, 1729.80 (ester C=O), 1602.81 (-N=N-), 1253.90 (C-O), 1138.46, 835.55; **^{1}H NMR (400 MHz, $CDCl_3$): δ (In ppm)**: 8.42 (s, 1H, Ar-H), 8.06 (d, *J* = 2.3 Hz, 1H, Ar-H), 8.01 (d, *J* =

2.1 Hz, 1H, Ar-H), 7.99 (d, *J* = 8.0 Hz, 2H, Ar-H), 7.93 (d, *J* = 8.8 Hz, 2H, Ar-H), 7.57 (d, *J* = 9.2 Hz, 2H, Ar-H), 7.04 (d, *J* = 8.8 Hz, 2H, Ar-H), 5.39 (brd, *J* = 3.6 Hz, 1H, olefinic), 4.67 (m, 1H, CHOCO), 4.09 (t, *J* = 6.1 Hz, 2H, OCH_2), 2.43-2.32 (m, 4H, 2 X allylic CH_2), 1.99–0.92 (m, 34H, 6 X CH, 9 X CH_2, 1 X $CH_{2\ chain}$, 2 X CH_3, 1 X CH_2-COO), 0.88 (d, *J* = 2.4 Hz, 6H, 2 X CH_3), 0.68 (s, 3H, CH_3) ; **^{13}C NMR (400MHz, $CDCl_3$): δ (In ppm):** 172.84 (C=O), 161.84 (Ar C-O-), 150.31, 139.62, 134.57, 129.23, 129.04, 127.92, 127.20, 127.08, 126.92, 126.65, 124.73, 122.62, 117.27, 114.76, 73.95 (CHOCO), 67.73 (Ar-O-C-), 56.64, 56.08, 49.97, 42.28, 39.68, 39.52, 38.10, 36.99, 36.18, 35.77, 34.29, 31.89, 28.55, 28.23, 28.02, 27.80, 24.26, 23.82, 22.85, 22.59, 21.79, 21.08, 19.31, 11.80; **Elemental Analysis**: $C_{47}H_{62}N_2O_3$:(cal): C, 80.30; H, 8.89; N, 3.98; found C, 80.27; H, 8.81; N, 3.92; %;

Cholesteryl 5-(4-((E)-naphthalen-2-yldiazenyl)phenoxy)pentanoate (VII-4):

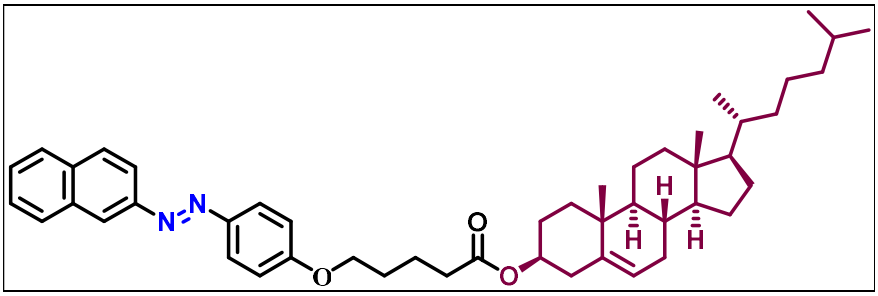

Orange solid, Yield: 72 %; **IR** ν_{max}/cm^{-1}: 3053.73, 2930.87 (C_{sp3}-H), 2866.51, 1732.07 (ester C=O), 1600.86 (-N=N-), 1248.22 (C-O), 1140.00, 836.54; **^{1}H NMR (400 MHz, $CDCl_3$): δ (In ppm)**: 8.42 (s, 1H, Ar-H), 8.07 (d, *J* = 2 Hz, 1H, Ar-H), 8.00 (d, *J* = 2.2 Hz, 1H, Ar-H), 7.98 (d, *J* = 8.8 Hz, 2H, Ar-H), 7.93 (d, *J* = 8.8 Hz, 2H, Ar-H), 7.56 (d, *J* = 9.2 Hz, 2H, Ar-H), 7.04 (d, *J* = 8.8 Hz, 2H, Ar-H), 5.40 (brd, *J* = 3.4 Hz, 1H, olefinic), 4.63 (m, 1H, CHOCO), 4.10 (t, *J* = 6.0 Hz, 2H, OCH_2), 2.43-2.32 (m, 4H, 2 X allylic CH_2), 1.99–0.92 (m, 36H, 6 X CH, 9 X CH_2, 2 X $CH_{2\ chain}$, 2 X CH_3, 1 X CH_2-COO), 0.88 (d, *J* = 2.3 Hz, 6H, 2 X CH_3), 0.68 (s, 3H, CH_3) ; **^{13}C NMR (400MHz, $CDCl_3$): δ (In ppm):** 172.83 (C=O), 161.46 (Ar C-O-), 150.30, 139.60, 134.51, 129.23, 129.04, 129.02, 127.91, 127.01, 126.90, 126.64, 124.77, 124.71, 122.68, 117.28, 114.75, 73.92 (CHOCO), 67.78 (Ar-O-C-), 56.64, 56.08, 49.90, 42.23, 39.67, 39.51, 38.14, 36.95, 36.12, 35.78, 34.27, 31.88, 31.82, 28.55, 28.02, 27.80, 24.26, 23.89, 22.84, 21.70, 21.01, 19.35, 11.83; **Elemental Analysis**: $C_{48}H_{64}N_2O_3$:(cal): C, 80.40; H, 9.00; N, 3.91; found C, 80.37; H, 8.97; N, 3.90; %;

Cholesteryl 6-(4-((E)-naphthalen-2-yldiazenyl)phenoxy)hexanoate (VII-5):

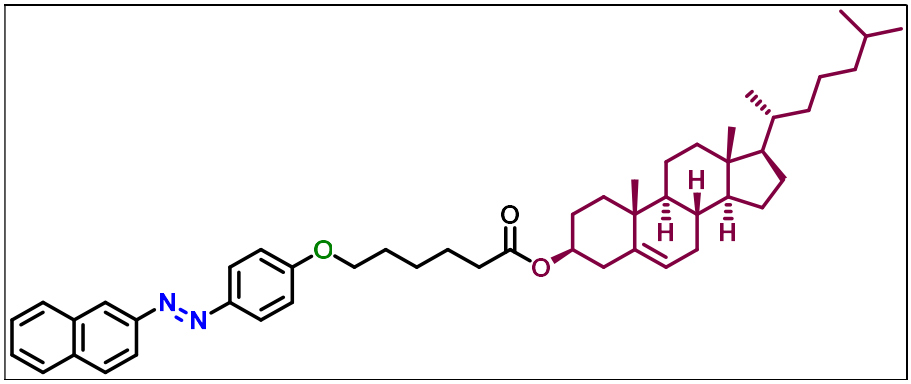

Orange solid, Yield: 71 %; **IR** ν_{max}/cm^{-1}: 3053.69, 2929.52 (C_{sp3}-H), 2851.96, 1729.23 (ester C=O), 1602.30 (-N=N-), 1253.90 (C-O), 1138.26, 833.97; **^{1}H NMR (400 MHz, $CDCl_3$): δ (In ppm)**: 8.45 (s, 1H, Ar-H), 8.08 (d, *J* = 2.3 Hz, 1H, Ar-H), 8.02 (d, *J* = 2.1 Hz, 1H, Ar-H), 7.99 (d, *J* = 8.6 Hz, 2H, Ar-H), 7.93 (d, *J* = 8.8 Hz, 2H, Ar-H), 7.57 (d, *J* = 9.2 Hz, 2H, Ar-H), 7.04 (d, *J* = 8.8 Hz, 2H, Ar-H), 5.41 (brd, *J* = 3.4 Hz, 1H, olefinic), 4.68 (m, 1H, CHOCO), 4.01 (t, *J* = 6.0 Hz, 2H, OCH_2), 2.38-2.33 (m, 4H, 2 X allylic CH_2), 1.88–0.92 (m, 38H, 6 X CH, 9 X CH_2, 3 X CH_2 chain, 2 X CH_3, 1 X CH_2-COO), 0.88 (d, *J* = 2.4 Hz, 6H, 2 X CH_3), 0.68 (s, 3H, CH_3) ; **^{13}C NMR (400MHz, $CDCl_3$): δ (In ppm):** 173.00 (C=O), 161.87 (Ar C-O-), 150.21, 139.77, 134.93, 129.20, 129.04, 129.02, 127.94, 127.15, 126.96, 126.69, 124.75, 124.75, 122.65, 117.30, 114.70, 73.73 (CHOCO), 68.24 (Ar-O-C-), 56.69, 56.12, 50.01, 42.39, 39.70, 39.52, 38.17, 36.63, 36.18, 35.87, 34.65, 31.92, 31.80, 29.13, 28.23, 28.04, 27.84, 24.23, 23.81, 22.89, 22.55, 21.00, 19.39, 11.89; **Elemental Analysis**: $C_{49}H_{66}N_2O_3$:(cal): C, 80.50; H, 9.10; N, 3.83; found C, 80.45; H, 9.07; N, 3.80; %;

Cholesteryl 8-(4-((E)-naphthalen-2-yldiazenyl)phenoxy)octanoate (VII-7):

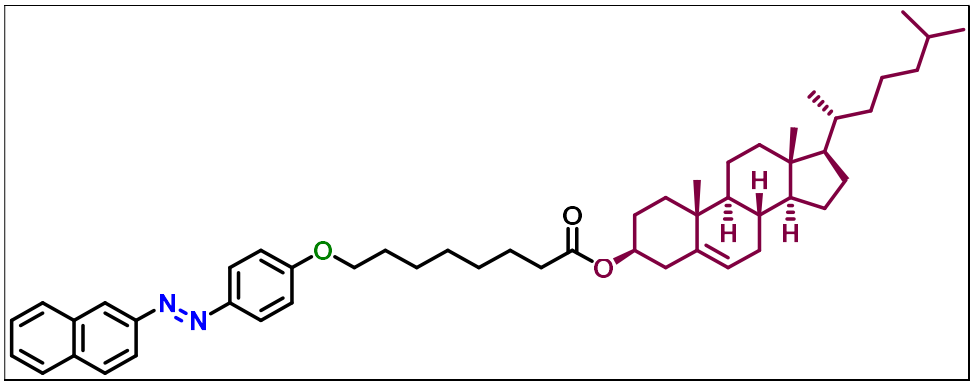

Orange solid, Yield: 73 %; **IR** ν_{max}/cm^{-1}: 3054.68, 2934.20 (C_{sp3}-H), 2851.75, 1735.25 (ester C=O), 1604.61 (-N=N-), 1261.55 (C-O), 1142.91, 840.47; **^{1}H NMR (400 MHz, $CDCl_3$): δ (In ppm)**: 8.42 (s, 1H, Ar-H), 7.98 (d, *J* = 2.4 Hz, 1H, Ar-H), 7.92 (d, *J* = 2.1 Hz, 1H, Ar-H), 7.89 (d, *J* = 8.8 Hz, 2H, Ar-H), 7.82 (d, *J* = 8.8 Hz, 2H, Ar-H), 7.47 (d, *J* = 9.2 Hz, 2H, Ar-H), 6.94 (d, *J* = 8.8 Hz, 2H, Ar-H), 5.29 (brd, *J* = 3.6 Hz, 1H, olefinic), 4.54 (m, 1H, CHOCO), 3.97 (t, *J* = 6.0 Hz, 2H, OCH_2), 2.24-2.19 (m, 4H, 2 X allylic CH_2), 1.93–0.93 (m, 42H, 6 X CH, 9 X CH_2, 5 X CH_2 chain, 2 X CH_3, 1 X CH_2-COO), 0.88 (d, *J* = 2.3 Hz, 6H, 2 X CH_3), 0.58 (s, 3H, CH_3) ; **^{13}C NMR (400MHz, $CDCl_3$): δ (In ppm):** 173.25 (C=O), 161.70 (Ar C-O-), 150.38, 139.70, 134.53, 129.24, 129.09, 129.02, 127.91, 127.19, 126.90, 126.62, 124.77, 124.71, 122.63, 117.38, 114.76, 73.77 (CHOCO), 68.27 (Ar-O-C-), 56.68, 56.13, 50.02, 42.28, 39.73, 39.53, 38.19, 36.96, 36.19, 35.80, 34.67, 31.91, 31.87, 29.13, 28.24, 28.03, 27.84, 25.85, 24.29, 23.85, 22.84, 22.58, 21.04, 19.32, 11.86; **Elemental Analysis**: $C_{51}H_{70}N_2O_3$:(cal): C, 80.69; H, 9.29; N, 3.69; found C, 80.64; H, 9.22; N, 3.66; %;

Cholesteryl 10-(4-((E)-naphthalen-2-yldiazenyl)phenoxy)decanoate (VII-9):

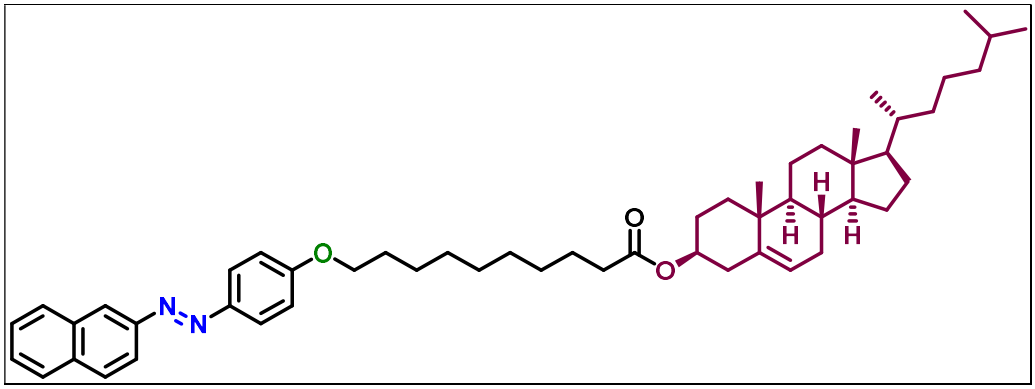

Orange solid, Yield: 69 %; **IR** ν_{max}/cm^{-1}: 3056.32, 2939.25 (C_{sp3}-H), 2850.77, 1734.61 (ester C=O), 1604.26 (-N=N-), 1246.28 (C-O), 1138.29, 839.45; **^{1}H NMR (400 MHz, $CDCl_3$): δ (In ppm)**: 8.42 (s, 1H, Ar-H), 8.08 (d, *J* = 2.6 Hz, 1H, Ar-H), 8.02 (d, *J* = 2 Hz, 1H, Ar-H), 7.99 (d, *J* = 8.2 Hz, 2H, Ar-H), 7.92 (d, *J* = 8.8 Hz, 2H, Ar-H), 7.55 (d, *J* = 9.2 Hz, 2H, Ar-H), 7.04 (d, *J* = 8.8 Hz, 2H, Ar-H), 5.39 (brd, *J* = 3.6 Hz, 1H, olefinic), 4.63 (m, 1H, CHOCO), 4.07 (t, *J* = 6.0 Hz, 2H, OCH_2), 2.34-2.28 (m, 4H, 2 X allylic CH_2), 2.00–0.92 (m, 46H, 6 X CH, 9 X CH_2, 7 X CH_2 chain, 2 X CH_3, 1 X CH_2-COO), 0.88 (d, *J* = 2.3 Hz, 6H, 2 X CH_3), 0.68 (s, 3H, CH_3) ; **^{13}C NMR (400MHz, $CDCl_3$): δ (In ppm):** 173.37 (C=O), 161.73 (Ar C-O-), 150.35, 139.70, 134.52, 129.25,

129.04, 127.92, 127.22, 126.98, 126.64, 124.78, 124.06, 122.64, 117.33, 114.74, 73.72 (CHOCO), 68.35 (Ar-O-C-), 56.66, 56.10, 49.99, 42.30, 39.71, 39.53, 38.17, 36.99, 36.18, 35.82, 34.72, 31.85, 29.74, 29.20, 28.25, 28.04, 27.83, 25.06, 24.30, 23.85, 22.87, 22.60, 21.03, 19.35, 11.87; **Elemental Analysis**: $C_{53}H_{74}N_2O_3$:(cal): C, 80.87; H, 9.48; N, 3.56; found C, 80.84; H, 9.45; N, 3.54; %;

Cholesteryl 11-(4-((E)-naphthalen-2-yldiazenyl)phenoxy)undecanoate (VII-10):

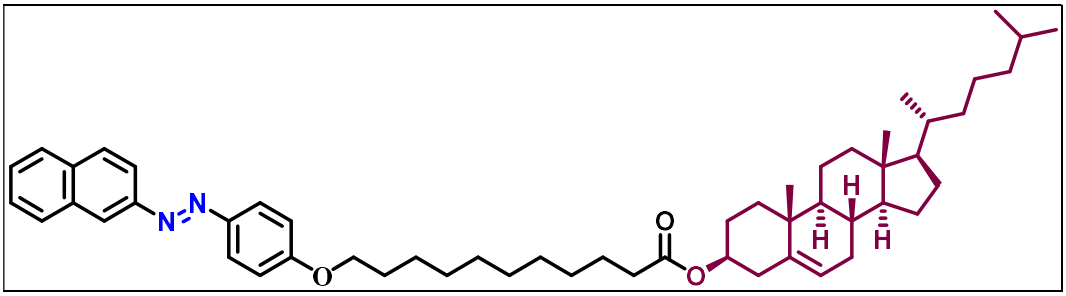

Orange solid, Yield: 71 %; **IR** ν_{max}/cm^{-1}: 3055.87, 2936.07 (C_{sp3}-H), 2851.16, 1736.20 (ester C=O), 1601.23 (-N=N-), 1255.78 (C-O), 1141.60, 838.49; **^{1}H NMR (400 MHz, $CDCl_3$): δ (In ppm)**: 8.42 (s, 1H, Ar-H), 8.08 (d, *J* = 2.4 Hz, 1H, Ar-H), 8.03 (d, *J* = 2.0 Hz, 1H, Ar-H), 7.99 (d, *J* = 8.8 Hz, 2H, Ar-H), 7.93 (d, *J* = 8.8 Hz, 2H, Ar-H), 7.56 (d, *J* = 9.2 Hz, 2H, Ar-H), 7.05 (d, *J* = 8.8 Hz, 2H, Ar-H), 5.39 (brd, *J* = 3.6 Hz, 1H, olefinic), 4.63 (m, 1H, CHOCO), 4.03 (t, *J* = 6.0 Hz, 2H, OCH_2), 2.43-2.32 (m, 4H, 2 X allylic CH_2), 1.99–0.92 (m, 48H, 6 X CH, 9 X CH_2, 8 X CH_2 chain, 2 X CH_3, 1 X CH_2-COO), 0.88 (d, *J* = 2.3 Hz, 6H, 2 X CH_3), 0.68 (s, 3H, CH_3) ; **^{13}C NMR (400MHz, $CDCl_3$): δ (In ppm):** 173.39 (C=O), 161.74 (Ar C-O-), 150.35, 139.71, 134.52, 129.25, 129.11, 129.05, 127.93, 127.22, 126.98, 126.64, 124.78, 124.72, 122.63, 117.33, 114.75, 73.72 (CHOCO), 68.37 (Ar-O-C-), 56.67, 56.11, 49.99, 42.30, 39.71, 39.53, 38.18, 37.00, 36.19, 35.82, 34.74, 31.91, 29.49, 29.22, 28.26, 28.05, 27.83, 25.07, 24.30, 23.85, 22.87, 22.61, 21.03, 19.36, 11.87; **Elemental Analysis**: $C_{54}H_{76}N_2O_3$:(cal): C, 80.95; H, 9.56; N, 3.50; found C, 80.94; H, 9.56; N, 3.53; %;

5.5.3.2 Cholesteryl ω-(4-((E)-(naphthalen-2-ylimino)methyl)phenoxy)alkanoate (VIII-n):

5.5.3.2.1 (E)-4-((naphthalen-2-ylimino)methyl)phenol (NpAmOH)

The synthesis of (E)-4-((naphthalen-2-ylimino)methyl)phenol (NpAmOH) is described in Chapter 2, Section 2A.5.3.2.

5.5.3.2.2 Cholesteryl ω-bromoalkanoates (ChBr-n)

The synthesis of Cholesteryl ω-bromoalkanoates (ChBr-n) is given in section 5.5.3.1.2.

5.5.3.2.3 Cholesteryl ω-(4-((E)-(naphthalen-2-ylimino)methyl)phenoxy)alkanoate (VIII-n)

In a round bottom flask with a reflux system and stirring for 15 minutes, (E)-4-((naphthalen-2-ylimino)methyl)phenol (**NpAmOH**) (0.52 mmol) and **ChBr-n** (0.5 mmol) were dissolved in acetone. Additions of anhydrous K_2CO_3 (2.17 g, 15.7 mmol) and a catalytic amount of KI were made to the reaction mixture, and the system was refluxed for about 48 h (monitored by TLC). The hot solution was filtered and washed with acetone after the reaction was finished. The filtrate was then collected and evaporated in a rotary evaporator. Cold petroleum ether was added to the concentrated extracts, and the resulting precipitate was filtered and washed two times with this same solvent. To obtain the desired product, the crude precipitate was recrystallised twice from ethanol.

5.5.3.2.4 Characterization of dimers VIII-n:

Cholesteryl 2-(4-((E)-(naphthalen-2-ylimino)methyl)phenoxy)acetate (VIII-1)

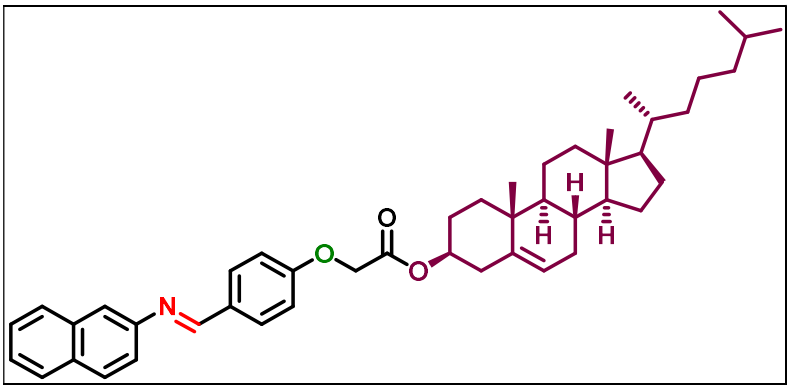

White solid, Yield: 66 %; **IR** ν_{max}/cm^{-1}: 3054.95, 2945.76 (C_{sp3}-H), 2862.82, 1731.62 (ester C=O), 1604.12 (-CH=N-), 1248.98 (C-O), 1167.49, 827.95; **^{1}H NMR (400 MHz, $CDCl_3$): δ (In ppm)**: 8.55 (s, 1H, -N=CH-), 7.83 (d, *J* = 8.8 Hz, 2H, Ar-H), 7.79 (d, *J* = 8.4 Hz, 2H, Ar-H), 7.77 (d, *J* = 8.4 Hz, 1H, Ar-H), 7.50 (s, 1H, Ar-H), 7.37 (d, *J* = 8.0 Hz, 1H, Ar-H), 7.35 (d, *J* = 7.6 Hz, 2H, Ar-H), 6.94 (d, *J* = 8.8 Hz, 2H, Ar-H), 5.31 (brd, *J* = 3.2 Hz, 1H, olefinic), 4.61 (m, 1H, CHOCO), 4.58 (t, *J* = 6.4 Hz, 2H, OCH_2), 2.30-2.28 (m, 4H, 2 X allylic CH_2), 1.92–0.91 (m, 30H, 6 X CH, 9 X CH_2, 2 X CH_3), 0.86 (d, *J* = 2.3 Hz, 6H, 2 X CH_3), 0.60 (s, 3H, CH_3) ; **^{13}C NMR (400MHz, $CDCl_3$): δ**

(In ppm): 172.22 (C=O), 160.86 (Ar C-O-), 158.93 (CH=N), 150.38, 138.69, 133.12, 129.55, 128.09, 127.83, 126.76, 125.23, 124.07, 121.60, 120.39, 116.43, 113.63, 72.78 (CHOCO), 67.03 (Ar-O-C-), 55.65, 55.07, 52.41, 48.97, 41.27, 38.60, 38.49, 37.12, 35.93, 35.14, 34.76, 33.62, 30.82, 28.09, 27.97, 27.20, 26.95, 24.81, 23.29, 22.72, 21.81, 19.99, 10.89; **Elemental Analysis**: $C_{46}H_{59}NO_3$:(cal): C, 81.98; H, 8.82; N, 2.08; found C, 81.94; H, 8.81; N, 2.06; %;

Cholesteryl 3-(4-((E)-(naphthalen-2-ylimino)methyl)phenoxy)propanoate (VIII-2)

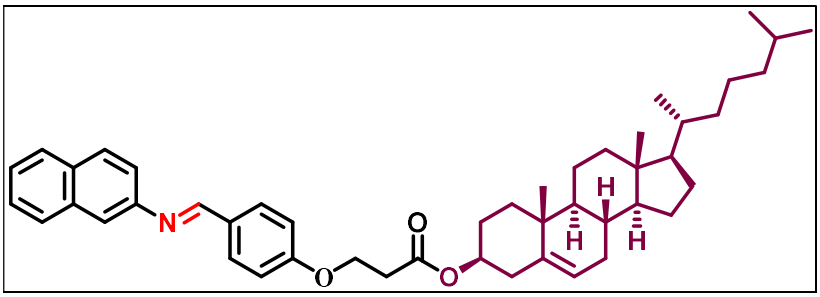

White solid, Yield: 68 %; **IR** ν_{max}/cm^{-1}: 3054.11, 2945.22 (C_{sp3}-H), 2864.93, 1730.14 (ester C=O), 1603.71 (-CH=N-), 1250.62 (C-O), 1170.66, 826.18; **^{1}H NMR (400 MHz, $CDCl_3$): δ (In ppm)**: 8.53 (s, 1H, -N=CH-), 7.86 (d, *J* = 8.8 Hz, 2H, Ar-H), 7.80 (d, *J* = 8.4 Hz, 2H, Ar-H), 7.75 (d, *J* = 8.4 Hz, 1H, Ar-H), 7.50 (s, 1H, Ar-H), 7.40 (d, *J* = 8.0 Hz, 1H, Ar-H), 7.36 (d, *J* = 7.6 Hz, 2H, Ar-H), 6.91 (d, *J* = 8.4 Hz, 2H, Ar-H), 5.29 (brd, *J* = 3.2 Hz, 1H, olefinic), 4.64 (m, 1H, CHOCO), 3.96 (t, *J* = 6.4 Hz, 2H, OCH_2), 2.27-2.24 (m, 4H, 2 X allylic CH_2), 2.09–0.90 (m, 32H, 6 X CH, 9 X CH_2, 2 X CH_3, 1 X CH_2-COO), 0.79 (d, *J* = 2.3 Hz, 6H, 2 X CH_3), 0.59 (s, 3H, CH_3) ; **^{13}C NMR (400MHz, $CDCl_3$): δ (In ppm):** 169.96 (C=O), 160.43 (Ar C-O-), 159.69 (CH=N), 149.82, 139.18, 134.13, 130.17, 128.93, 127.87, 126.38, 125.24, 123.16, 121.28, 117.62, 114.89, 75.47 (CHOCO), 65.49 (Ar-O-C-), 56.66, 56.10, 53.48, 49.97, 42.31, 39.69, 39.52, 37.97, 36.18, 35.81, 31.90, 31.83, 28.25, 28.04, 27.69, 24.29, 23.83, 22.86, 22.60, 21.03, 19.33, 11.88; **Elemental Analysis**: $C_{47}H_{61}NO_3$:(cal): C, 82.05; H, 8.94; N, 2.04; found C, 82.01; H, 8.92; N, 2.04; %;

Cholesteryl 4-(4-((E)-(naphthalen-2-ylimino)methyl)phenoxy)butanoate (VIII-3)

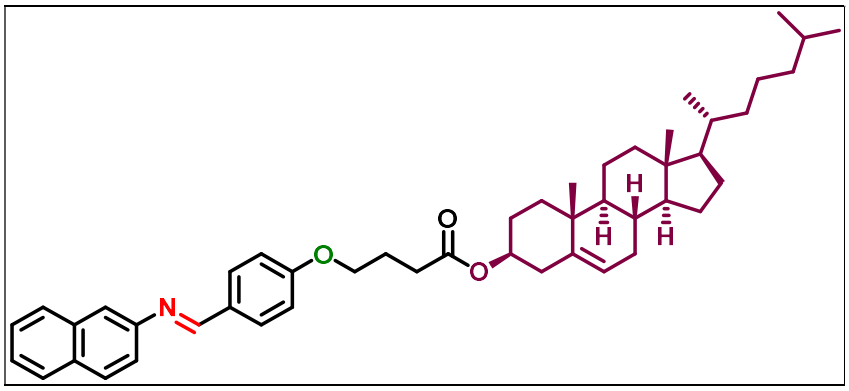

White solid, Yield: 68 %; **IR** ν_{max}/cm^{-1}: 3053.40, 2944.74 (C_{sp3}-H), 2864.79, 1732.63 (ester C=O), 1604.42 (-CH=N-), 1238.98 (C-O), 1166.49, 826.95; **^{1}H NMR (400 MHz, $CDCl_3$): δ (In ppm)**: 8.56 (s, 1H, -N=CH-), 7.91 (d, *J* = 8.8 Hz, 2H, Ar-H), 7.88 (d, *J* = 8.4 Hz, 2H, Ar-H), 7.59 (d, *J* = 8.4 Hz, 1H, Ar-H), 7.50 (s, 1H, Ar-H), 7.45 (d, *J* = 8.0 Hz, 1H, Ar-H), 7.38 (d, *J* = 7.6 Hz, 2H, Ar-H), 7.01 (d, *J* = 8.4 Hz, 2H, Ar-H), 5.39 (brd, *J* = 3.2 Hz, 1H, olefinic), 4.69 (m, 1H, CHOCO), 4.07 (t, *J* = 6.4 Hz, 2H, OCH_2), 2.41- 2.33 (m, 4H, 2 X allylic CH_2), 2.01–0.90 (m, 34H, 6 X CH, 9 X CH_2, 1 X CH_2 chain, 2 X CH_3, 1 X CH_2-COO), 0.88 (d, *J* = 2.3 Hz, 6H, 2 X CH_3), 0.70 (s, 3H, CH_3) ; **^{13}C NMR (400MHz, $CDCl_3$): δ (In ppm):** 173.37 (C=O), 161.96 (Ar C-O-), 160.00 (CH=N), 150.04, 139.71, 134.18, 129.05, 128.88, 127.84, 126.33, 125.14, 122.63, 121.40, 120.39, 117.53, 114.73, 76.74 (CHOCO), 68.21 (Ar-O-C-), 56.68, 56.12, 50.00, 42.31, 39.72, 39.53, 38.18, 37.00, 35.82, 34.73, 31.91, 29.74, 28.04, 27.83, 26.03, 25.07, 24.30, 23.85, 22.87, 21.04, 19.36, 11.88; **Elemental Analysis**: $C_{48}H_{63}NO_3$:(cal): C, 82.12; H, 9.05; N, 2.00; found C, 82.10; H, 8.99; N, 1.97; %;

Cholesteryl 5-(4-((E)-(naphthalen-2-ylimino)methyl)phenoxy)pentanoate (VIII-4)

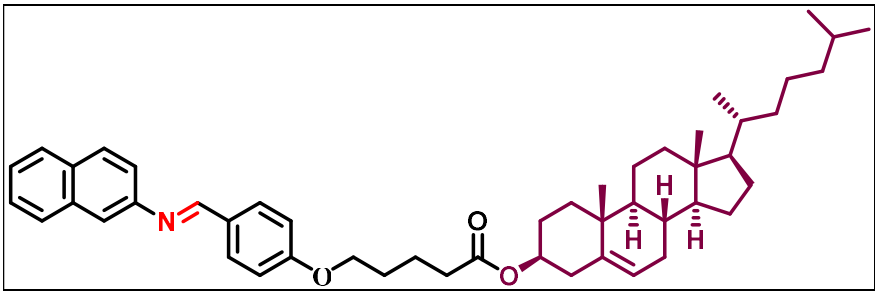

White solid, Yield: 71 %; **IR** ν_{max}/cm^{-1}: 3055.13, 2945.62 (C_{sp3}-H), 2865.95, 1728.83 (ester C=O), 1605.15 (-CH=N-), 1250.30 (C-O), 1169.50, 826.84; **^{1}H NMR (400 MHz,**

$CDCl_3$): δ (In ppm): 8.53 (s, 1H, -N=CH-), 7.91 (d, *J* = 8.8 Hz, 2H, Ar-H), 7.88 (d, *J* = 8.4 Hz, 2H, Ar-H), 7.59 (d, *J* = 8.4 Hz, 1H, Ar-H), 7.50 (s, 1H, Ar-H), 7.45 (d, *J* = 8.0 Hz, 1H, Ar-H), 7.38 (d, *J* = 7.6 Hz, 2H, Ar-H), 7.01 (d, *J* = 8.4 Hz, 2H, Ar-H), 5.41 (brd, *J* = 3.2 Hz, 1H, olefinic), 4.64 (m, 1H, CHOCO), 4.07 (t, *J* = 6.4 Hz, 2H, OCH_2), 2.41-2.33 (m, 4H, 2 X allylic CH_2), 2.01–0.90 (m, 36H, 6 X CH, 9 X CH_2, 2 X CH_2 chain, 2 X CH_3, 1 X CH_2-COO), 0.88 (d, *J* = 2.3 Hz, 6H, 2 X CH_3), 0.70 (s, 3H, CH_3) ; **^{13}C NMR (400MHz, $CDCl_3$): δ (In ppm):** 172.82 (C=O), 161.73 (Ar C-O-), 159.89 (CH=N), 150.03, 139.65, 134.19, 129.24, 128.88, 127.85, 126.39, 125.15, 122.71, 121.37, 120.39, 117.54, 114.74, 76.73 (CHOCO), 67.61 (Ar-O-C-), 56.69, 56.14, 50.03, 42.32, 39.74, 39.54, 38.18, 37.00, 35.81, 34.28, 31.92, 28.58, 28.25, 27.84, 24.30, 23.85, 22.85, 22.59, 21.71, 21.04, 19.35, 11.87; **Elemental Analysis**: $C_{49}H_{65}NO_3$:(cal): C, 82.19; H, 9.15; N, 1.96; found C, 82.13; H, 9.11; N, 1.93; %;

Cholesteryl 6-(4-((E)-(naphthalen-2-ylimino)methyl)phenoxy)hexanoate (VIII-5)

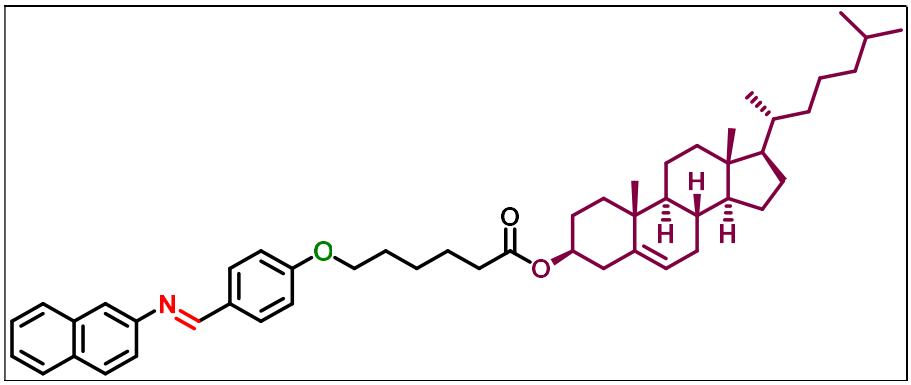

White solid, Yield: 69 %; **IR** ν_{max}/cm^{-1}: 3055.24, 2946.71 (C_{sp3}-H), 2866.73, 1729.50 (ester C=O), 1605.02 (-CH=N-), 1250.62 (C-O), 1170.53, 826.64; **^{1}H NMR (400 MHz, $CDCl_3$): δ (In ppm)**: 8.56 (s, 1H, -N=CH-), 7.86 (d, *J* = 8.8 Hz, 2H, Ar-H), 7.80 (d, *J* = 8.4 Hz, 2H, Ar-H), 7.76 (d, *J* = 8.0 Hz, 1H, Ar-H), 7.49 (s, 1H, Ar-H), 7.40 (d, *J* = 8.0 Hz, 1H, Ar-H), 7.36 (d, *J* = 7.6 Hz, 2H, Ar-H), 6.90 (d, *J* = 8.4 Hz, 2H, Ar-H), 5.38 (brd, *J* = 3.2 Hz, 1H, olefinic), 4.66 (m, 1H, CHOCO), 3.96 (t, *J* = 6.4 Hz, 2H, OCH_2), 2.27-2.24 (m, 4H, 2 X allylic CH_2), 2.09–0.90 (m, 38H, 6 X CH, 9 X CH_2, 3 X CH_2 chain, 2 X CH_3, 1 X CH_2-COO), 0.84 (d, *J* = 2.3 Hz, 6H, 2 X CH_3), 0.59 (s, 3H, CH_3) ; **^{13}C NMR (400MHz, $CDCl_3$): δ (In ppm):** 173.04 (C=O), 161.84 (Ar C-O-), 159.30 (CH=N), 150.03, 139.67, 134.15, 129.17, 128.93, 127.84, 126.39, 125.14, 122.67, 121.37, 121.23, 117.53, 114.73, 73.87 (CHOCO), 67.85 (Ar-O-C-), 56.70, 56.14,

50.03, 42.32, 39.74, 39.53, 38.18, 37.00, 35.80, 34.58, 31.92, 28.88, 28.24, 27.84, 24.30, 23.85, 22.84, 22.58, 21.05, 19.34, 11.83; **Elemental Analysis**: $C_{50}H_{67}NO_3$:(cal): C, 82.26; H, 9.25; N, 1.92; found C, 82.22; H, 9.21; N, 1.91; %;

Cholesteryl 8-(4-((E)-(naphthalen-2-ylimino)methyl)phenoxy)octanoate (VIII-7)

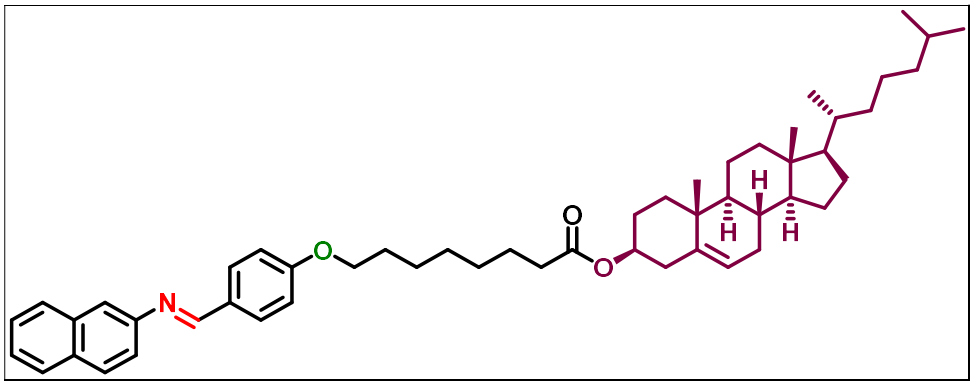

White solid, Yield: 65 %; **IR** ν_{max}/cm^{-1}: 3058.45, 2952.08 (C_{sp3}-H), 2866.81, 1726.38 (ester C=O), 1604.00 (-CH=N-), 1256.16 (C-O), 1169.70, 832.26; **^{1}H NMR (400 MHz, $CDCl_3$): δ (In ppm)**: 8.54 (s, 1H, -N=CH-), 7.81 (d, *J* = 8.8 Hz, 2H, Ar-H), 7.78 (d, *J* = 8.4 Hz, 2H, Ar-H), 7.75 (d, *J* = 8.4 Hz, 1H, Ar-H), 7.49 (s, 1H, Ar-H), 7.40 (d, *J* = 8.0 Hz, 1H, Ar-H), 7.36 (d, *J* = 7.6 Hz, 2H, Ar-H), 6.91 (d, *J* = 8.4 Hz, 2H, Ar-H), 5.29 (brd, *J* = 3.2 Hz, 1H, olefinic), 4.65 (m, 1H, CHOCO), 3.95 (t, *J* = 6.4 Hz, 2H, OCH_2), 2.25-2.19 (m, 4H, 2 X allylic CH_2), 1.91–0.90 (m, 42H, 6 X CH, 9 X CH_2, 5 X CH_2 $_{chain}$, 2 X CH_3, 1 X CH_2-COO), 0.86 (d, *J* = 2.3 Hz, 6H, 2 X CH_3), 0.59 (s, 3H, CH_3) ; **^{13}C NMR (400MHz, $CDCl_3$): δ (In ppm):** 172.23 (C=O), 160.87 (Ar C-O-), 158.93 (CH=N), 148.98, 138.64, 133.13, 129.55, 128.03, 127.83, 126.79, 125.28, 124.09, 121.60, 120.34, 116.48, 113.68, 72.72 (CHOCO), 67.06 (Ar-O-C-), 55.63, 55.07, 52.41, 48.96, 41.26, 38.67, 38.48, 37.13, 35.95, 35.14, 34.76, 33.62, 30.86, 28.07, 27.97, 27.20, 24.81, 23.25, 22.79, 21.81, 21.54, 19.99, 10.82; **Elemental Analysis**: $C_{52}H_{71}NO_3$:(cal): C, 82.38; H, 9.44; N, 1.85; found C, 82.33; H, 9.42; N, 1.81; %;

Cholesteryl 10-(4-((E)-(naphthalen-2-ylimino)methyl)phenoxy)decanoate (VIII-9)

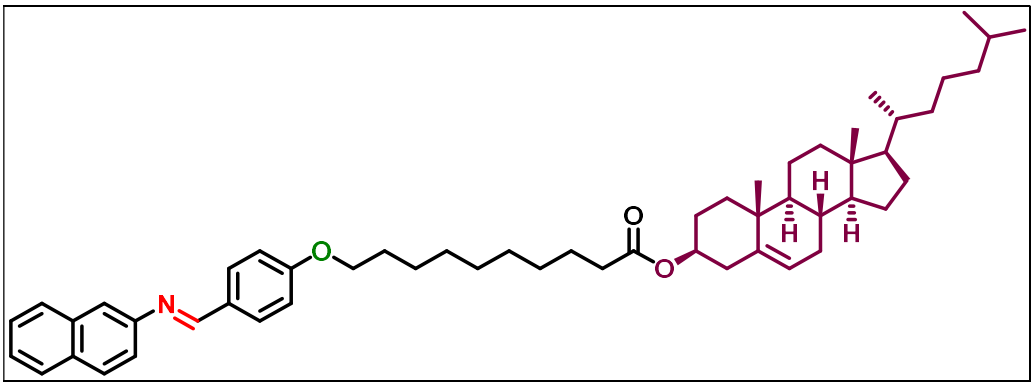

White solid, Yield: 66 %; **IR** ν_{max}/cm^{-1}: 3056.87, 2956.80 (C_{sp3}-H), 2867.03, 1725.47 (ester C=O), 1603.89 (-CH=N-), 1251.43 (C-O), 1171.98, 829.92; **^{1}H NMR (400 MHz, $CDCl_3$): δ (In ppm)**: 8.53 (s, 1H, -N=CH-), 7.93 (d, *J* = 8.8 Hz, 2H, Ar-H), 7.88 (d, *J* = 8.4 Hz, 2H, Ar-H), 7.86 (d, *J* = 8.4 Hz, 1H, Ar-H), 7.50 (s, 1H, Ar-H), 7.47 (d, *J* = 8.0 Hz, 1H, Ar-H), 7.45 (d, *J* = 7.6 Hz, 2H, Ar-H), 7.01 (d, *J* = 8.4 Hz, 2H, Ar-H), 5.31 (brd, *J* = 3.2 Hz, 1H, olefinic), 4.66 (m, 1H, CHOCO), 4.05 (t, *J* = 6.4 Hz, 2H, OCH_2), 2.34-2.28 (m, 4H, 2 X allylic CH_2), 1.89–0.92 (m, 46H, 6 X CH, 9 X CH_2, 7 X CH_2 $_{chain}$, 2 X CH_3, 1 X CH_2-COO), 0.88 (d, *J* = 2.3 Hz, 6H, 2 X CH_3), 0.69 (s, 3H, CH_3) ; **^{13}C NMR (400MHz, $CDCl_3$): δ (In ppm):** 173.36 (C=O), 161.95 (Ar C-O-), 160.00 (CH=N), 150.04, 139.71, 134.18, 129.06, 128.89, 127.85, 126.34, 125.15, 122.64, 121.40, 120.39, 117.54, 114.73, 76.75 (CHOCO), 68.19 (Ar-O-C-), 56.68, 56.12, 50.00, 42.31, 39.72, 39.54, 38.19, 37.00, 35.83, 34.73, 31.92, 29.38, 28.05, 27.84, 26.01, 25.07, 24.31, 23.86, 22.88, 21.04, 19.36, 11.84; **Elemental Analysis**: $C_{54}H_{75}NO_3$:(cal): C, 82.50; H, 9.62; N, 1.78; found C, 82.46; H, 9.59; N, 1.78; %;

Cholesteryl 11-(4-((E)-(naphthalen-2-ylimino)methyl)phenoxy)undecanoate (VIII-10)

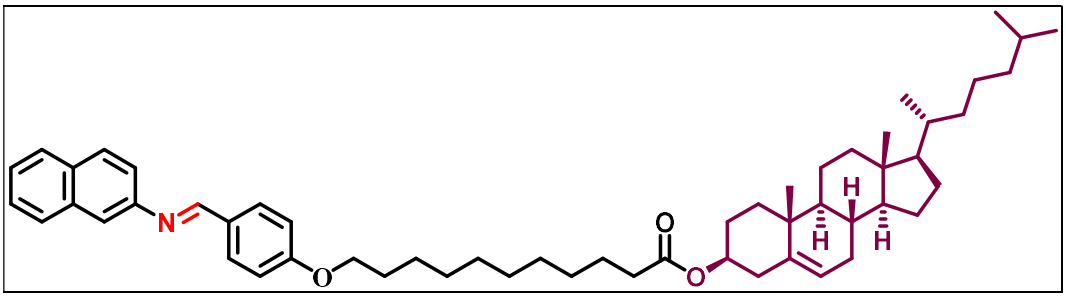

White solid, Yield: 68 %; **IR** ν_{max}/cm^{-1}: 3056.80, 2936.41 (C_{sp3}-H), 2867.07, 1725.61 (ester C=O), 1604.13 (-CH=N-), 1253.60 (C-O), 1172.54, 827.19; **^{1}H NMR (400 MHz,**

$CDCl_3$): δ (In ppm): 8.53 (s, 1H, -N=CH-), 7.91 (d, *J* = 8.8 Hz, 2H, Ar-H), 7.88 (d, *J* = 8.4 Hz, 2H, Ar-H), 7.59 (d, *J* = 8.4 Hz, 1H, Ar-H), 7.51 (s, 1H, Ar-H), 7.45 (d, *J* = 8.0 Hz, 1H, Ar-H), 7.38 (d, *J* = 7.6 Hz, 2H, Ar-H), 7.01 (d, *J* = 8.4 Hz, 2H, Ar-H), 5.39 (brd, *J* = 3.2 Hz, 1H, olefinic), 4.64 (m, 1H, CHOCO), 4.05 (t, *J* = 6.4 Hz, 2H, OCH_2), 2.38-2.28 (m, 4H, 2 X allylic CH_2), 2.04–0.92 (m, 48H, 6 X CH, 9 X CH_2, 8 X CH_2 chain, 2 X CH_3, 1 X CH_2-COO), 0.88 (d, *J* = 2.3 Hz, 6H, 2 X CH_3), 0.69 (s, 3H, CH_3) ; **^{13}C NMR (400MHz, $CDCl_3$): δ (In ppm):** 172.32 (C=O), 160.89 (Ar C-O-), 158.97 (CH=N), 148.96, 138.64, 133.11, 129.55, 127.97, 127.83, 126.78, 125.34, 124.22, 121.58, 120.33, 116.48, 113.67, 72.67 (CHOCO), 67.13 (Ar-O-C-), 55.61, 55.04, 52.41, 48.93, 41.24, 38.65, 38.47, 37.11, 35.93, 35.12, 34.76, 33.66, 30.85, 28.26, 28.03, 27.20, 26.98, 24.94, 24.00, 23.24, 22.78, 21.81, 21.54, 19.97, 10.81; **Elemental Analysis**: $C_{55}H_{79}NO_3$:(cal): C, 82.55; H, 9.70; N, 1.75; found C, 82.51; H, 9.69; N, 1.73; %;

5.6 Spectras

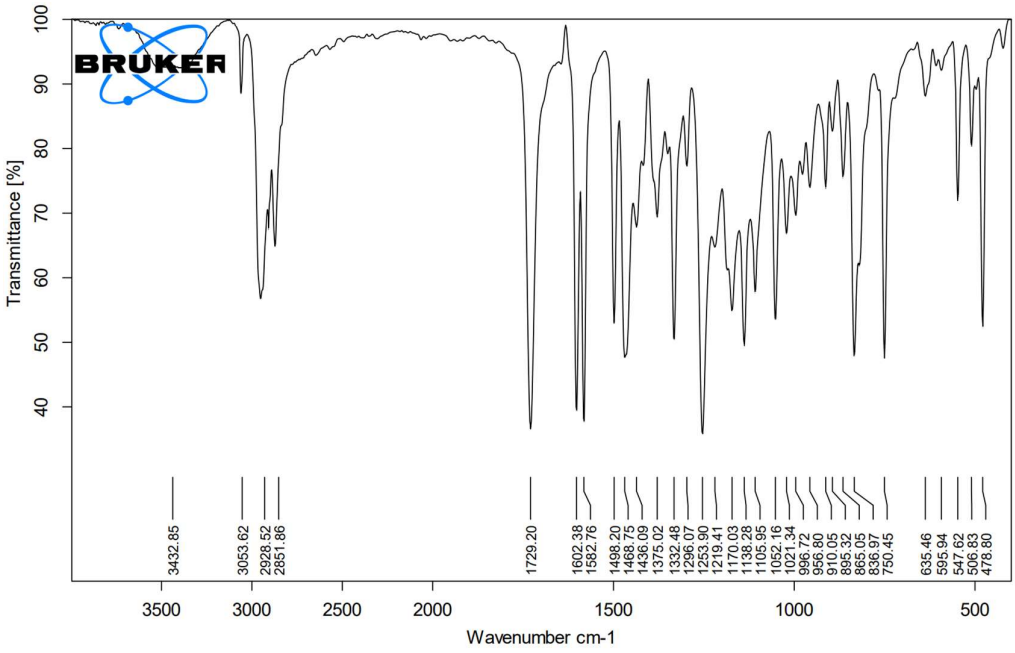

Fig. S5.1: FT-IR spectra of *VII-1*

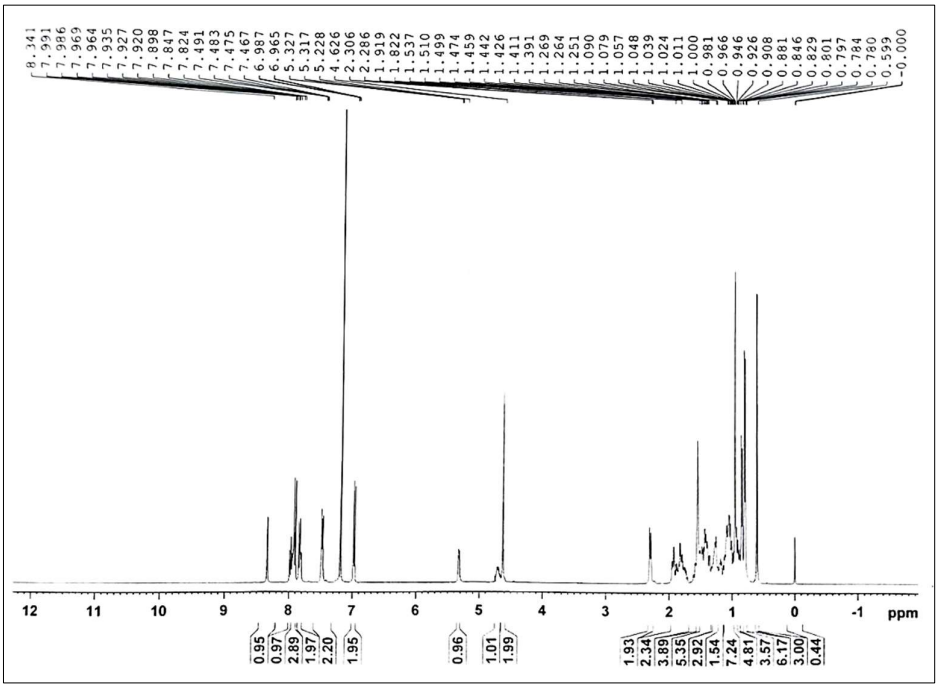

Fig. S5.2: ^{1}H-NMR spectra of *VII-1*

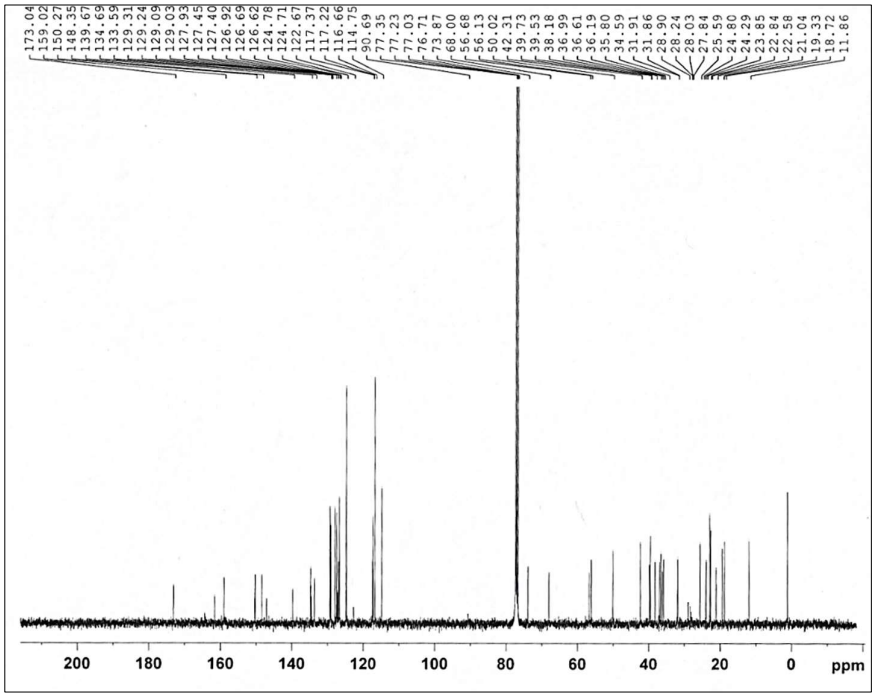

Fig. S5.3: ^{13}C-NMR spectra of *VII-1*

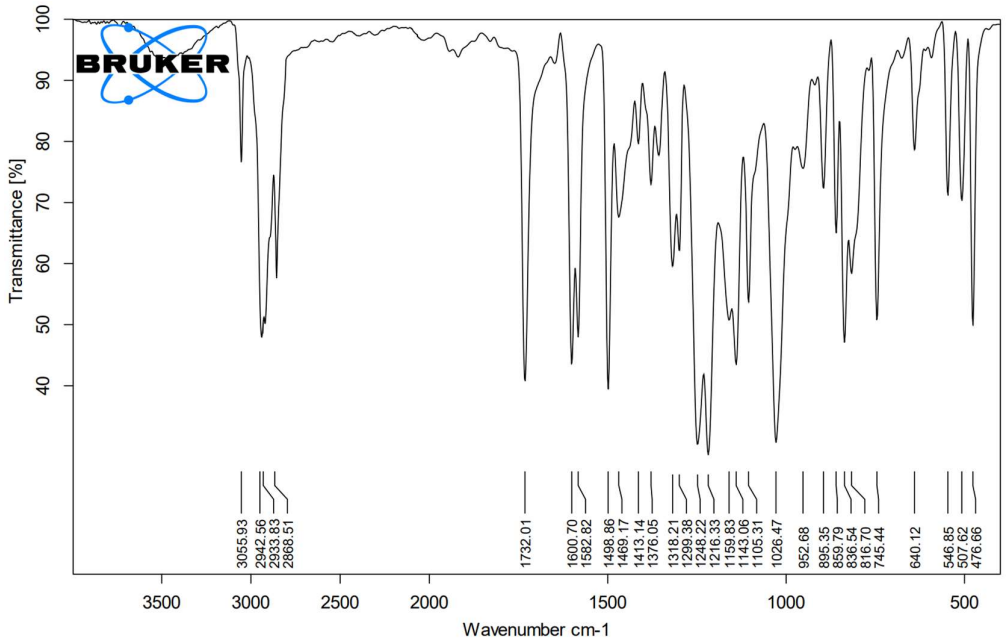

Fig. S5.4: FT-IR spectra of *VII-2*

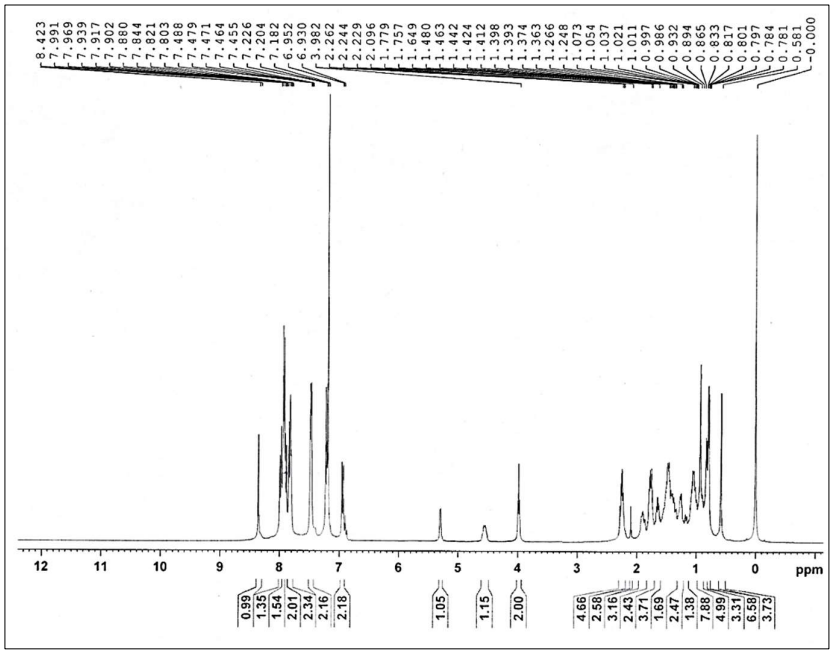

Fig. S5.5: ^{1}H-NMR spectra of *VII-2*

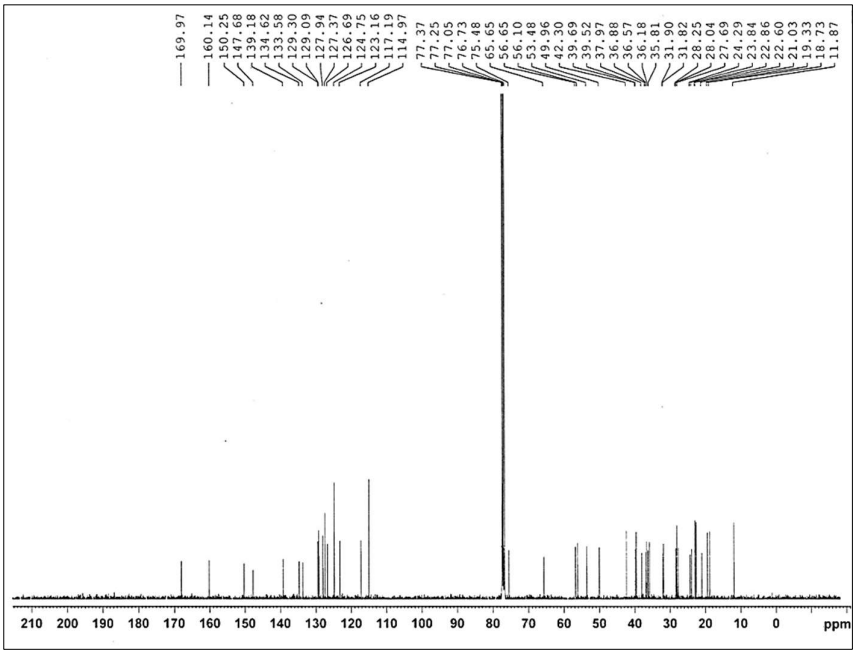

Fig. S5.6: ^{13}C-NMR spectra of *VII-2*

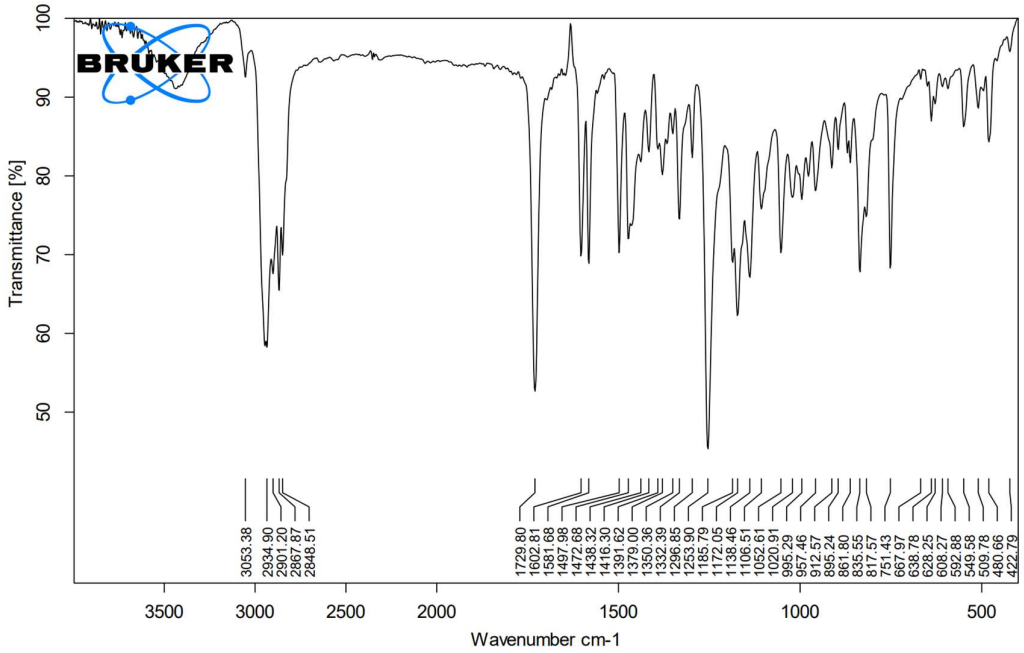

Fig. S5.7: FT-IR spectra of *VII-3*

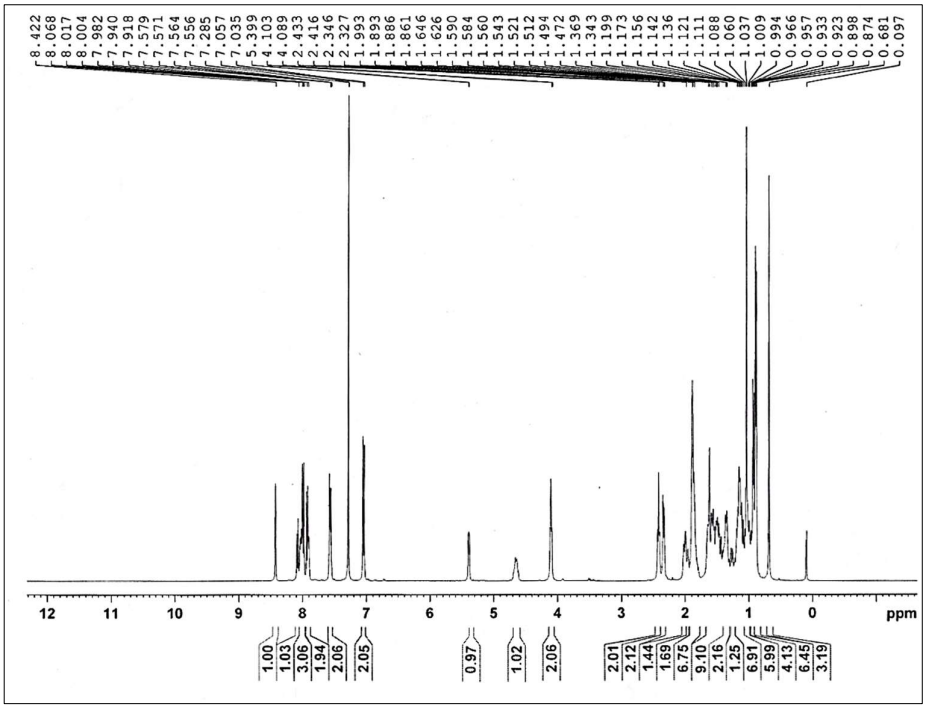

Fig. S5.8: ^{1}H-NMR spectra of *VII-3*

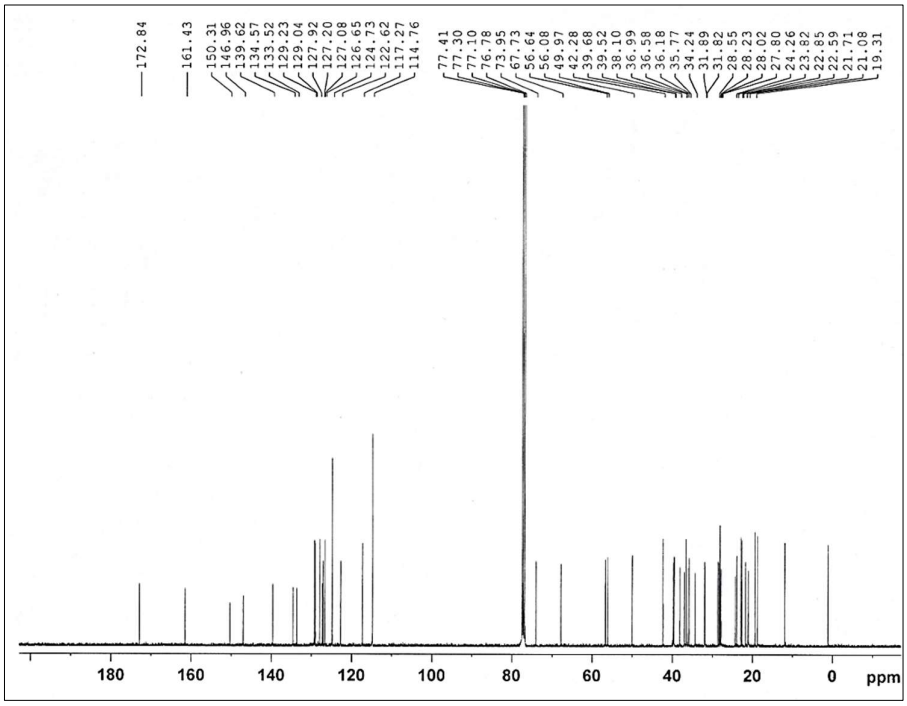

Fig. S5.9: ^{13}C-NMR spectra of *VII-3*

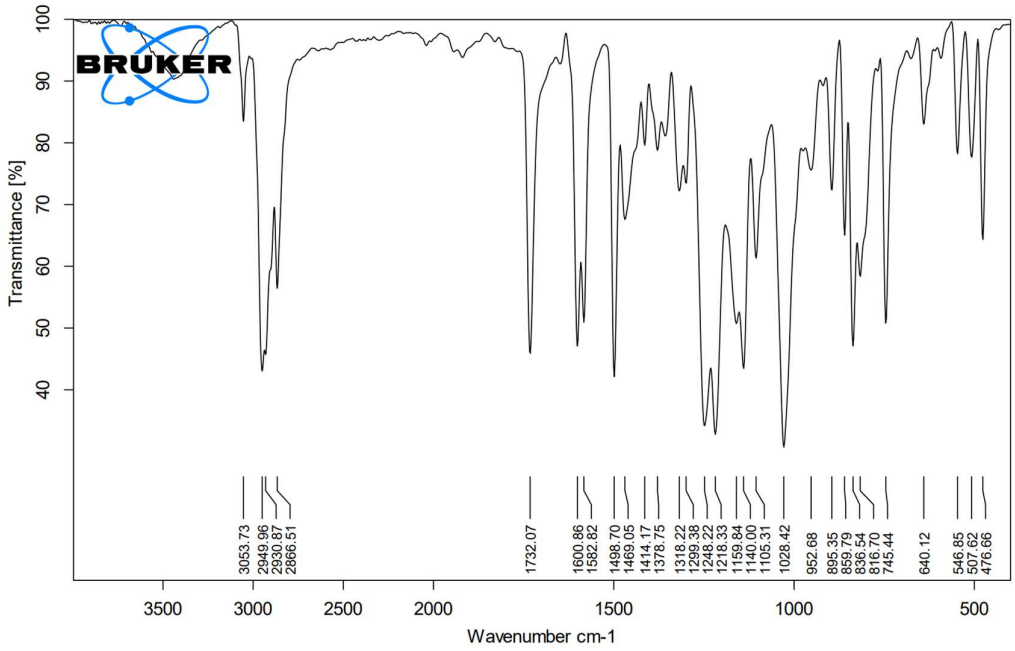

Fig. S5.10: FT-IR spectra of *VII-4*

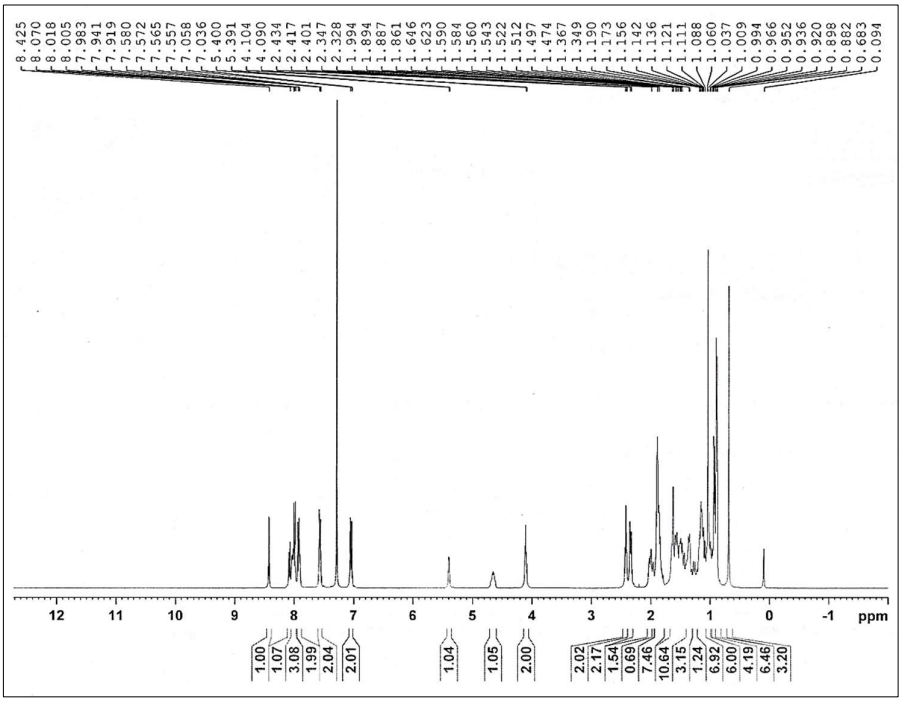

Fig. S5.11: ^{1}H-NMR spectra of *VII-4*

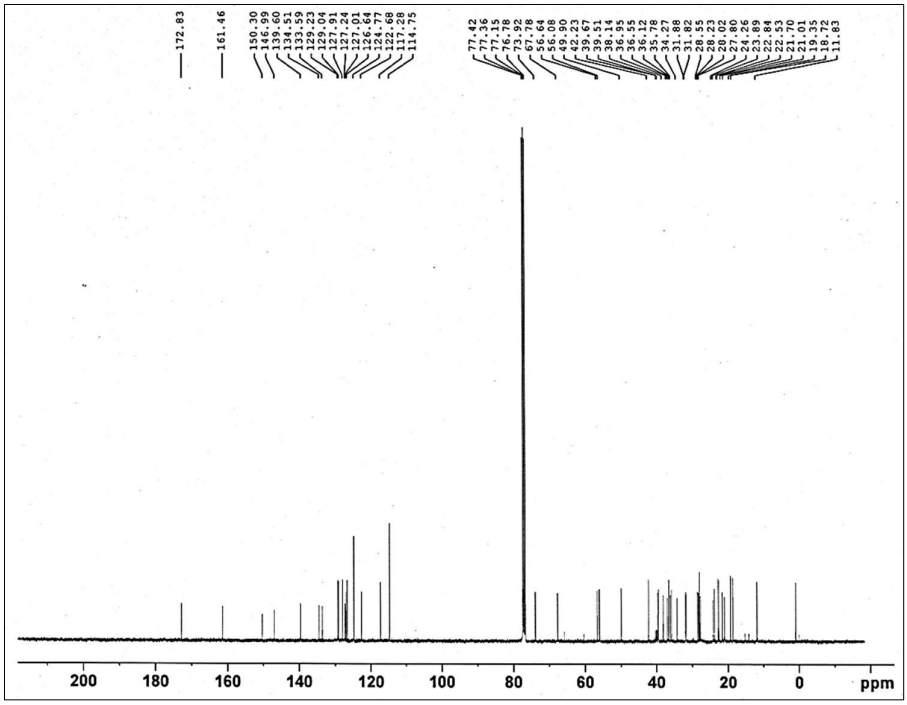

Fig. S5.12: ^{13}C-NMR spectra of *VII-4*

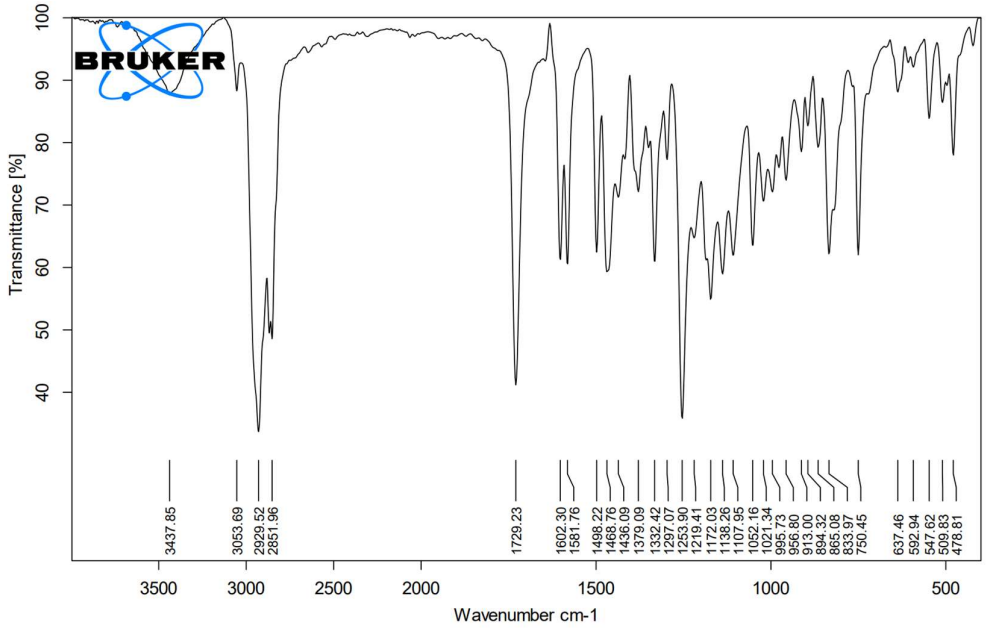

Fig. S5.13: FT-IR spectra of *VII-5*

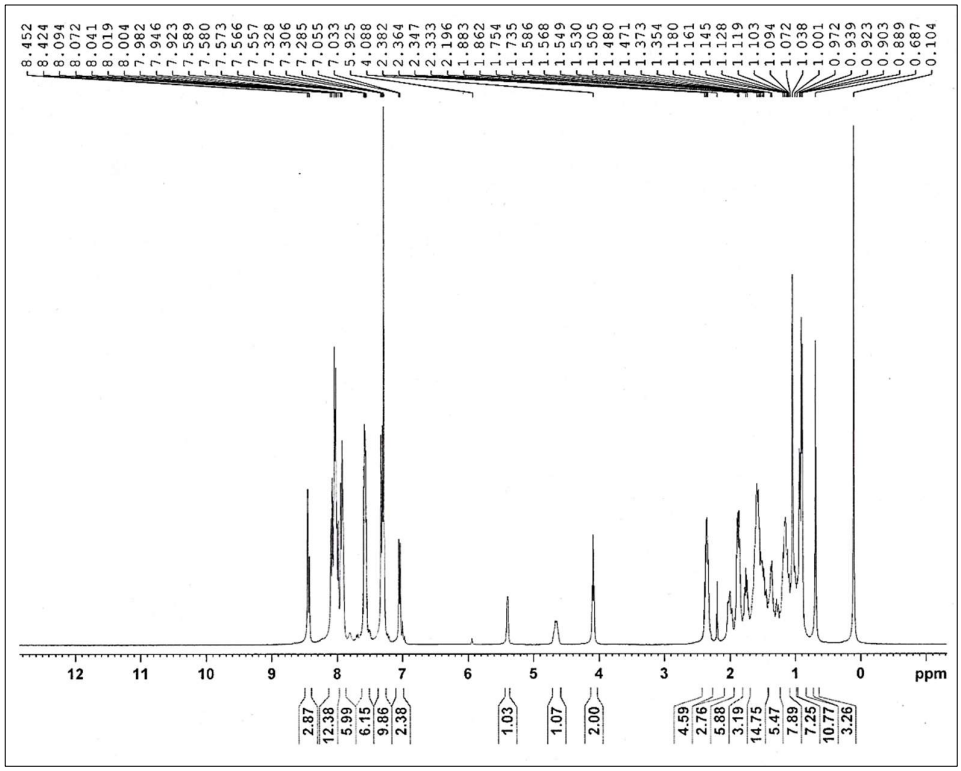

Fig. S5.14: ^{1}H-NMR spectra of *VII-5*

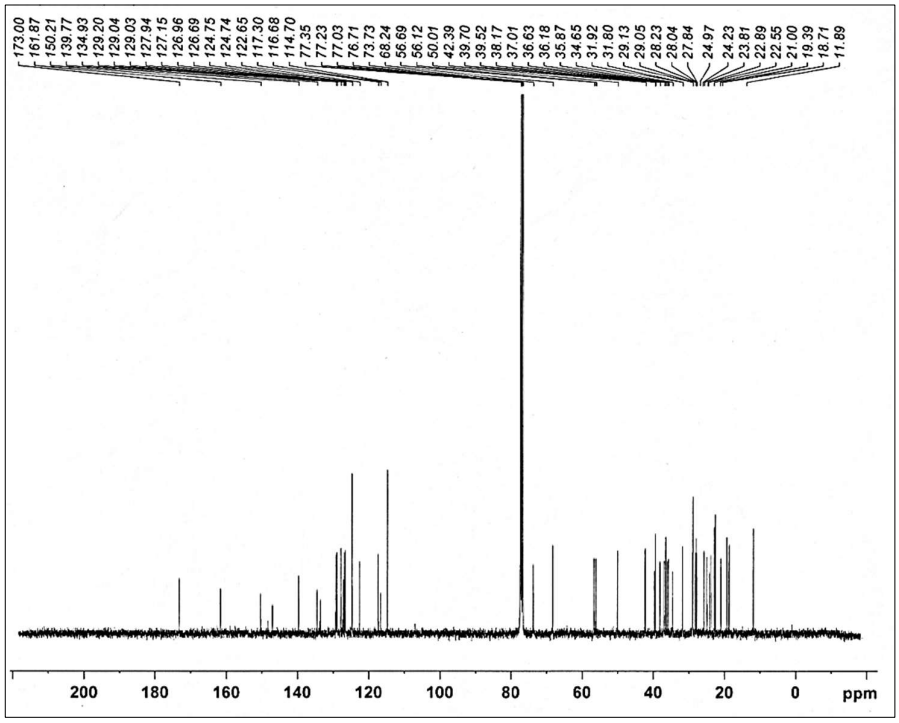

Fig. S5.15: ^{13}C-NMR spectra of *VII-5*

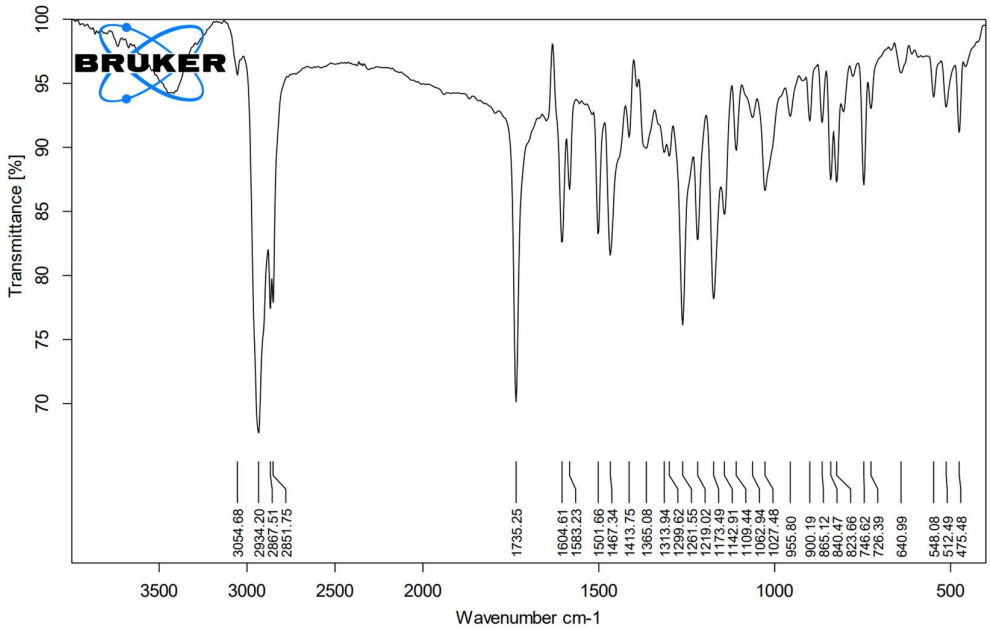

Fig. S5.16: FT-IR spectra of *VII-7*

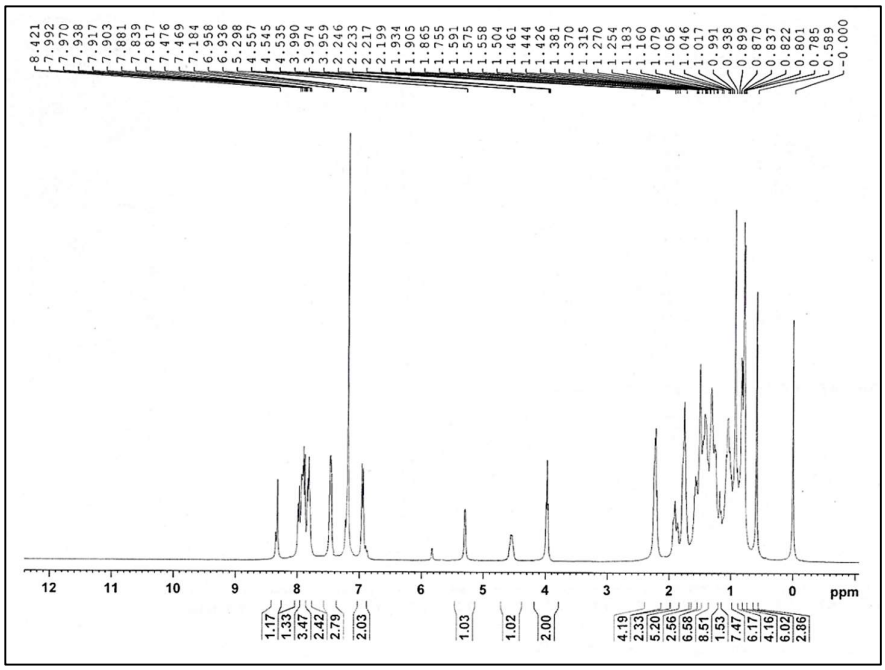

Fig. S5.17: ^{1}H-NMR spectra of *VII-7*

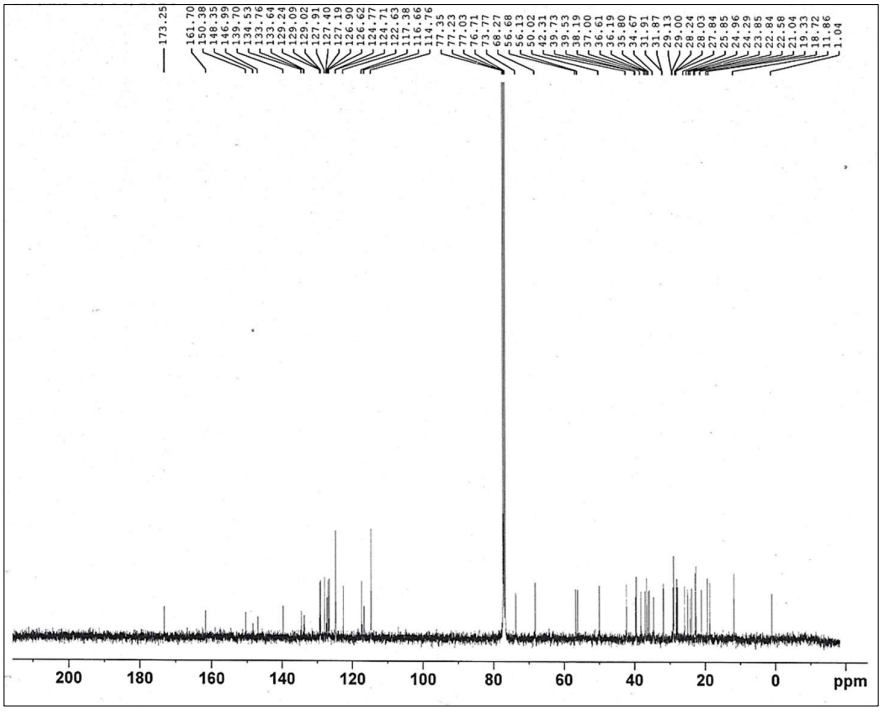

Fig. S5.18: ^{13}C-NMR spectra of *VII-7*

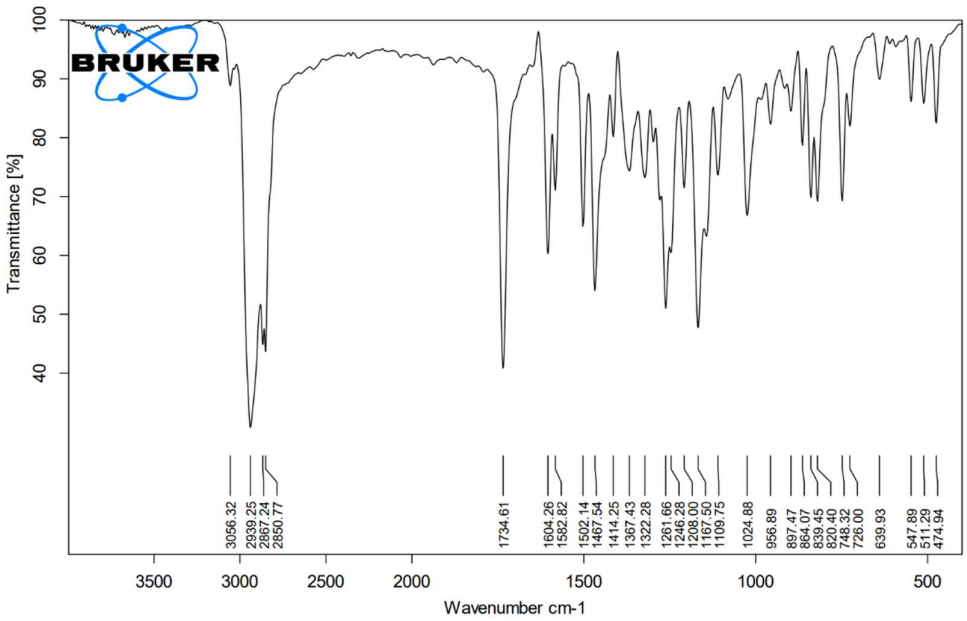

Fig. S5.19: FT-IR spectra of *VII-9*

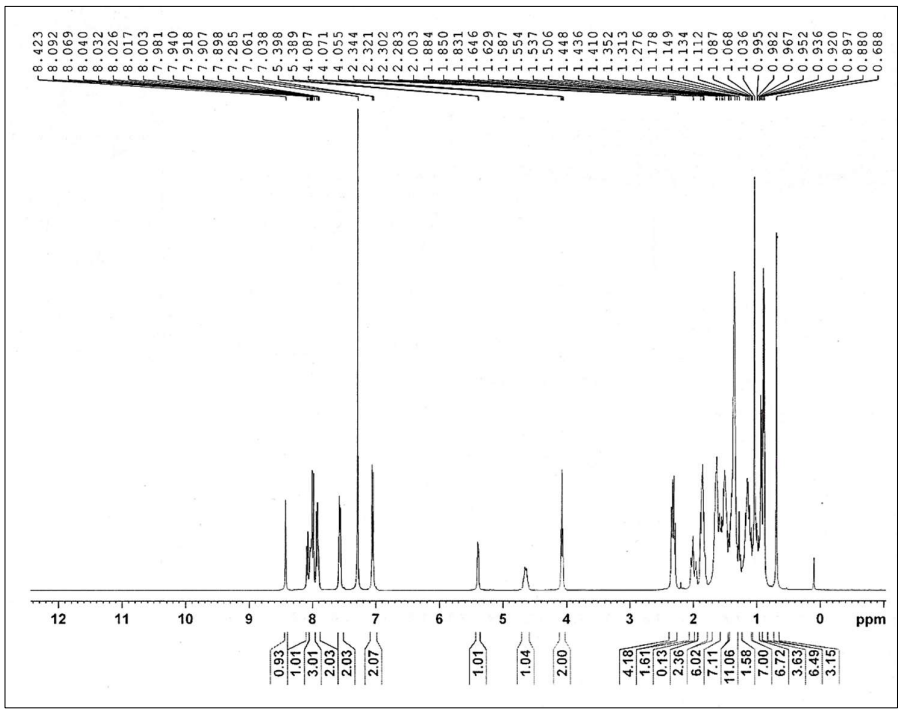

Fig. S5.20: ^{1}H-NMR spectra of *VII-9*

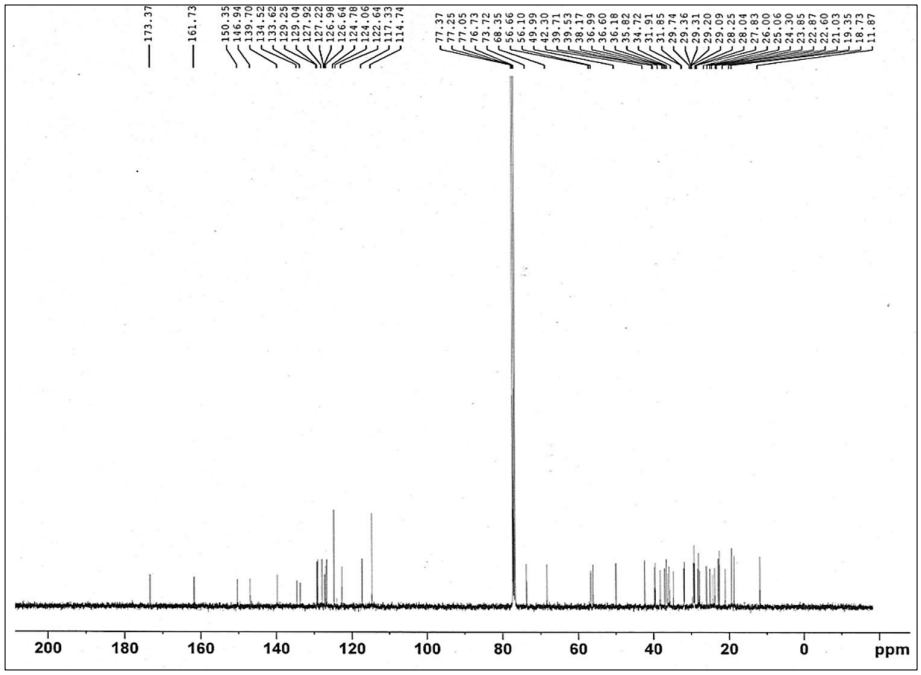

Fig. S5.21: ^{13}C-NMR spectra of *VII-9*

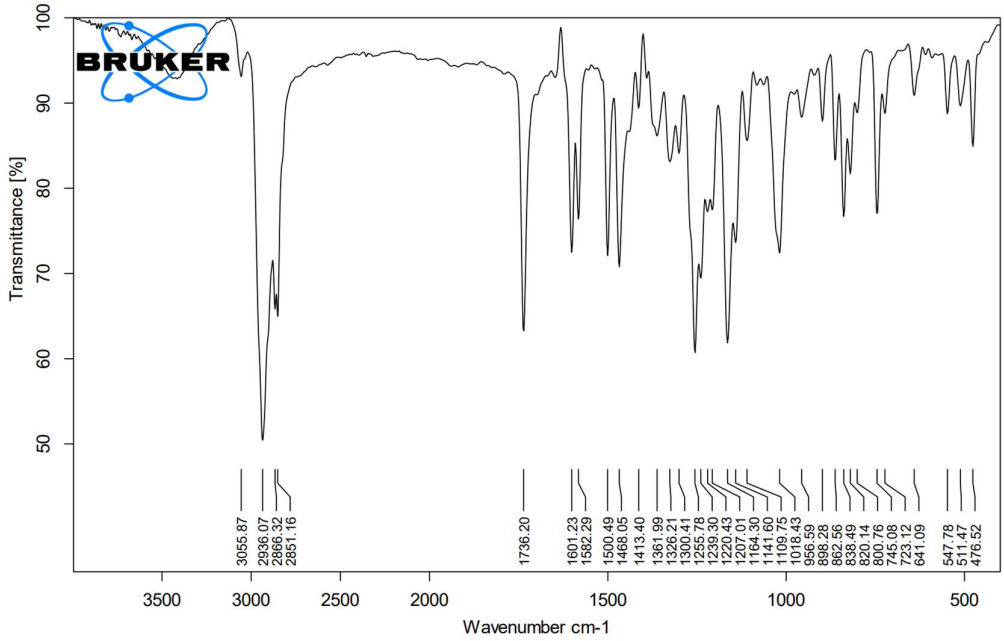

Fig. S5.22: FT-IR spectra of *VII-10*

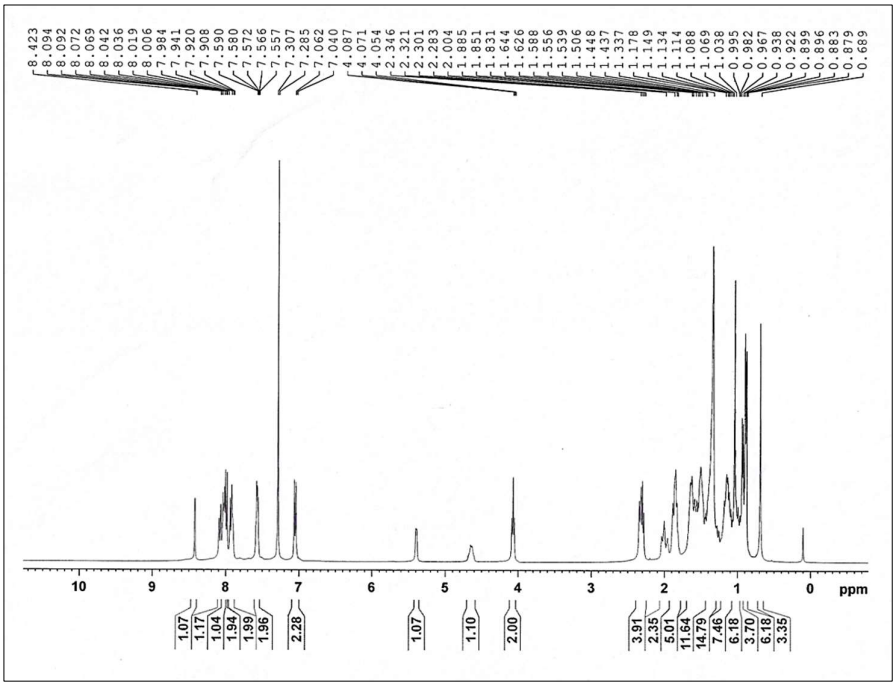

Fig. S5.23: ^{1}H-NMR spectra of *VII-10*

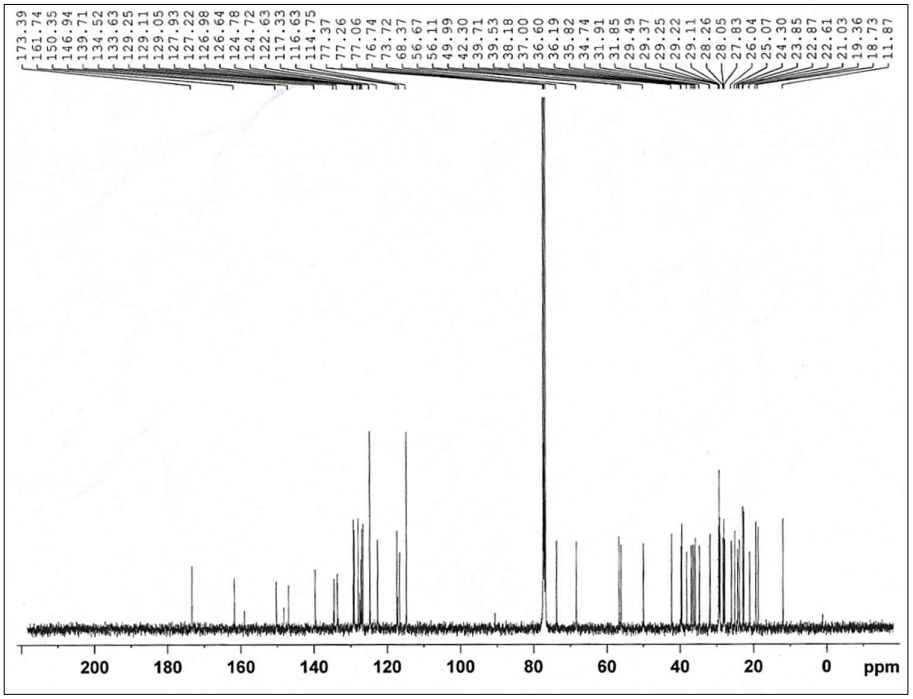

Fig. S5.24: ^{13}C-NMR spectra of *VII-10*

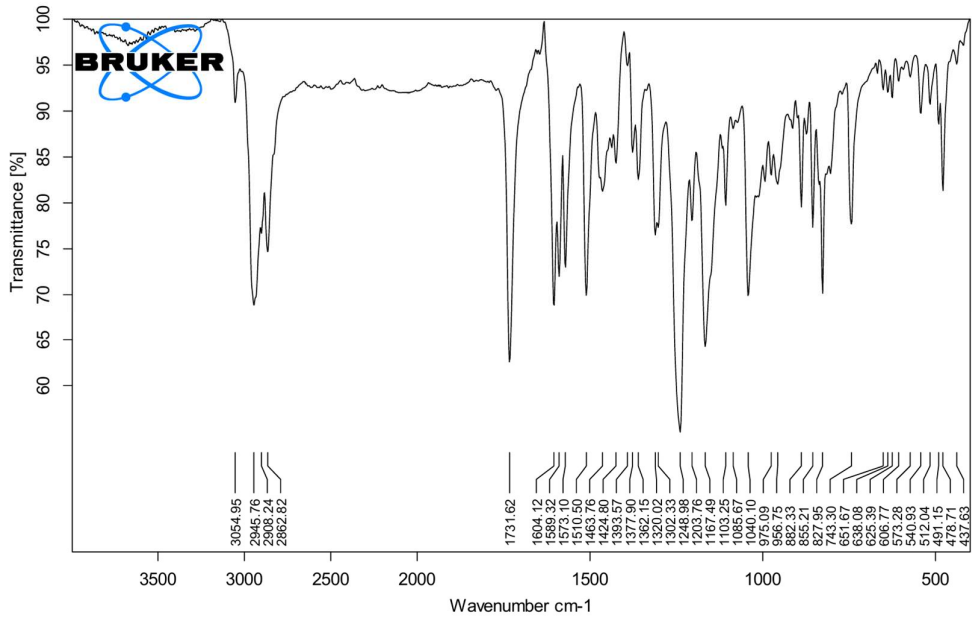

Fig. S5.25: FT-IR spectra of *VIII-1*

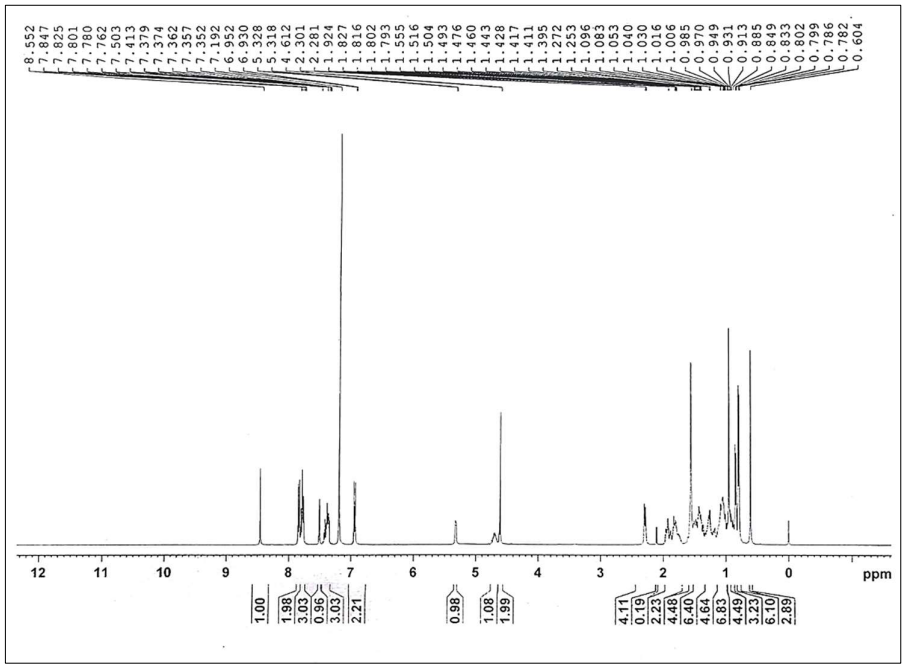

Fig. S5.26: ^{1}H-NMR spectra of *VIII-1*

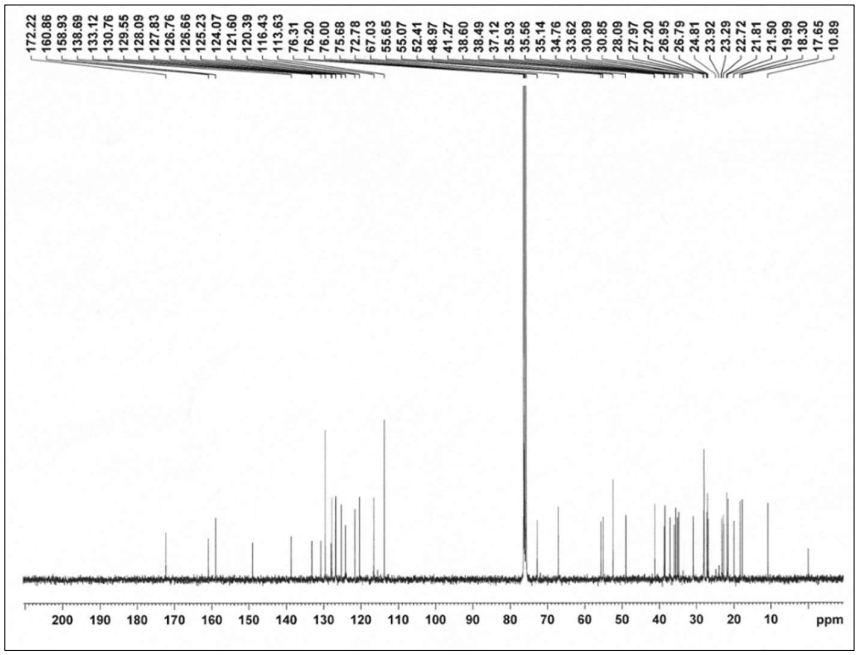

Fig. S5.27: ^{13}C-NMR spectra of *VIII-1*

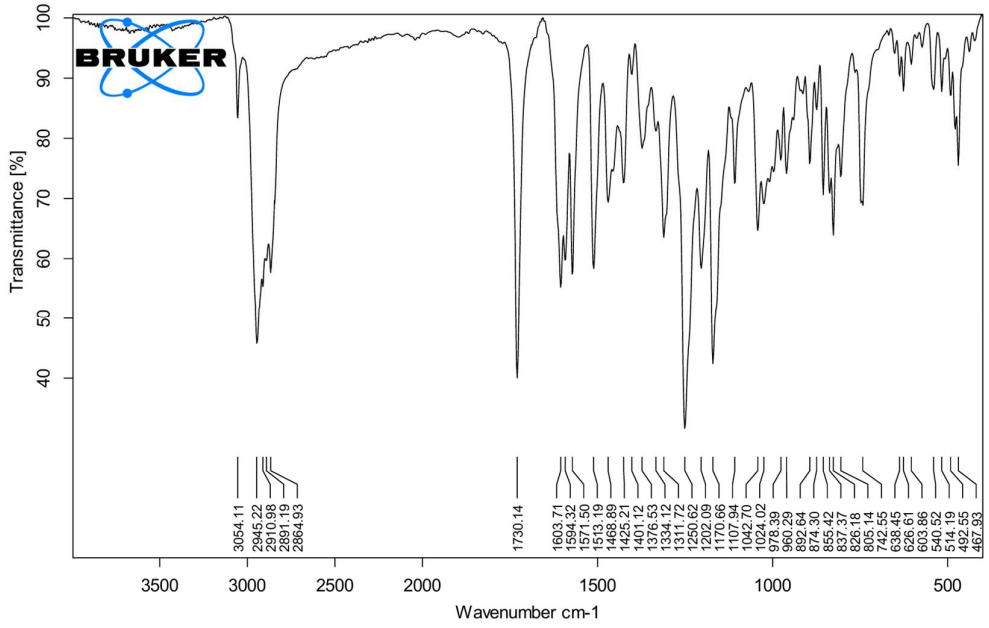

Fig. S5.28: FT-IR spectra of *VIII-2*

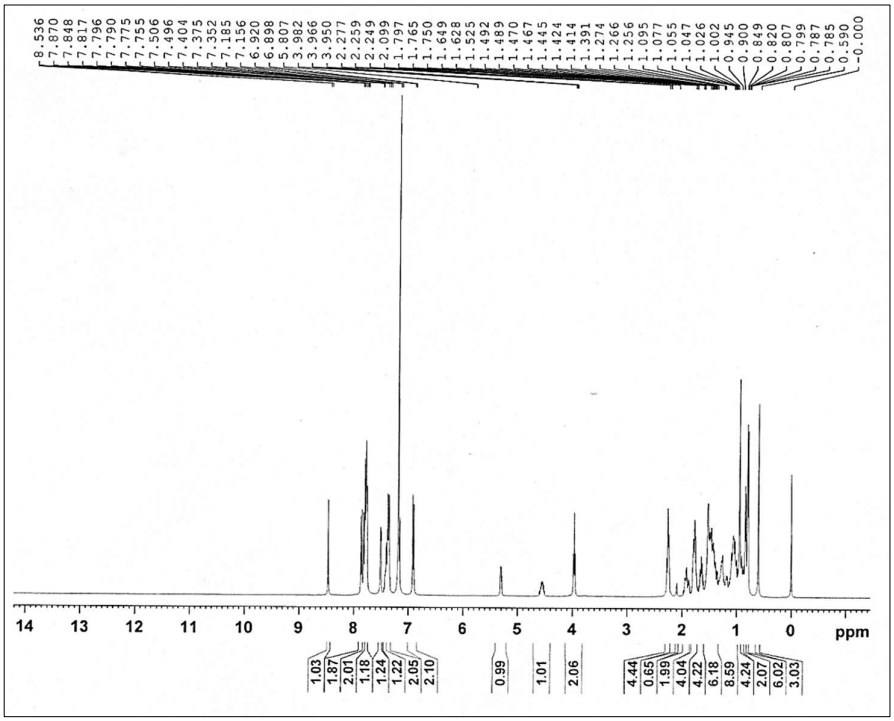

Fig. S5.29: ^{1}H-NMR spectra of *VIII-2*

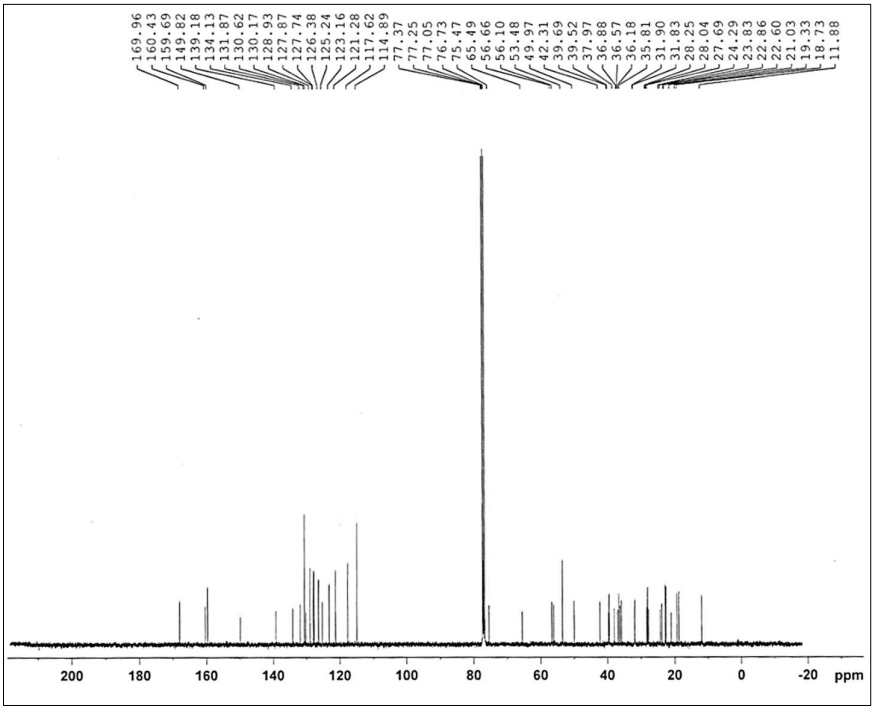

Fig. S5.30: ^{13}C-NMR spectra of *VIII-2*

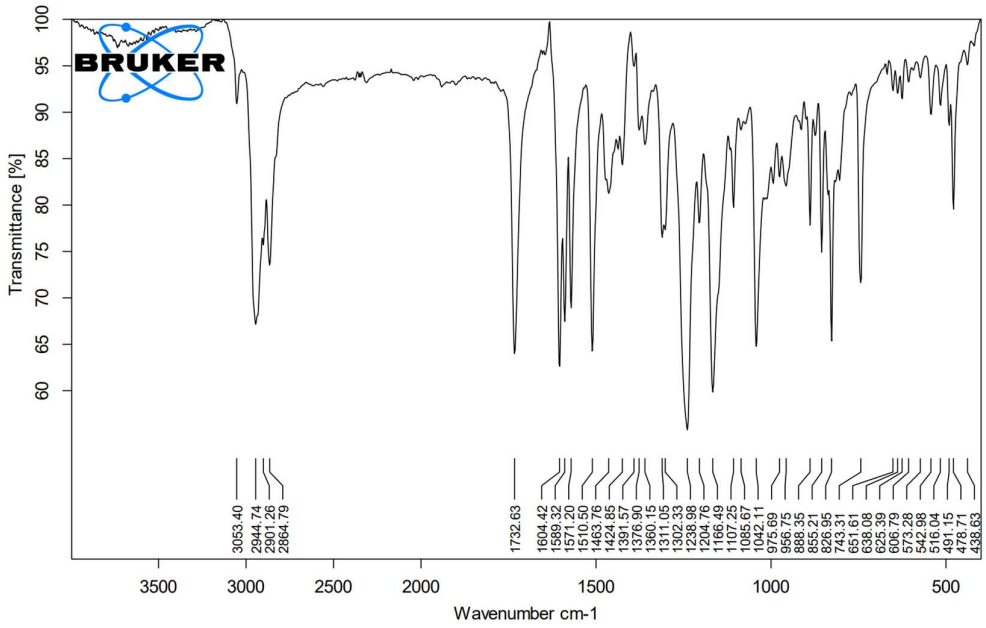

Fig. S5.31: FT-IR spectra of *VIII-3*

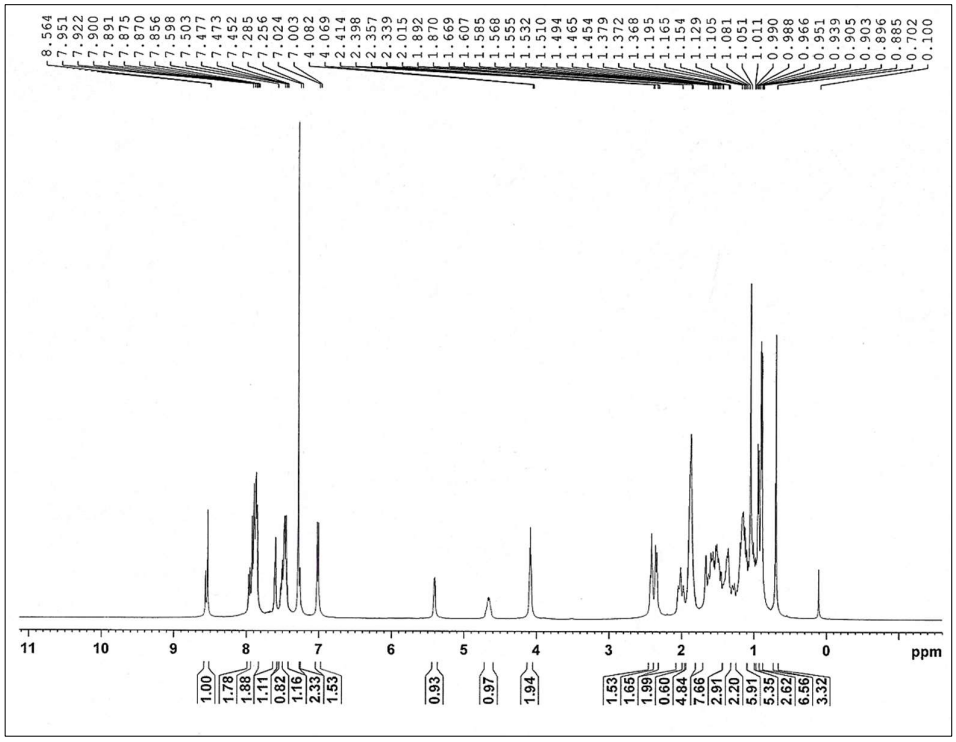

Fig. S5.32: ^{1}H-NMR spectra of *VIII-3*

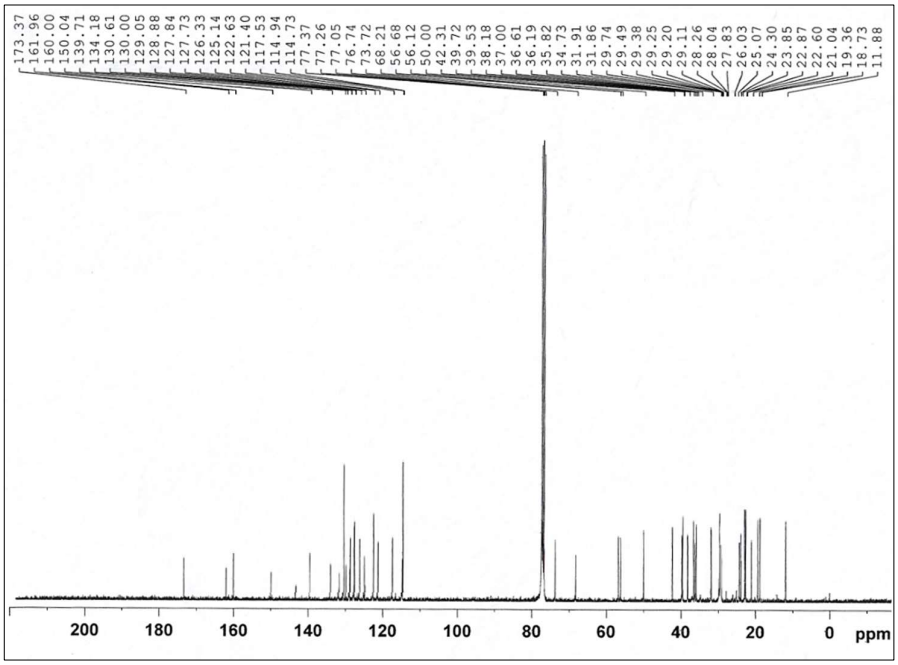

Fig. S5.33: ^{13}C-NMR spectra of *VIII-3*

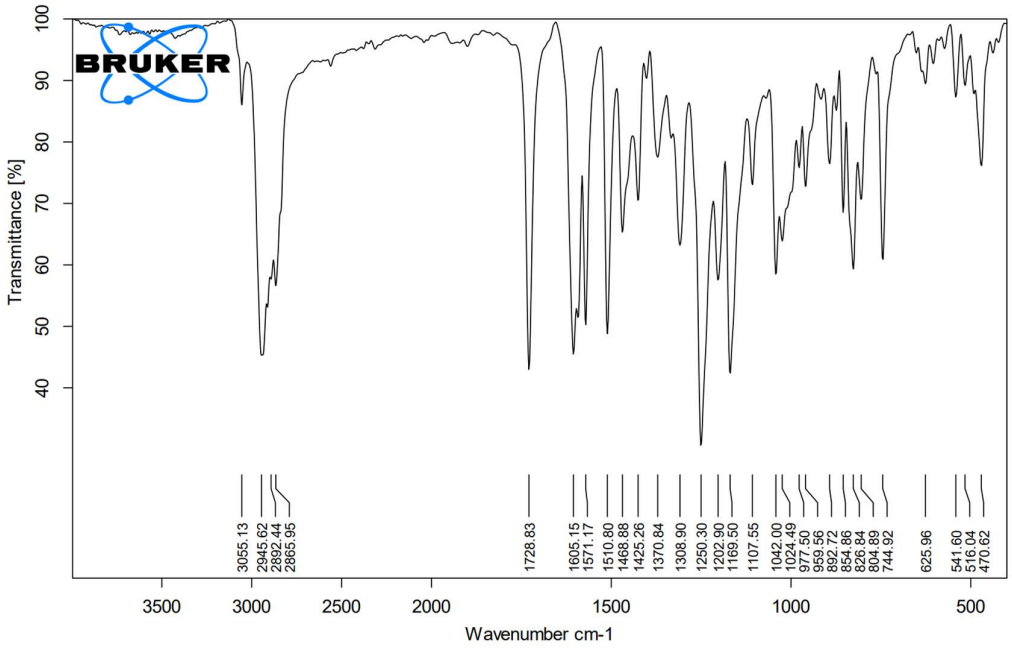

Fig. S5.34: FT-IR spectra of *VIII-4*

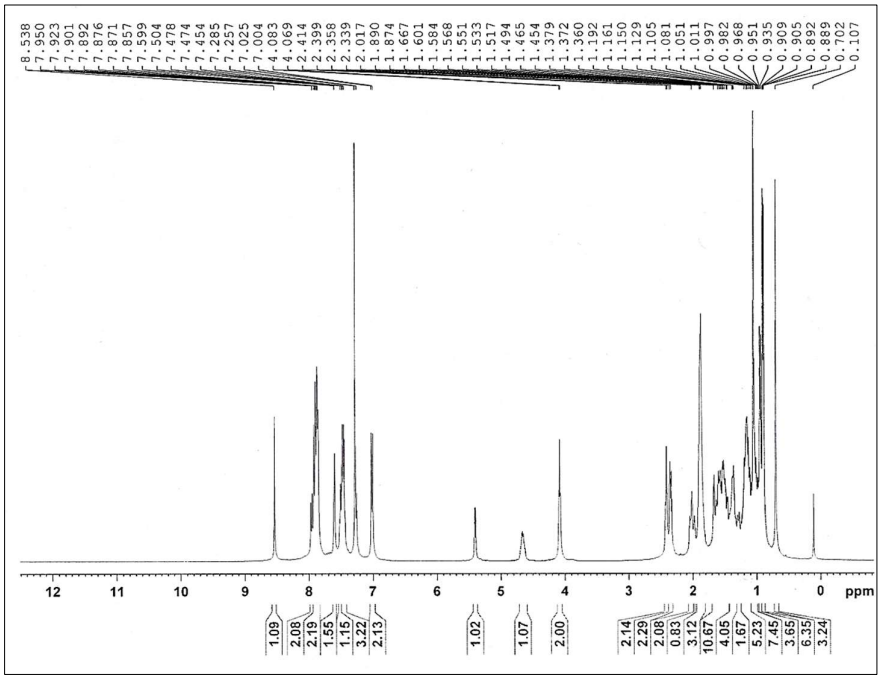

Fig. S5.35: ^{1}H-NMR spectra of *VIII-4*

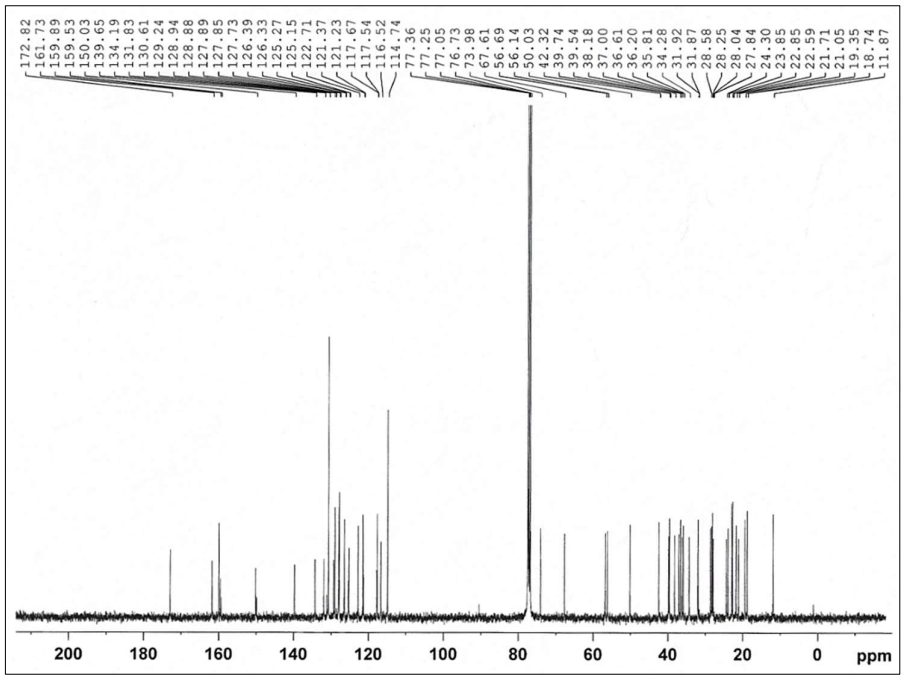

Fig. S5.36: ^{13}C-NMR spectra of *VIII-4*

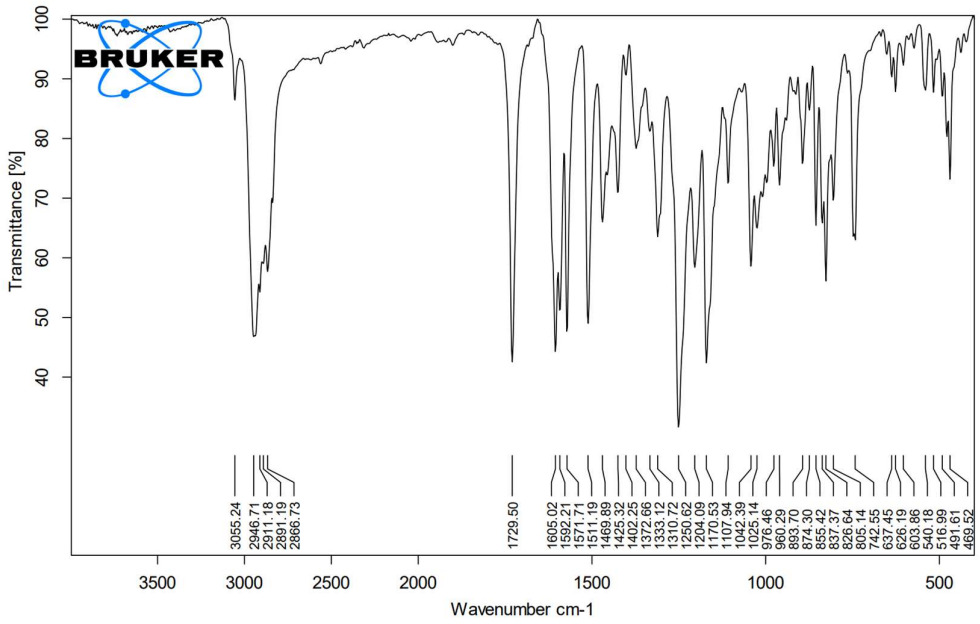

Fig. S5.37: FT-IR spectra of *VIII-5*

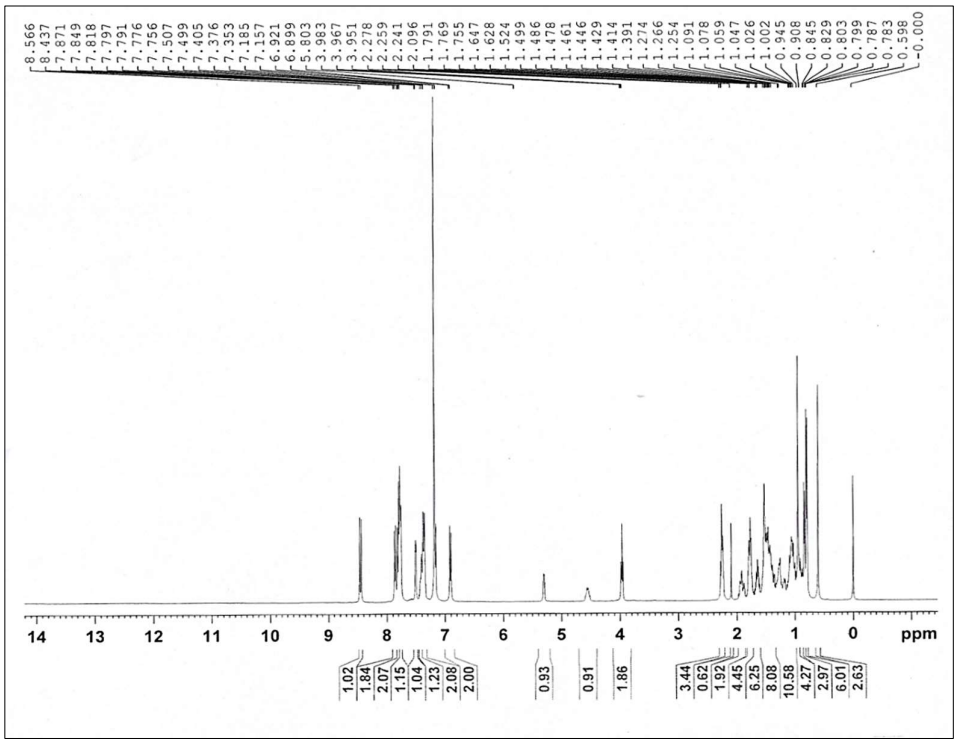

Fig. S5.38: ^{1}H-NMR spectra of *VIII-5*

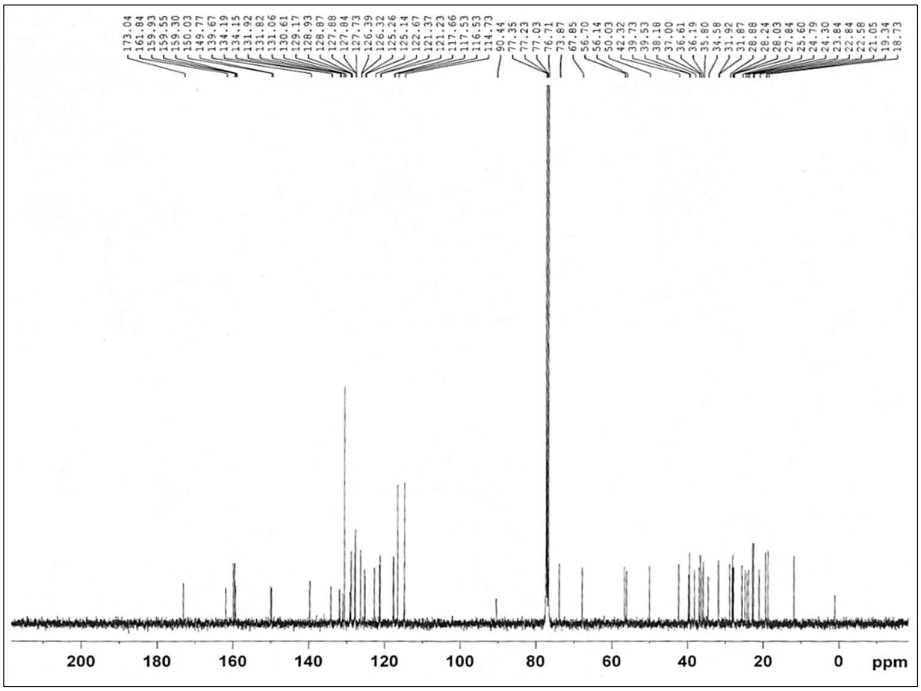

Fig. S5.39: ^{13}C-NMR spectra of *VIII-5*

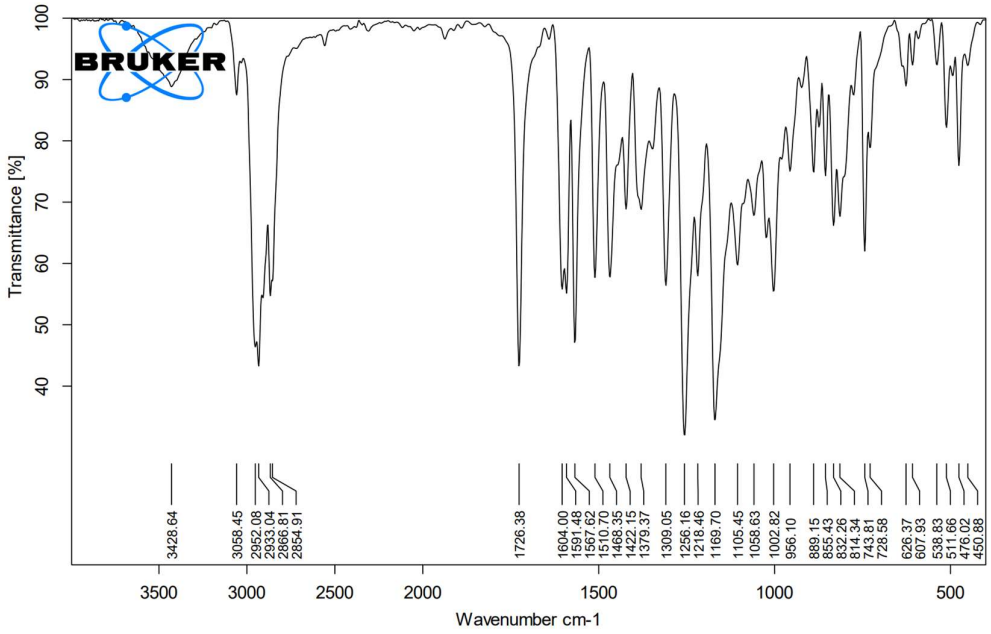

Fig. S5.40: FT-IR spectra of *VIII-7*

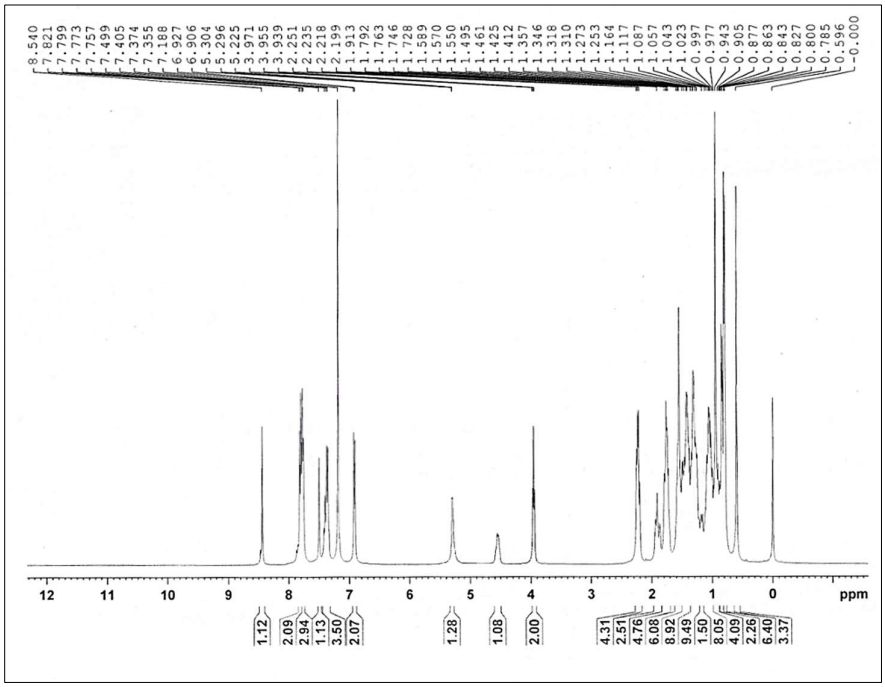

Fig. S5.41: ^{1}H-NMR spectra of *VIII-7*

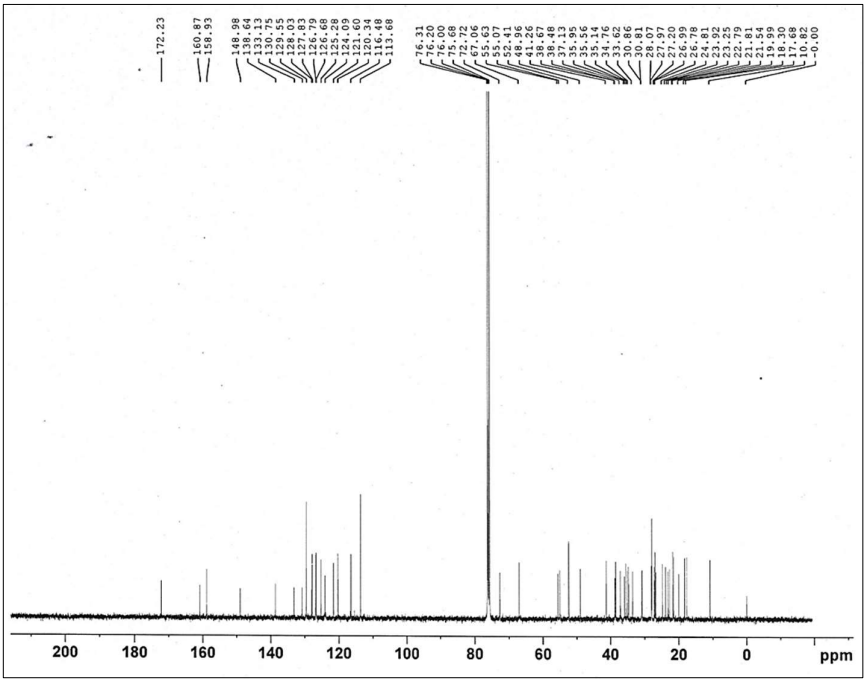

Fig. S5.42: ^{13}C-NMR spectra of *VIII-7*

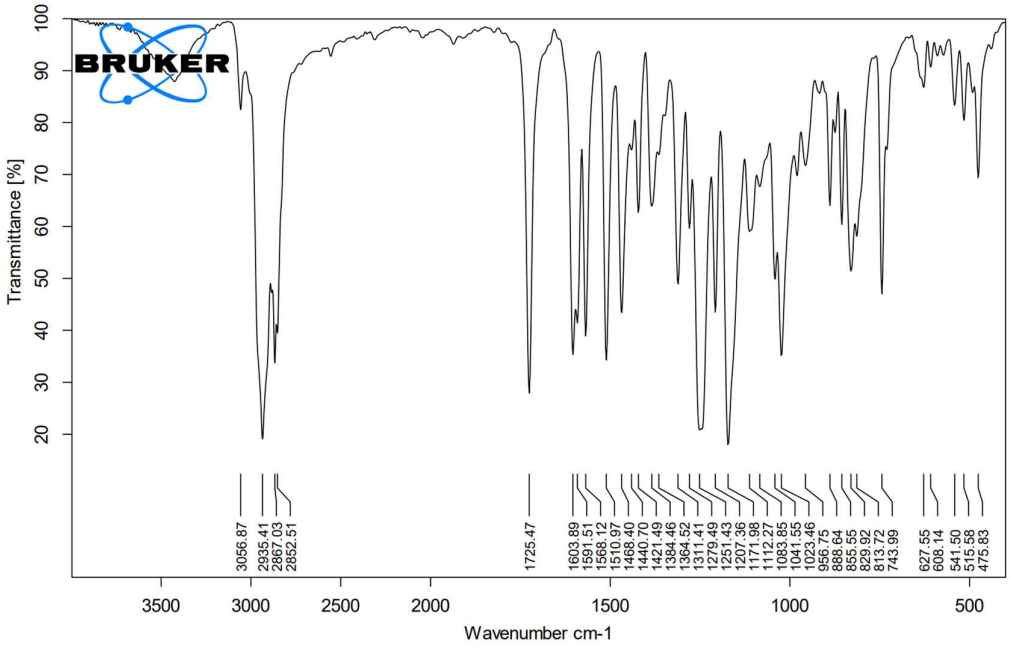

Fig. S5.43: FT-IR spectra of *VIII-9*

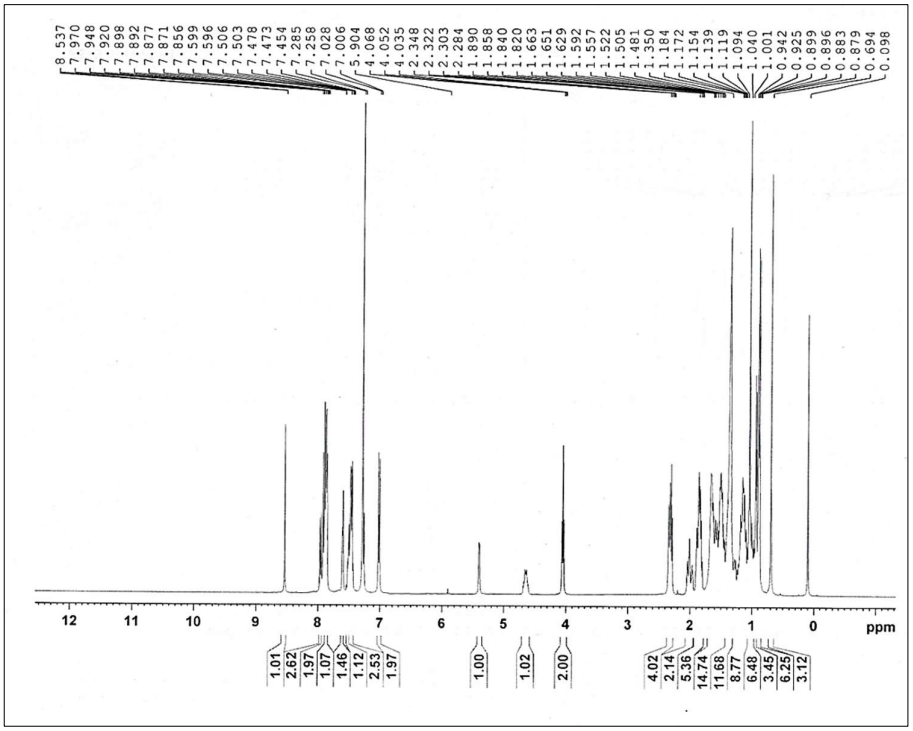

Fig. S5.44: ^{1}H-NMR spectra of *VIII-9*

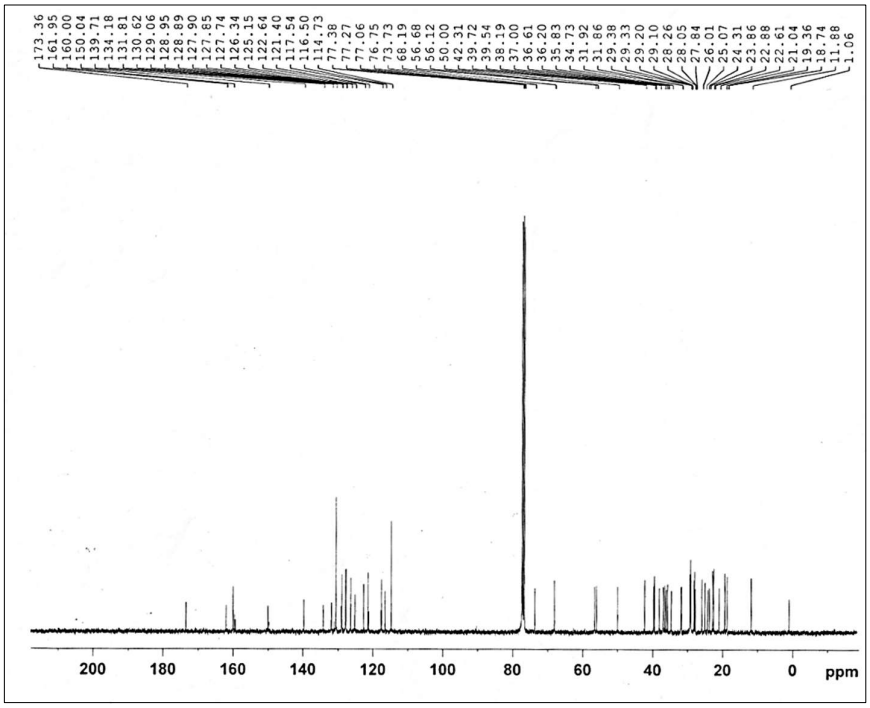

Fig. S5.45: ^{13}C-NMR spectra of *VIII-9*

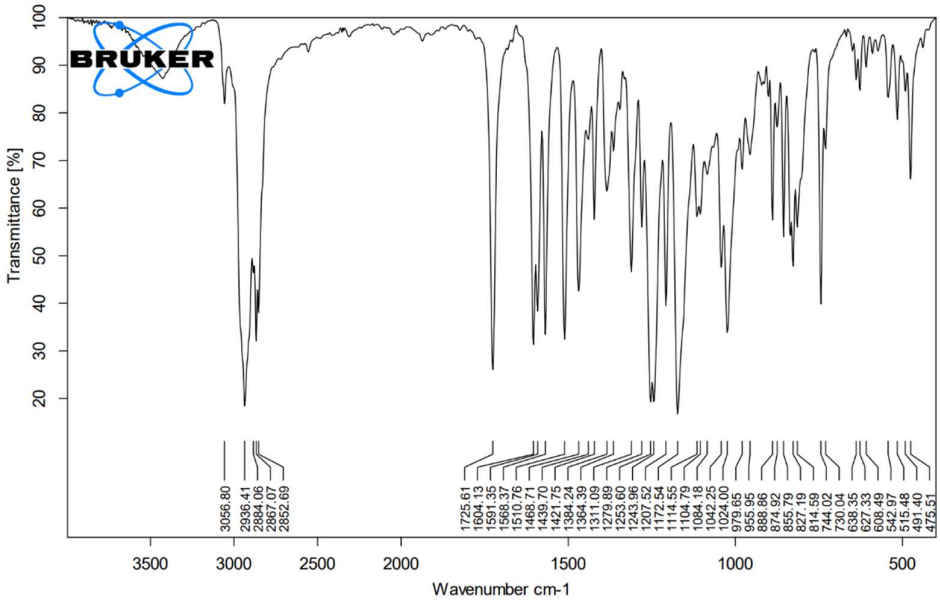

Fig. S5.46: FT-IR spectra of *VIII-10*

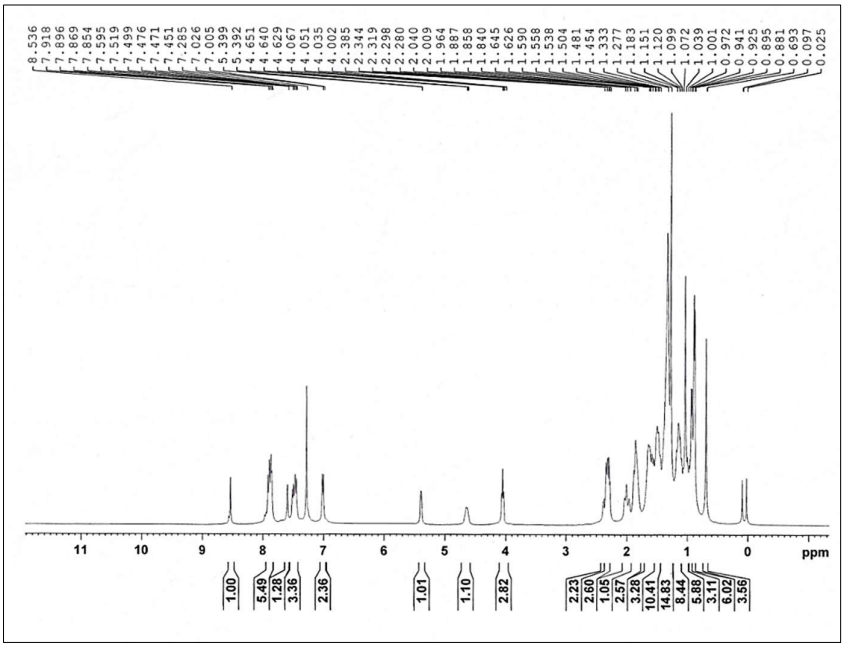

Fig. S5.47: ^{1}H-NMR spectra of *VIII-10*

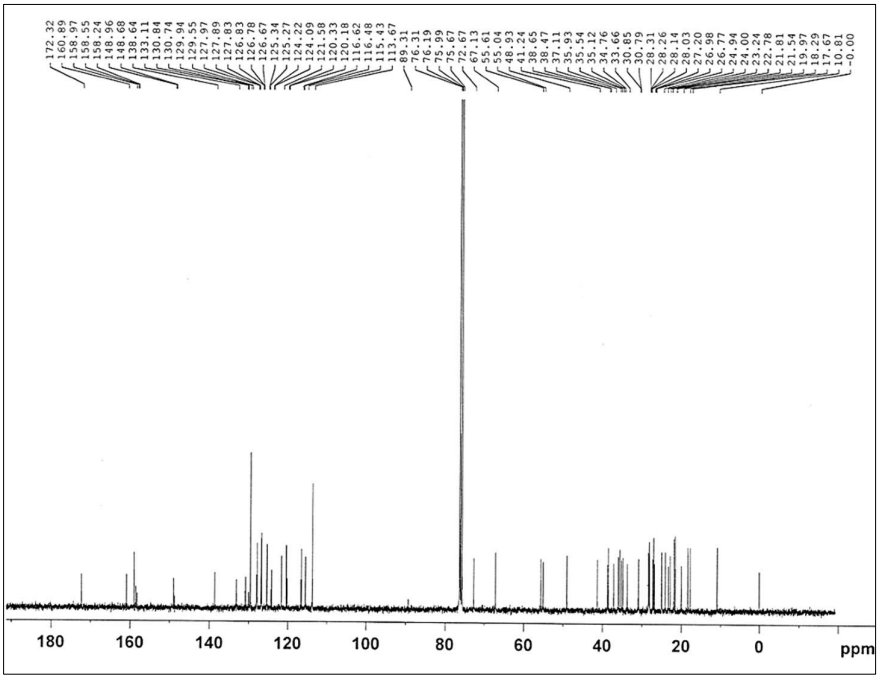

Fig. S5.48: ^{13}C-NMR spectra of *VIII-10*

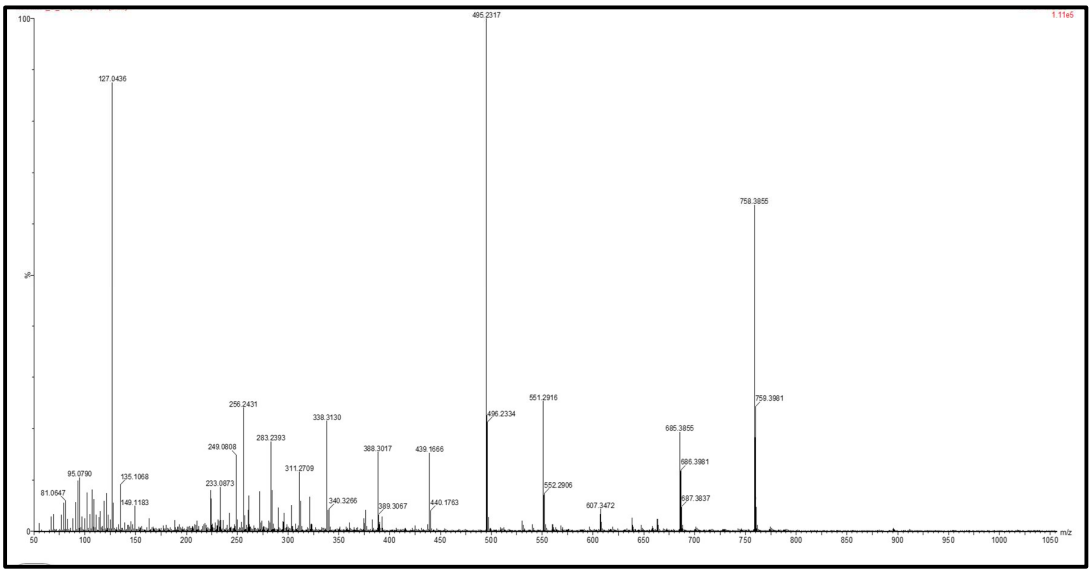

Fig. S5.49: Mass spectra of *VII-7*

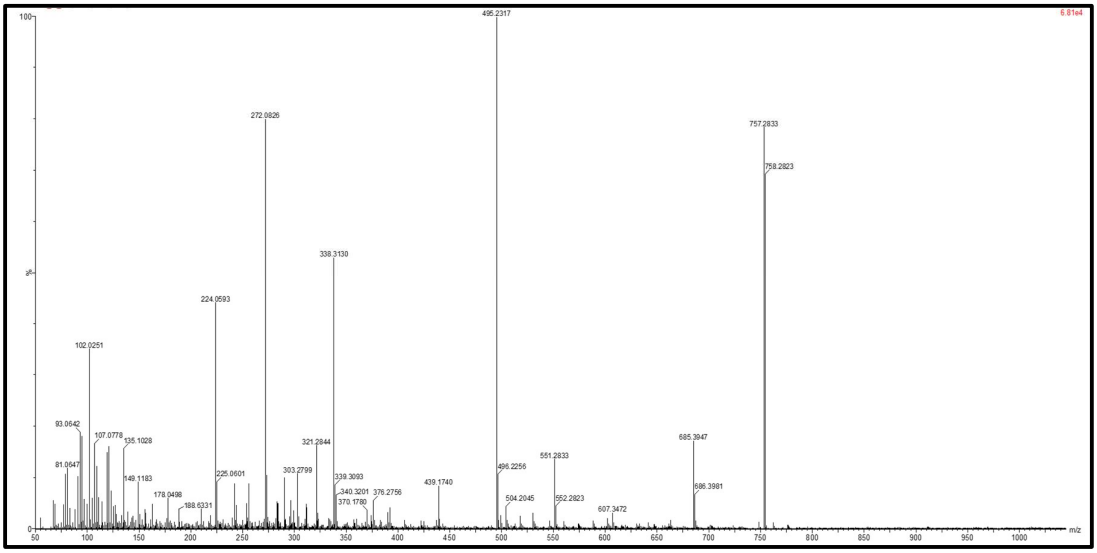

Fig. S5.50: Mass spectra of *VIII-7*

5.7 DSC thermograms of the prepared dimers

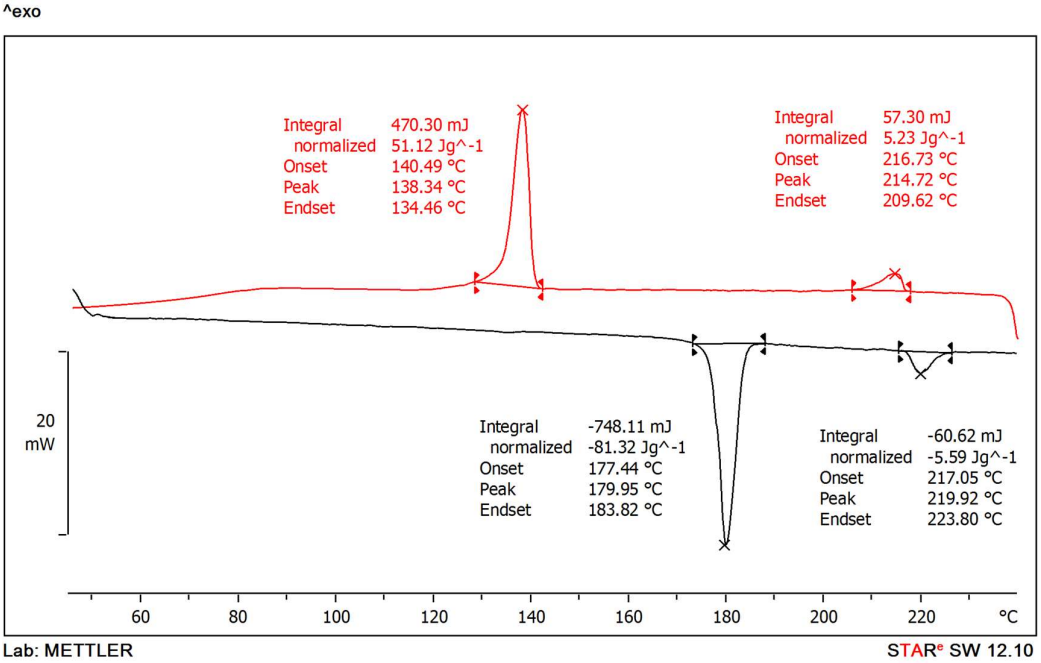

Fig. S5.51: DSC thermogram of *VII-3*

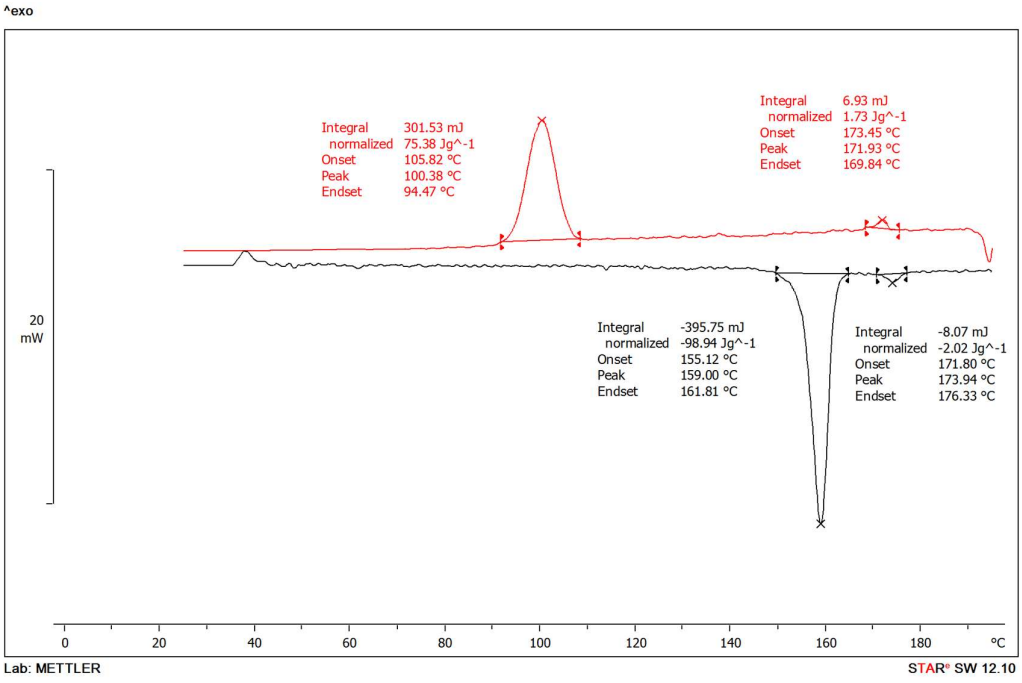

Fig. S5.52: DSC thermogram of *VII-4*

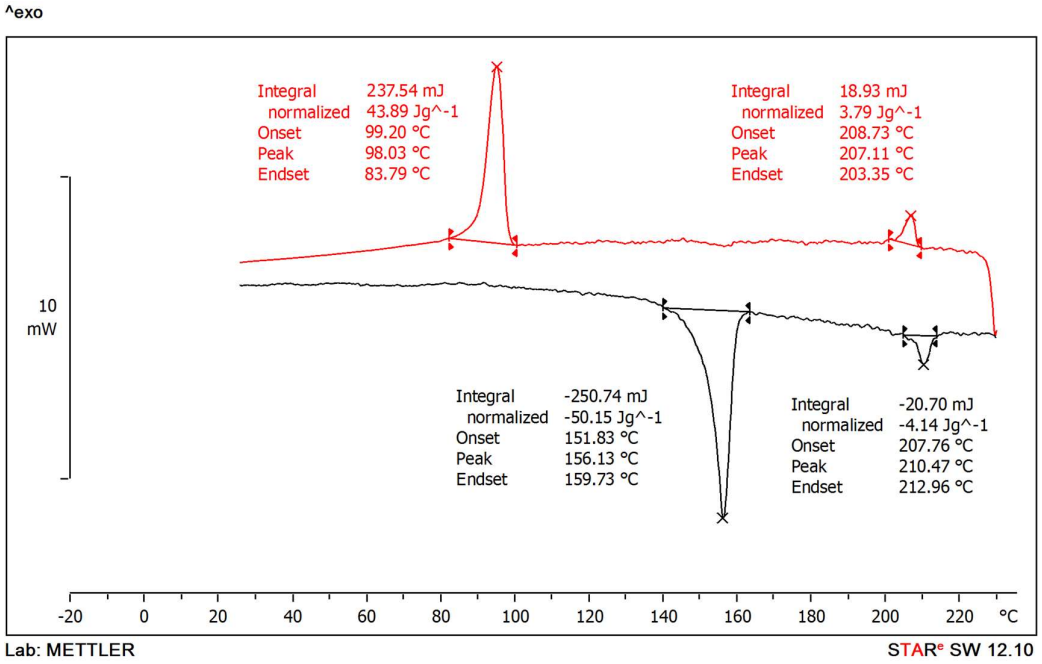

Fig. S5.53: DSC thermogram of *VII-5*

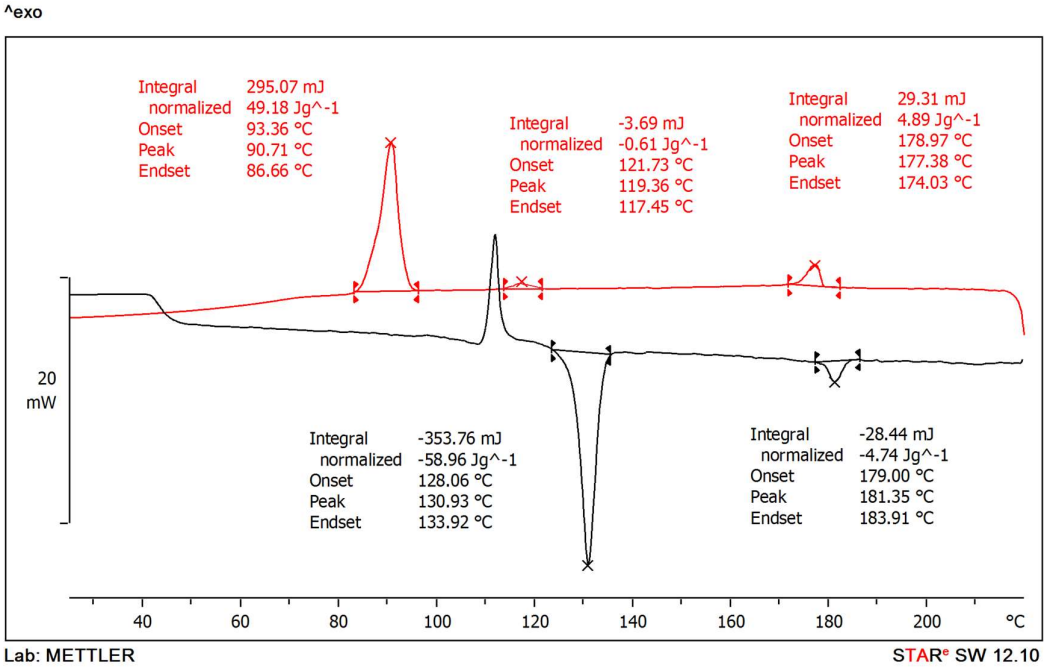

Fig. S5.54: DSC thermogram of *VII-7*

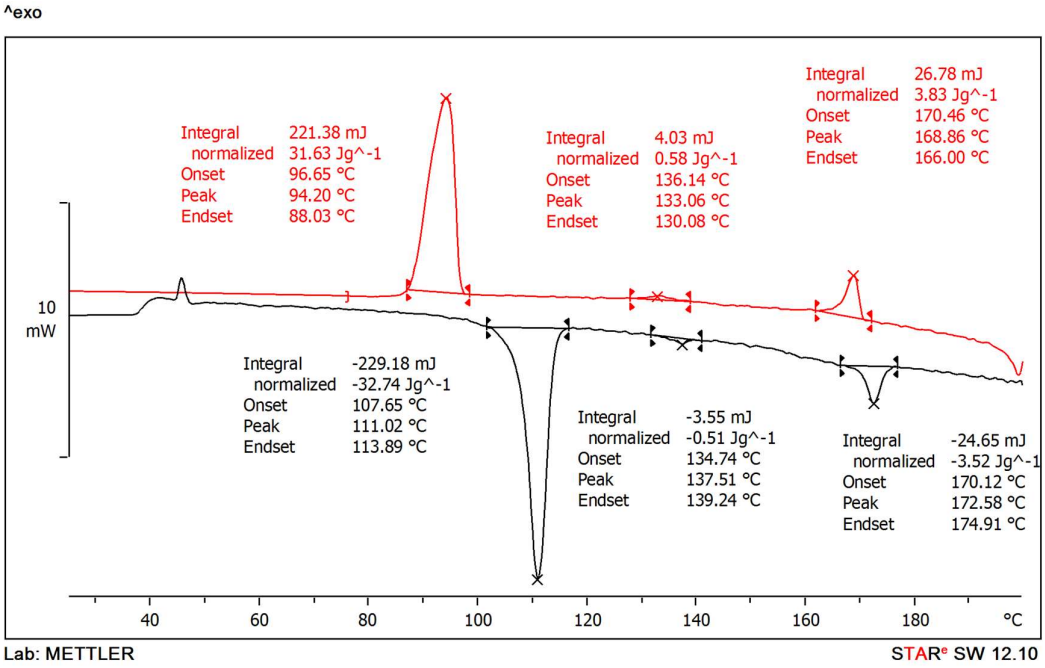

Fig. S5.55: DSC thermogram of *VII-9*

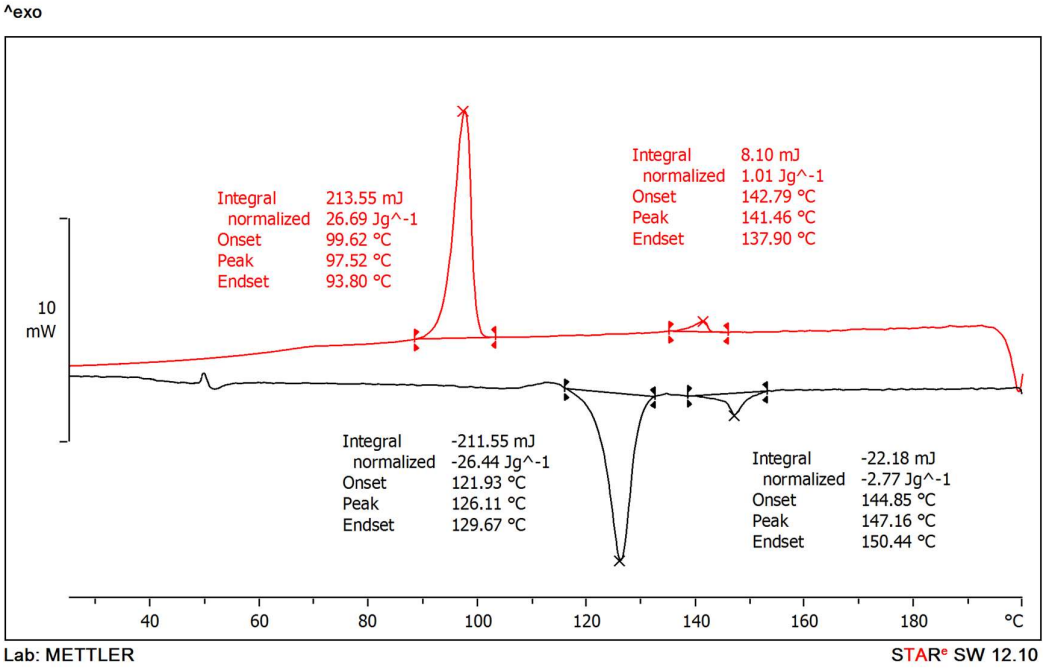

Fig. S5.56: DSC thermogram of *VII-10*

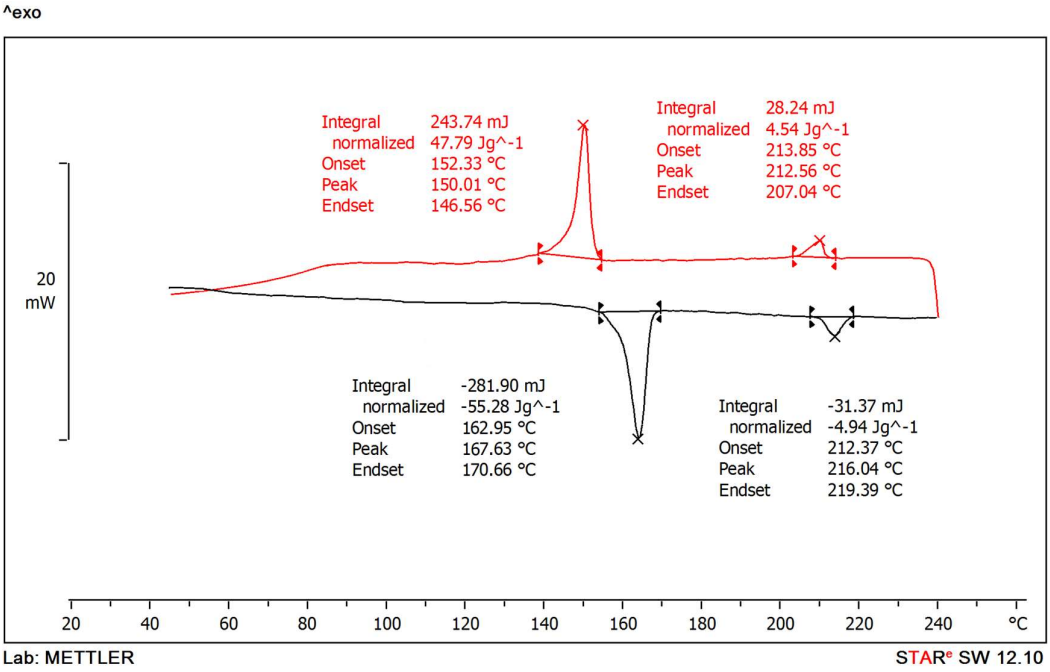

Fig. S5.57: DSC thermogram of *VIII-3*

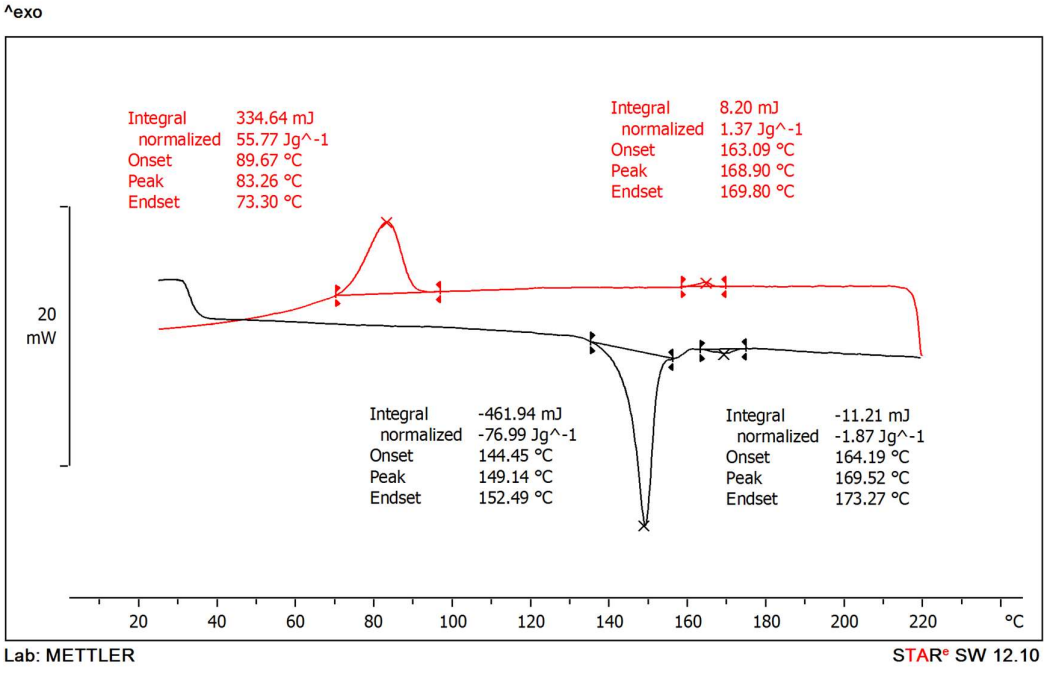

Fig. S5.58: DSC thermogram of *VIII-4*

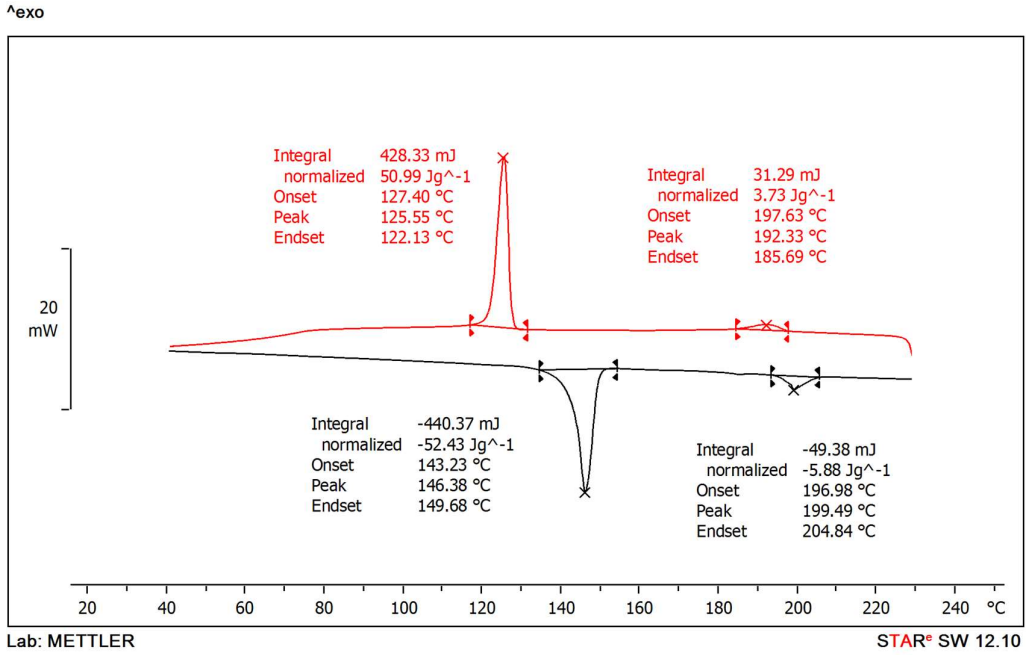

Fig. S5.59: DSC thermogram of *VIII-5*

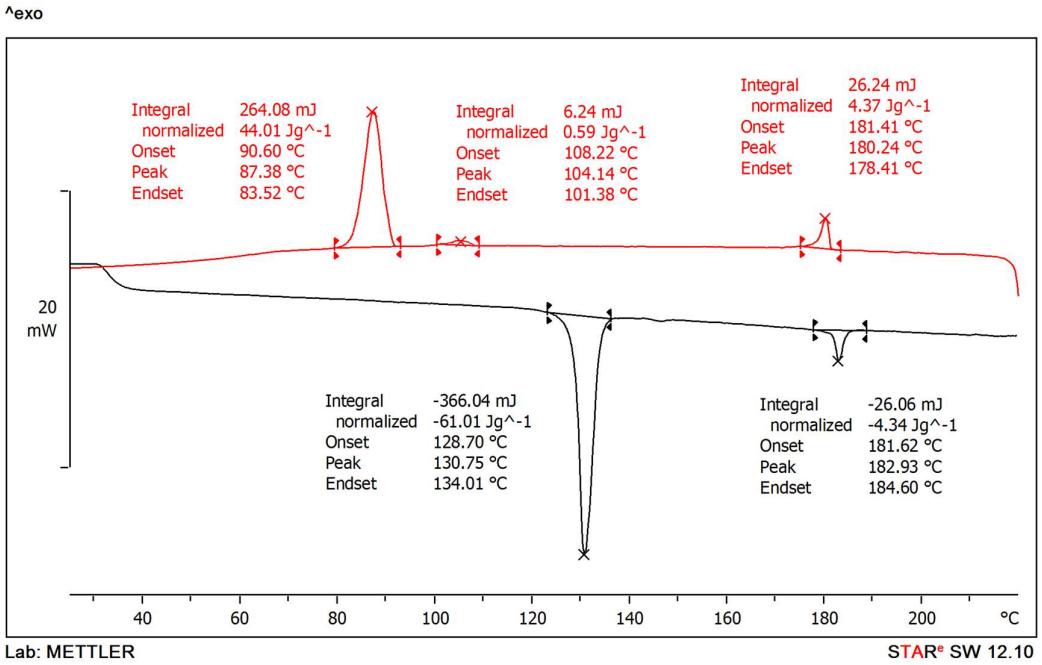

Fig. S5.60: DSC thermogram of *VIII-7*

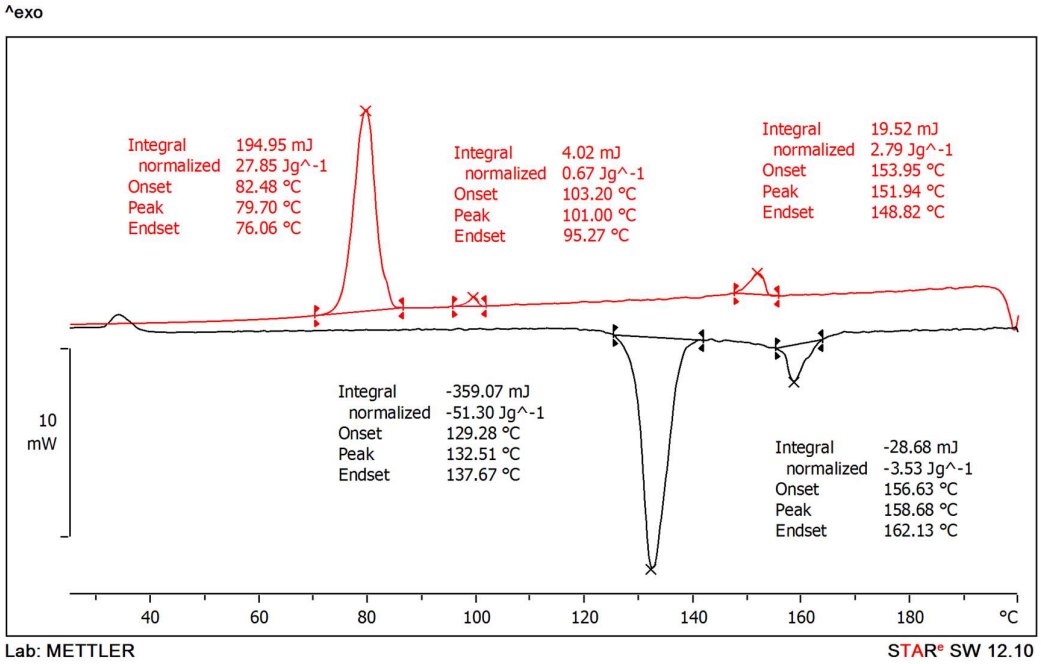

Fig. S5.61: DSC thermogram of *VIII-9*

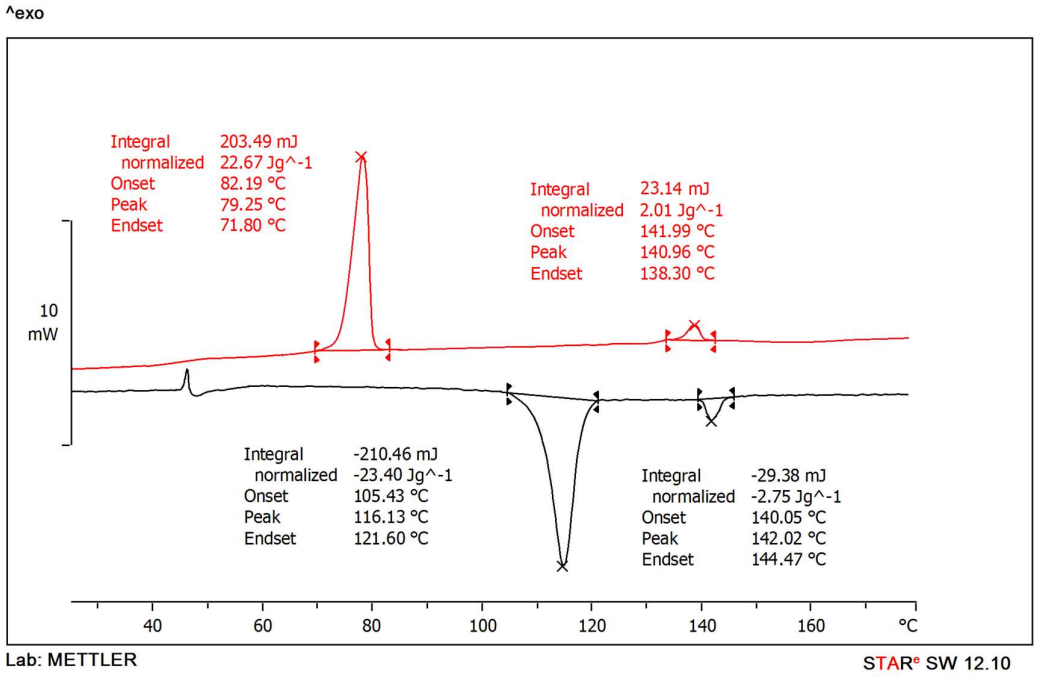

Fig. S5.62: DSC thermogram of *VIII-10*

5.8 References:

1 F. Hardouin, M. F. Achard, Jung-Il Jin, Jin-Wook Shin and Yong-Kuk Yun, *J. Phys. II Fr.*, 1994, **4**, 627–643.

2 C. V Yelamaggad, I. S. Shashikala, G. Liao, D. S. S. Rao, S. K. Prasad, Q. Li and A. Jakli, *Chem. Mater.*, 2006, **18**, 6100–6102.

3 M. Gupta and S. K. Pal, *Liq. Cryst.*, 2015, **42**, 1250–1256.

4 Z. Fang and C. Wu, *Liq. Cryst.*, 2020, **47**, 1086–1099.

5 C. V Yelamaggad, G. Shanker, U. S. Hiremath and S. Krishna Prasad, *J. Mater. Chem.*, 2008, **18**, 2927–2949.

6 Z. Fang, K. Zou and C. Wu, *Liq. Cryst.*, 2020, **47**, 1473–1486.

7 C. V Yelamaggad and S. A. Bhat, *Liq. Cryst.*, 2022, **49**, 995–1009.

8 V. Bhat S, V. A. Raghunathan and S. Kumar, *J. Mol. Liq.*, 2021, **340**, 117219.

9 V. Punjani, G. Mohiuddin, S. Chakraborty, P. Barman, A. Baghla, M. B. Kanakala, M. K. Das, C. Yelamaggad and S. K. Pal, *Soft Matter*, 2024, **20**, 7012–7020.

10 B. S. Ranjitha, M. Alaasar and G. Shanker, *J. Mol. Struct.*, 2024, **1305**, 137626.

11 A. Krishna KM, S. Sony, S. Dhingra and M. Gupta, *ACS Mater. Lett.*, 2023, **5**, 3248–3254.

12 U. S. Hiremath, G. G. Nair and D. S. S. Rao, *Liq. Cryst.*, 2016, **43**, 711–728.

13 Y.-P. Goh, W.-S. Yam, F.-W. Yip and G. Hegde, *Curr. Org. Synth.*, 2021, **18**, 352–365.

14 K. C. Majumdar, S. Chakravorty, N. Pal and R. K. Sinha, *Tetrahedron*, 2009, **65**, 7998–8006.

15 J. Xiong, X. Lin, H. Guo, F. Yang and J. Lai, *Liq. Cryst.*, 2018, **45**, 362–369.

16 C. V Yelamaggad, N. L. Bonde, A. S. Achalkumar, D. S. Shankar Rao, S. K. Prasad and A. K. Prajapati, *Chem. Mater.*, 2007, **19**, 2463–2472.

17 C. V Yelamaggad, A. S. Achalkumar, N. L. Bonde and A. K. Prajapati, *Chem. Mater.*, 2006, **18**, 1076–1078.

18 B. N. Veerabhadraswamy, S. A. Bhat, U. S. Hiremath and C. V Yelamaggad, *Chemphyschem*, 2019, **20**, 2836–2851.

19 V. A. Mallia and N. Tamaoki, *Chem. Soc. Rev.*, 2004, **33**, 76–84.

20 T.-Y. Guo, Z.-P. Chen, J.-F. Lin, Z.-Z. Cai, H.-L. Xie, A. Reheman and Y.-G. Jia, *J. Mol. Struct.*, 2023, **1283**, 135282.

21 C. V. Yelamaggad, M. Mathews, T. Fujita and N. Iyi, *Liq. Cryst.*, 2003, **30**, 1079–1087.

22 M. Rabari, Y. Parmar and A. K. Prajapati, *Liq. Cryst.*, 2023, **50**, 2552–2570

23 M. Rabari, S. Solanki and A. K. Prajapati, *Dye. Pigment.*, 2023, **220**, 111757.

24 M. Rabari, R. S. Kumar CH and A. K. Prajapati, *J. Mol. Struct.*, 2023, **1293**, 136252.

25 M.-Y. Zheng, Y.-S. Wei, Y.-Z. Gu and S. Wang, *Mol. Cryst. Liq. Cryst.*, 2014, **593**, 151–164.

26 B. S. Ranjitha, D. Sandhya Kumari, A. Shetty, G. Shanker, M. Alaasar, R. Pashameah and G. Hegde, *J. Mol. Liq.*, 2023, **383**, 121985.

27 C. Wu, *Mater. Lett.*, 2007, **61**, 1380–1383.

28 V. A. Mallia and N. Tamaoki, *J. Mater. Chem.*, 2003, **13**, 219–224.

29 N. Tamaoki, Y. Aoki, M. Moriyama and M. Kidowaki, *Chem. Mater.*, 2003, **15**, 719–726.

30 H. Huang, Y. Cong, B. Hu and B. Zhang, *Liq. Cryst.*, 2021, **48**, 564–578.

31 K. Kim, E. Do, Y. Kwon and J. Jin, *Liq. Cryst.*, 2005, **32**, 229–237.

32 A. Alshargabi, G. Y. Yeap, W. A. K. Mahmood, C. C. Han, H. C. Lin and D. Takeuchi, *Liq. Cryst.*, 2015, **42**, 1337–1349.

33 R. W. Date, G. Luckhurst, M. Shuman and J. Seddon, *J. Phys. II France,* 1995, **5,** 587-605.

34 Y. Tian, X. Xu, Y. Zhao, X. Tang and T. Li, *Liq. Cryst.*, 1997, **22**, 87–96.

35 P. Tolédano, B. Mettout and A. Primak, *Eur. Phys. J. E*, 2004, **14**, 49–54.

36 D. D. Sarkar, R. Deb, N. Chakraborty, G. Mohiuddin, R. K. Nath and V. S. R. Nandiraju, *Liq. Cryst.*, 2013, **40**, 468–481.

37 K. C. Majumdar, T. Ghosh, S. Chakravorty, N. Pal, D. S. Shankar Rao and S. K. Prasad, *Liq. Cryst.*, 2010, **37**, 1539–1547.

38 M. Hagar, H. A. Ahmed and G. R. Saad, *J. Mol. Liq.*, 2019, **273**, 266–273.

39 M. Rabari and A. K. Prajapati, *J. Mol. Struct.*, 2024, **1307**, 137971.

40 M. Rabari and A. K. Prajapati, *J. Mol. Struct.*, 2024, **1308**, 138101.

41 D. W. Lee, J. Il Jin, M. Laguerre, M. F. Achard and F. Hardouin, *Liq. Cryst.*, 2000, **27**, 145–152.

42 J. W. Lee, Y. Park, J. Il Jin, M. F. Achard and F. Hardouin, *J. Mater. Chem.*,

2003, **13**, 1367–1372.

43 E. Do, K. Kim, Y. Kwon and J. Jin, *Liq. Cryst.*, 2006, **33**, 511–519.

44 T. E. A. Frizon, A. A. Vieira, F. C. Giacomelli, R. Cercená, A. Dal Bó, E. Zapp, E. Junca, A. A. Chepluki, C. D. Tomasi, L. B. Ribeiro, S. Saba and J. Rafique, *Liq. Cryst.*, 2022, **49**, 758–768.

45 G.-Y. Yeap, A. Alshargabi, W. A. K. Mahmood, C.-C. Han, H.-C. Lin, M. Santo and M. M. Ito, *Tetrahedron*, 2015, **71**, 3939–3945.